الجمهورية الجزائرية الديمقراطية الشعبية
Democratic and Popular of Algeria

وزارة التعليم العالي والبحث العلمي
Mining of Higher Education and Scientific Research
جامعة الشهيد الشيخ العربي التبسي – تبسة
Echahid Cheikh Larbi Tebessi University – Tebessa
معـــــــهد المـــناجم
Institute of Mines
قسم المناجم و الجيوتكنولوجيا
Departement of Mines and Geotechnology

MEMOIRE

Present for the award of the Master's degree

Major: Geotechnics

Option: Geotechnics

Geotechnical modeling of slope stability: case study and risk assessment 'open trench excavation in BEKKARIA'

Made by
BOUAZDIA Maroua.

In front of a jury

Mebrouk Faouzi	**President**	**MAA**	**Echahid Cheikh Larbi Tebessi University – Tebessa**
Berrah Yacine	**Acadimic Supervisor**	**MCA**	**Echahid Cheikh Larbi Tebessi University – Tebessa**
Djellali Adel	**Examiner**	**PR**	**Echahid Cheikh Larbi Tebessi University – Tebessa**

Academic year: 2024/2025

الجمهورية الجزائرية الديمقراطية الشعبية
République Algérienne Démocratique et Populaire

Ministère de l'Enseignement Supérieur
et de la Recherche Scientifique
Université Larbi Tebessi – Tébessa
Institut des Mines
Département mines et géotechnologie

وزارة التعليم العالي و البحث العلمي
جامعةالعربي التبسي – تبسة
معهد المناجم
قسم المناجم و الجيوتكنولوجيا

Année universitaire : 2024/2025Tébessa le : 7/6/2025

Lettre de soutenabilité

Noms et prénoms des étudiants :

BOUAZDIA MAROUA

Niveau : Master 2 Option : Géotechnique

Thème :Geotechnical Modeling of Slope Stability :Case Study And Risk Assessment 'open tranche Bekkaria'

Nom et prénom de l'encadreur : BERRAH YACINE

Chapitres réalisés	Signature de l'encadreur
Chapter I: Slope Stability Causality And Effects	
Chapter II:Geological, Hydrogeological and Geomorphological Condition.	
CHAPTER III: Geotechnical Investigation and Data Collection.	
CHAPTRE IV:Case study, Resultes and discussion.	

الجمهورية الجزائرية الديمقراطية الشعبية
وزارة التعليم العالي و البحث العلمي

مؤسسة التعليم العالي: جامعة العربي التبسي-تبسة

تصريح شرفي خاص بالالتزام بقواعد النزاهة العلمية لانجاز بحث

أنا الممضي أدناه،

السيد(ة): بوازدية مروى الصفة: طالبة

الحامل لبطاقة التعريف الوطنية رقم: 293229141 والصادرة بتاريخ: 03/10/2024

المسجل بمعهد: المناجم. قسم: المناجم و الجيوتكنولوجيا

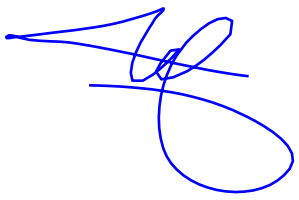
والمكلف بانجاز أعمال بحث (مذكرة التخرج، مذكرة ماستر) ، عنوانها:

Geotechnicalmodelingofslopestability:casestudyandrisk assessment‘open trench excavation in BEKKARIA '

أصرح بشرفي أني ألتزم بمراعاة المعايير العلمية والمنهجية و معايير الأخلاقيات المهنية والنزاهة الأكاديمية المطلوبة في انجاز البحث المذكور أعلاه.

التاريخ : 09/06/20

إمضاء المعني(ة)



الجمهورية الجزائرية الديمقراطية الشعبية

وزارة الشهيد الشيخ التعليم العالي و البحث العلمي

جامعة العربي التبسي- تبسة

مقرر رقم: 227 مؤرخ في: 04 جوان 2025

يتضمن الترخيص بمناقشة مذكرة الماستر

إنّ مدير جامعة العربي التبسي بتبسة،

- بموجب القرار الوزاري رقم 318 و المؤرخ في 05 ماي 2021 المتضمن تعيين السيد "قواسمية عبد الكريم" مديرا لجامعة العربي التبسي - تبسة،

-و بمقتضى المرسوم التنفيذي رقم : 12- 363 مؤرخ في 8 أكتوبر 2012، يعدل و يتمم المرسوم التنفيذي رقم 09 - 08 المؤرخ في : 04 جانفي 2009 و المتضمن إنشاء جامعة العربي التبّسي بتبسة،

-وبمقتضى المرسوم التنفيذي رقم 08-265 المؤرّخ في 17 شعبان عام 1429 الموافق 19 غشت سنة 2008 الذي يحدّد نظام الدراسات للحصول على شهادة الليسانس وشهادة الماستر وشهادة الدّكتوراه، لاسيما المادة 9 منه،

-وبموجب القرار رقم 362 المؤرّخ في 09 جوان 2014 الذي يحدّد كيفيات إعداد ومناقشة مذكّرة الماستر، لاسيما المادة 7 منه،

- وبموجب القرار رقم 1080 المؤرّخ في 13 أكتوبر 2015 والمتضمّن تأهيل ماستر الفروع ذات تسجيل وطني بجامعة تبسة.

- وبموجب القرار رقم 375 المؤرّخ في 15 جوان 2020 المعدل لملحق القرار 1080 المؤرّخ في 13 أكتوبر 2015 والمتضمّن تأهيل ماستر الفروع ذات تسجيل وطني بجامعة تبسة، اختصاص جيوتقني

-وبموجب المقرّر رقم 227 المؤرّخ في 2025/06/04 والمتضمّن تعيين لجنة مناقشة مذكّرة الماستر،

-وبعد الاطّلاع على مقرر تعيين لجنة مناقشة مذكرة الماستر المؤرّخ في2025/06/04

يقرّر ما يأتي:

المادة الأولى: يُرخّصُ للطالب(ة) بوازدية مروى، المولود (ة) بتاريخ 2003/02/23 بـ **الماء الابيض - تبسة**، بمناقشة مذكّرة الماستر والموسُومة بـ

Geotechnical Modeling of Slope Stability: Case Study and Risk Assessment

المادة 2: يكلّف رئيس قسم المناجم والجيوتكنولوجيا بتنفيذ هذا المقرّر الّذي يسلّم نسخة عنه إلى الطّالب المعني بالمناقشة وأعضاء لجنة المناقشة فور توقيعه، وبضمان نشره عبر فضاءات المؤسّسة المادية والرقمية.

المادة 3: تُحفظ نسخة عن هذا المقرّر ضمن الملفّ البيداغوجي للطّالب المعني وينشر في النّشرة الرّسمية لجامعة العربي التبسي.

حُرّر ب تبسة، 04 جوان 2025

عن المدير، وبتفويض منه

مدير معهد المناجم

د.عولمي زوبير

جامعة الشهيد الشيخ العربي التبسي تبسة

المدير

معهد المناجم

الجمهورية الجزائرية الديمقراطية الشعبية

وزارة التعليم العالي والبحث العلمي

جامعة العربي التبسي- تبسة

مقرر رقم : 193مؤرخ في : 04 جوان 2025

يتضمن تعيين لجنة مناقشة مذكرة الماستر

إنّ مدير جامعة العربي التبسي بتبسة،

- بموجب القرار الوزاري رقم 318 و المؤرخ في 05 ماي 2021 المتضمن تعيين السيد "قواسمية عبد الكريم" مديرا لجامعة العربي التبسي - تبسة،

- و بمقتضى المرسوم التنفيذي رقم : 12- 363 مؤرخ في 8 أكتوبر 2012، يعدل و يتمم المرسوم التنفيذي رقم 09 - 08 المؤرخ في : 04 جانفي 2009 و المتضمن إنشاء جامعة العربي التبّسي بتبسة،

- وبمقتضى المرسوم التنفيذي رقم 08-265 المؤرّخ في 17 شعبان عام 1429 الموافق 19 غشت سنة 2008 الذي يحدّد نظام الدراسات للحصول على شهادة الليسانس وشهادة الماستر وشهادة الدّكتوراه، لاسيما المادة 9 منه،

-وبموجب القرار رقم 362 المؤرّخ في 09 جوان 2014 الذي يحدّد كيفيات إعداد ومناقشة مذكّرة الماستر، لاسيما المادتان 10 و11 منه،

-وبموجب القرار رقم 1380 المؤرّخ في 09 أوت 2016 والمتضمّن مواءمة التكوينات في الماستر بعنوان جامعة تبسة في ميدان "علوم وتكنولوجيا".

-وبموجب القرار رقم رقم 921 المؤرّخ في 25 أوت 2021 المعدل لملحق القرار 1080 المؤرّخ في 13 أكتوبر 2015 والمتضمّن مواءمة التكوينات في الماستر بعنوان جامعة تبسة في ميدان "علوم وتكنولوجيا"، اختصاص جيوتقني

-وبعد الاطّلاع على محضر المجلس العلمي لمعهد المناجم رقم 03 المؤرّخ في 12 ديسمبر 2024،

يقرّر ما يأتي:

المادة الأولى: تُعيّنُ بموجب هذا المقرّر لجنة مناقشة مذكّرة الماستر المحضّرة من طرف الطّالب (ة): بوازدية مروى،

المولود (ة) بتاريخ 2003/02/23 بـ الماء الابيض - تبسة ،

والموسُومة بـ : Geotechnical Modeling of Slope Stability: Case Study and Risk Assessment

والمسجّل (ة) بمعهد المناجم

المادة 2: تتشكّل اللجنة المشار إليها في المادة الأولى من الأعضاء الآتي ذكرهم:

رقم	الاسم واللّقب	الرتبة	مؤسّسة الانتماء	الصّفة
1	مبروك فوزي	أستاذ مساعد – أ-	جامعة العربي التبسي - تبسة	رئيسا
2	براح ياسين	أستاذ محاضر - أ	جامعة العربي التبسي - تبسة	مشرفا
3	عادل جلالي	أستاذ	جامعة العربي التبسي - تبسة	ممتحنا

المادة 3: يكلّف رئيس قسم المناجم والجيوتكنولوجيا بتنفيذ هذا المقرّر الّذي يُسلّم نسخةً عنه إلى كلّ من الطّالب المعني والمشرف على المذكّرة وأعضاء لجنة المناقشة فور توقيعه.

المادة 4: تحفظ نسخة عن هذا المقرّر في الملفّ البيداغوجي للطالب المعني، ويُنشر في النّشرة الرّسمية لجامعة العربي التبسي.

حُرّر ب تبسة، في 04 جوان 2025

عن المدير، وبتفويض منه

مدير المعهد

مدير معهد المناجم
د.عولمي زوبير

جامعة الشهيد الشيخ العربي التبسي تبسة
معهد المناجم

Scanned with CamScanner

Abstract
This study investigates slope stability challenges in a geologically complex mountainous terrain where a phosphate transport railway is being constructed. Combining advanced numerical modeling (PLAXIS 2D/2024) with comprehensive field investigations, the research evaluates stability across three distinct geological facies: unstable diapiric gypsum-clay formations requiring reinforcement, competent limestone strata demonstrating inherent stability, and plastic clays showing critical susceptibility to failure. Key findings reveal rainfall infiltration reduces safety factors by 25-40% in weak formations, while dynamic train loads induce progressive deformations (<5 mm) in plastic clays. The study establishes optimal slope designs (65° benched excavations) and proposes targeted mitigation measures including drainage systems and soil nailing. By developing a validated modeling framework for multi-lithological terrains, this research provides both practical solutions for the current project and a methodological template for similar infrastructure developments in geologically challenging environments. The results emphasize the necessity of lithology-specific engineering approaches and real-time monitoring to ensure long-term slope stability
Keywords: Slope stability analysis; Geotechnical modeling; Diapiric formations; PLAXIS 2D simulation; Rainfall-induced landslides; Mining infrastructure.

ملخص

تتناول هذه الدراسة تحديات استقرار المنحدرات في منطقة جبلية ذات تركيب جيولوجي معقد حيث يتم إنشاء خط سكك حديدية لنقل الفوسفات. من خلال الجمع بين النمذجة الرقمية المتقدمة PLAXIS 2D/2024 والتحقيقات الميدانية الشاملة، تقيم البحث الاستقرار عبر ثلاثة أنماط جيولوجية متميزة: تكوينات غير مستقرة منالتكوينات المندفعة (Diapir) من العصر الترياسي خصائص جيوتقنية حرجة بسبب احتوائها على طبقات من الجبس والطين اللدن التي تحتاج إلى تعزيز، طبقات حجر جيري متماسكة تظهر استقراراً ذاتياً، وطين لدن يظهر حساسية حرجة للانهيار. تكشف النتائج الرئيسية أن تسرب مياه الأمطار يقلل عوامل الأمان بنسبة 25-40% في التكوينات الضعيفة، بينما تسبب الأحمال الديناميكية للقطارات تشوهات تراكمية> 5مم) في الطين اللدن. توصلت الدراسة إلى تصاميم مثالية للمنحدرات (حفريات متدرجة بزاوية 65°) وتقترح إجراءات تخفيف مستهدفة تشمل أنظمة الصرف وتثبيت التربة بالمسامير.

الكلمات المفتاحية :تحليل استقرار المنحدرات؛ النمذجة الجيوتقنية؛ التكوينات المندفعة؛ محاكاةPLAXIS 2D ؛ انهيارات أرضية ناتجة عن الأمطار؛ طريق السكة الحديدية(البنية التحتية للتعدين)

Résumé

Cette étude examine les défais de stabilité des pentes dans un terrain montagneux géologiquement complexe où une voie ferrée pour le transport de phosphate est en construction. En combinant la modélisation numérique avancée (PLAXIS 2D /2024) avec des investigations de terrain complètes, la recherche évalue la stabilité à travers trois faciès géologiques distincts : des formations instables de gypse-argile diapirique nécessitant un renforcement, des strates de calcaire compétentes démontrant une stabilité inhérente, et des argiles plastiques montrant une susceptibilité critique à la rupture. Les principaux résultats révèlent que l'infiltration des précipitations réduit les facteurs de sécurité de 25 à 40% dans les formations faibles, tandis que les charges dynamiques des trains induisent des déformations progressives (<5 mm) dans les argiles plastiques. L'étude établit des conceptions optimales de pente (excavations en gradins à 65°) et propose des mesures d'atténuation ciblées incluant des systèmes de drainage et des clouages des sols.

Mots-clés : Stabilité des pentes; Modélisation géotechnique; Formations diapiriques; PLAXIS 2D;Infiltration des pluies ;Clouage du sol; Infrastructure minière

Table of Contents

Abstract.....iii

ملخص.....iv

Résumé.....v

List of figures.....viii

Liste des tableaux.....xii

General Introduction.....xiii

Chapter I: SLOPE STABILITY CAUSALITY AND EFFECTS

I.1 Introduction.....2

I.2. Ground Movements and Slope Failures.....3

I.2.1 Overview of Ground Movements.....3

I.2.2 Main Types of Ground Movements.....3

I.2.3 Causes of Ground Movements and Slope Failures.....5

I.2.4 Engineering Hazards Associated with Ground Movements.....7

I.2.5 Engineering Hazards Associated with Ground Movements.....7

I.3. Types of Slope Failures 8
I.3.1 Classification of Slope Failures by Material Type 8
I.3.2 Classification by Mechanism 13
I.3.3 Classification by Movement Speed 14
I.4 Causes of Slope Failures 15
I.4.1 Natural Causes 15
I.4.2 Human-Induced Causes 17
I.4.3 Comparative Analysis of Natural and Human-Induced Causes 17
I.5 Parameters Influencing Slope Stability and Factor of Safety 18
I.5.1 Factor of Safety (FoS) 18
I.5.2 Key Geotechnical Parameters Affecting Slope Stability 20
I.6 Methods of slope failure analysis 22
I.6.2 Numerical Methods (e.g., Finite Element Method - FEM) 25
I.6.2 Numerical Methods 26
I.6.3 Comparison between Limit Equilibrium Method (LEM) and Finite Element Method (FEM) 28
I.6.4 Summary and Recommendations 29
I.7 Importance of Modeling Slope Stability 30
I.8 Consquences of Slope Failures 30
I.8.1 Human Losses 30
I.8.3 Environmental Impact 31
I.8.4 Socioeconomic Impact 31
I.9Conclusion: 32

Chapter II:Geological, Hydrogeological and Geomorphological Condition.

II.1.Introduction: 34
I.2. Location of the Study Area: 35
II.2.1. Regional Geographic Setting: 35

II.2.2 Local Geographic Setting : 35
II.3. Geomorphological Setting of the Bekkaria Region (Tébessa, NE Algeria): 37
II.4. Geological Context 37
II.4.1. Regional Geologie: 37
II.4.2Geogical map : 38
II.4.3 Local Geology 39
II.5.Stratigraphic Summary of the Tébessa 40
II.6.Tectonic Features in the Tebessa Region: 42
II.7. Hydrogeological and Climatological Conditions of the Bekkaria Region: 43
II.7.1. Piezometry and Groundwater Levels 43
II.7.2. Climate Classification, Precipitation, and Temperature 44
II.7.3. Implications for Open-Trench Slope Stability 45

II.7.4. Impact of These Factors on Slope Stability 45
II.7.5. Recommendations for Data Collection and Stability Management 46
II.8Conclution : 46

CHAPTER III:Geotechnical Investigation and Data Collection

III.1. Introduction: 49
III.2.Geotechnical investigation: 50
III.2.1Boreholes Investigation 50
III.2.2Detailed Lithological Description of Boreholes : 51
III.2.3Water Table : 53
III.3 Geophysics: 53
III.3.1Description : 53
III.3.2 Seismic Refraction Results (Vp Profiles) : 54
III.3.3 Profile Comparisons: 58
III.3.4 Core Data Validation : 58
III.3.5 Implications: 58
III.4Presentation of Project : 58
III.4.1 Site Overview and Field Observations: 58
III.4.2 Geological and Topographic Mapping: 59
III.4.3Representative Field Photos: 60
III.4.4Geological Observations and Geotechnical Stability Implications 62
III.4.5 Project Description 63
III.5 Geotechnical Tests and data extraction 65
III.5.1 Results of Physical, Mechanical, and Chemical Analyses 65
III.5.1.1Turonian Limestones: 65
III.6Conlusion: 70
CHAPTER IV : CASE STADY:RUSULTS AND DISCUSSION .

IV.1 Introduction: 71
IV .2Geotechnical Molding: 72
IV.2.1 Clayey soil formation (MIOPLIOCEN): 72
IV.2.2 Results and discussion of Clayey 77
IV.2.3 Interpretation 86
IV.2.4 Limestone Layer facies (Turonian) : 86
IV.2.5Results and discussion of Limestone 92
IV.2.6Interpritation (Limestone): 101
IV.2.7 Diapiric clayey soil formation (Triasic facies) : 101
IV.2.8Results and discussion: 106
IV.2.8 Interpretation (gypsum clayey facies Triassic) 116
IV.2.9 Risk Assessment Recommendations & Remediation Measures for Unstable Facies 117
IV.3 Conclusion 118
General Conclusion 120

List of figures

FigI.1:LandslidesMovement.(website1) 3
FigI.2: Rockfallmovement (GeoStru 2022). 4
FigI.3: DebriFlowmovement.((Keefer,2016)) 4
FigI.4:SoilCreep movement.(website2) 5
FigI.5: CircularFailure(Kolapoetal.,2022/U.S.Geological Survey,(2004)) 8
FigI.6:Translationalslide.(U.S.Geological Survey,(2004)) 9
FigI.7:Earthflow.(U.S.GeologicalSurvey,2004)) 9
FigI.8:Lateral SpreadsNiigata,Japan 1964(U.S.Geological Survey(2023)) 10
FigI.9:Typical Rockfall Diagram.(InspiredPencil (2023)) 11
FigI.10:TopplingFailureSchematic.(Wyllie,D.C.,&Mah,C.W. (2004)) 11
FigI.11:Planar Slide.(Acharyaetal.,2017) 12
FigI.12:WedgeFailure(Prodyogi.(2023)) 12
FigI.13: BucklingFailureSchematic.(Cuiet al., 2023) 13
FigI.14:BustrappedinfloodwatersduringheavyrainfallinHaldwani, India. (Kumari,2022) 16
FigI.15:Effectsof SeismicActivityonUrbanAreas.(SchematicsInkage,2024) 16
Fig I.16:Descriptionofslicingwithfracture surface. 23
References 122
ANNEX 127
FigureI.17:Theforcesactingon asurface accordingtoFELLENIUS 24
Figure I.18: Taylor's slope stability charts for homogeneous slopes under total stress conditions. (notasingenierocivil.blogspot.com, 2011; based on Taylor, 1937) 26
Fig I.19:Structuraldamagecaused byaman-madeslope failure(Kolapoet al., 2022) 31
FigII.1:Regional GeographicLocation (Tebessa). 35
FigII.2:Location of therailway crossing thestudyareaand theproject zone. 36
Fig II.3:Geological Map of Tebessa. 38
FigII.04:Geological Map ofStudy Area(Bekkaria). 39
Fig II.05: Complete Stratigraphic Column of the Tebessa Region: Lithostratigraphic Sequence from the Triassic to the Quaternary (Durozoy, J. P. (1956)). 41
FigII.06.TectonicsketchoftheTébessaregion(Kowalski etal.1997) 42
FigII.07:Carte-piezometrique-El-Ma-El-Abiod-et-Tebessa-janv-2009 44
FigureII.08:MonthlyAverage Temperature andPrecipitation(1991–2023)–Tébessa(ClimateProxyforBekkaria)(AdaptedfromClimate-Data.org, 45

Tutiempo.net, and Climate-Charts.com)
FigIII.1:Anexampleofboreholedrilled inthelimestonefacies. 50
FigIII-2: Preliminary geologicalsection along theaxisofthetrack 53
FigIII-3:MappingofGeophysicalInvestigationPointsandBoreholesonSatellite Imagery. 54
FigIII-4:Locationof GeophysicalProfilePS1ontheStudy Site. 55
FigIII-5:InterpritationResultsof PS1GeophisicalProfile. 55
FigIII-6:LocationofGeophysicalProfilePS2ontheStudySite. 56
FigIII-7:InterpritationResultsofPS1GeophisicalProfile. 56
FigIII-8:LocationofGeophysicalPro 57
FigIII-9:InterpritationResultsof PS3GeophisicalProfile. 57
Fig III-10:GeoMap View inTopographicPlan(COSIDER2024). 59
FigIII.11:OutcropofPliocene Moiclays 60
FigIII.12:TuronienLimestonesDipping TowardsTheSE 61
Fig III.13:Unstablerockyareaat thetop ofthehill. 61
FigIII.14:VariegatedTriassicClays. 61
Fig III.15:ExcavationWorkPlanView(COSIDER2024) 62
FigIII.16:CasagrandeSDC-03clayclassificationchart 65
FigIII.17:CasagrandeSDC-02clayclassificationchart 68
FigIV.1:TheCrosssection ofclayey soil. 72
Fig IV.2:TheGeometryClayeyLayer. 72
Fig IV.3:Inputmaterial. 73
FigIV.4: BoundariesConditions. 74
FigIV.5: Generate Mesh. 74
Fig IV.6: Flowcondition. 75
Fig IV.7: thenodesofcalculationphasesinP3AXIS. 75
FigIV.8:Configurationof calculationphasesinPLAXIS. 76
Fig IV.9:Mesh DeformationduringInitialPhases. 77
FigIV.10:TotalDeformationduringInitialPhases. 77
Fig IV.11 :Mesh DeformationduringPhase 01. 78
FigIV.12:TotalDeformationduringPhase01. 78
FigIV.13:Mesh DeformationduringExcavationPhase. 79
FigIV.14 :Total DeformationduringExcavationPhase. 79
FigIV.15 :Thesafety factor oftheExcavation Phase. 80
FigIV.16:MeshDeformationduringPhase04. 80

FigIV.17:TotalDeformationduringPhase04. 81
FigIV.18:MeshDeformationduringPhase05. 81
FigIV.19:TotalDeformation during Phase05. 82
FigIV.20:The safetyfactorofphase 05. 82
FigIV.21:MeshDeformationduringPhase06(dynamic). 83
Fig IV.22:Totaldisplacement duringphase06(dynamic). 83
Fig IV.23:Thesafetyfactorofphase06(Dynamic). 84
FigIV.24:MeshDeformationduringPhase 07(rainfall). 84
FigIV.25:Totaldisplacementduringphase 07(rainfall). 85
FigIV.26:The safetyfactorofthe phase07. 85
FigIV.27:DisplacementversusStrngthReductionFactor(Msf). 86
FigIV.28:TheCrosssection ofclayey soil. 87
FigIV.29:TheGeometryLimestoneLayer. 87
Fig IV.30:Inputmaterial. 88
FigIV.31: Generate Mesh. 89
FigIV.32: Flowcondition. 89
FigIV.33: thenodesofcalculationphases. 90
FigIV.34:ConfigurationofcalculationphasesinPLAXIS2D. 90
Fig IV.35:Mesh DeformationduringInitialPhases. 91
FigIV.36:TotalDeformationduringInitialPhases. 92
Fig IV.37 :Mesh DeformationduringPhase 01. 93
FigIV.38:TotalDeformationduringPhase01. 93
FigIV.39:MeshDeformationduringExcavationPhase. 94
FigIV.40:TotalDeformationduringExcavationPhase. 94
FigIV.41 :Thesafety factor oftheExcavation phase. 95
FigIV.42:MeshDeformationduringPhase04. 95
FigIV.43:TotalDeformationduringPhase04. 96
FigIV.44:MeshDeformationduringPhase05. 96
Fig IV.45:TotalDeformationduringPhase 05. 97
FigIV.46:The safetyfactorofphase 05. 97
FigIV.47:MeshDeformationduringPhase06(dynamic). 98
FigIV.48:Totaldisplacement duringphase06(dynamic). 98
FigIV.49:MeshDeformationduringPhase 07(rainfall). 100
FigIV.50:Totaldisplacementduringphase 07(rainfall). 100
FigIV.51:DisplacementversusStrngthReduction Factor (Msf). 101

FigIV.52:TheCrosssection ofclayey soil. 102
Fig IV.53:TheGeometryClayeyLayer. 102
FigIV.54:Inputmaterial. 103
FigIV.55: BoundariesConditions. 104
FigIV.56: Generate Mesh. 104
FigIV.57:Flowcondition. 105
FigIV.58:ConfigurationofcalculationphasesinPLAXIS2D. 106
FigIV.59: Completethecalculation phases. 107
FigIV.60:MeshDeformationduringInitialPhases 107
FigIV.61:TotalDeformationduringInitialPhases 107
FigIV.62:MeshDeformationduringPhase01 108
FigIV.63:TotalDeformationduringPhase01. 108
FigIV.64:MeshDeformationduringExcavationPhase. 109
Fig IV.65:TotalDeformationduringExcavationPhase. 109
FigIV.66MeshDeformationduringphase03. 110
FigIV.67:Totaldisplacementduringphase03. 110
FigIV.68:MeshDeformation duringPhase04. 111
FigIV.69:TotalDeformationduringPhase04 111
FigIV.70:MeshDeformationduringPhase05 112
FigIV.71:TotalDeformationduringPhase05. 112
FigIV.72:MeshDeformationduringPhase06(dynamic) 113
Fig IV.73:Total displacement duringphase06(dynamic) 113
FigIV.74:Thesafetyfactor ofthephasedynamic. 114
FigIV.75:Meshdeformation. 114
FigIV.76:Totaldisplacementduringphase 07(rainfall). 115
FigIV.77:MeshDeformationduringphase08. 115
FigIV.78:Thesafety factor ofthephase07. 116
FigIV.79:DisplacementversusStrengthReductionFactor (Msf). 116

Tableslist

TableI.1:Comparison between Natural andHuman-Induced CausesofSlope Failures. 18

TableI.2:ComparisonbetweenLimitEquilibriumMethod(LEM) andFiniteElement Method(FEM)(Duncan,J.M.,&Wright,S.G.(2005). 29

TableIII.1:SummaryofBoreholesLocation andCracteristics. 51

TableIII.2:Resultsof mechanicaltestsSDC-04/SDC-05. 64

TableIII.3:ResultsofthephysicaltestsSDC-03/SDC-06. 65

TableIII.4:Resultsofthemechanical testsSDC-03/SDC06. 66

TableIII.5:Resultsof SPTSDC-03and SDC-06 tests. 67

TableIII.6:Resultsofphysicaltestsof the SDC02survey. 67

TableIII.7:Resultsof chemical analysesof theSDC02 survey. 68

TableIV.1: Claylayer properties. 73

TableIV.1:Limestonelayer properties. 88

General Introduction

Slope stability analysis represents a fundamental challenge in geotechnical engineering, particularly in mountainous regions where complex terrain and variable geological conditions create significant engineering constraints. The construction of critical mining infrastructure, such as phosphate transport railways, demands rigorous stability assessment to prevent catastrophic failures that could compromise safety, disrupt operations, and incur substantial economic losses. This dissertation presents a comprehensive investigation of slope stability through a case study of a railway corridor traversing geologically complex terrain, employing integrated methodologies that combine theoretical analysis, field characterization, and advanced numerical modeling to develop practical engineering solutions.

The investigation begins with the establishment of a theoretical framework for understanding slope instability by examining the fundamental physical processes governing failure mechanisms. It explores the complex interplay between geological predisposition, hydrological triggers, and anthropogenic factors that collectively influence slope performance. The analysis covers various failure modes including rotational slips in homogeneous materials, planar failures along discontinuities, and compound movements in heterogeneous formations. Particular emphasis is placed on the limitations of conventional limit equilibrium methods and the advantages of advanced numerical techniques, specifically highlighting the capabilities of finite element analysis in PLAXIS 2D for modeling nonlinear material behavior, staged construction sequences, and dynamic loading conditions.

Following the theoretical background, a detailed characterization of the study area's natural setting is presented. The geological framework includes a diapiric Triassic sequence of gypsum-clay formations that exhibit challenging geotechnical behavior due to dissolution susceptibility and weathering. Competent limestone interbeds provide structural continuity in some sectors, while extensive deposits of soft, plastic clays create zones of potential instability. The hydrogeological regime is described through seasonal groundwater fluctuations and preferential flow paths along lithological contacts. Geomorphological features such as existing landslide scars, tension cracks, and erosional patterns provide critical insights into the site’s evolutionary history and current stability conditions. This comprehensive environmental assessment forms the essential foundation for subsequent geotechnical modeling and analysis.

To support this, a systematic geotechnical investigation program was conducted to characterize subsurface conditions and provide reliable input parameters for numerical modeling. The field campaign included geophysical surveys (electrical resistivity tomography and seismic refraction) to delineate subsurface heterogeneity. Borehole drilling provided stratigraphic control and high-quality samples for laboratory tests, including triaxial shear and consolidation testing. In-situ testing encompassed vane shear testing in clay zones and rock mass characterization in limestone areas. This multi-method

approach yielded a robust dataset for constructing accurate geotechnical profiles reflective of the site's complexity.

Finally, the collected data and developed models were applied to practical engineering scenarios. Finite element analyses evaluated slope stability under natural conditions, excavated profiles, and operational loading. Special attention was given to transient hydrological effects, with coupled flow-deformation modeling used to assess pore pressure development during rainfall events. Dynamic analyses quantified the effects of train-induced vibrations on slope deformation. The risk assessment framework synthesized numerical findings with field observations to identify critical failure mechanisms and propose targeted mitigation strategies, including optimized slope geometries, stabilization measures, and monitoring protocols. The study concludes with actionable recommendations for ensuring safe railway construction and long-term operational reliability in a geologically challenging environment.

CHAPTER I:

SLOPE STABILITY CAUSALITY AND EFFECTS

Chapter I :SLOPE STABILITY CAUSALITY AND EFFECTS

I.1 Introduction

Slope stability is a central concern in geotechnical and geo-environmental engineering due to its direct impact on the safety, functionality, and longevity of both natural and man-made slopes. From hillsides and mountainous terrains to engineered slopes such as road embankments and railway cuttings, the stability of these systems governs the feasibility and security of infrastructure development. Slope failureswhether sudden like landslides and rockfalls or progressive like soil creeppose significant threats to human lives, critical infrastructure, and environmental systems (Wyllie & Mah, 2004).

A slope is considered stable when it can resist disturbing forces, such as gravity, water infiltration, seismic activity, or human interventions, without experiencing movement or collapse (Duncan & Wright, 2005). However, when these driving forces exceed the resisting forces, instability occurs in various forms, each governed by specific failure mechanisms (Sidle & Ochiai, 2006).

In large-scale civil engineering projects, particularly those involving open trench construction such as railway lines, the concern for slope stability is heightened. Excavation activities often result in steep cut slopes, which become vulnerable to both natural and anthropogenic disturbances. Slope failure in such contexts can lead to severe structural damage, disruption of service, and economic losses, in addition to posing direct threats to human safety and environmental integrity (Petley, 2012; Smith & McDonald, 1998).

The assessment and prediction of slope behavior rely on the integration of geotechnical investigations, laboratory testing, observational data, and numerical modeling techniques. These methods aim to evaluate the Factor of Safety (FoS) and to anticipate potential failure scenarios under various loading and hydrological conditions (Fell et al., 2008). Given the increasing complexity of slope systemsexacerbated by climate change, urban expansion, and land-use alterationadvanced modeling approaches are indispensable for risk assessment and mitigation.

This chapter introduces the theoretical framework necessary to understand the mechanisms, causes, and impacts of slope instability. It begins with a classification of ground movements and slope failure types, explores the geotechnical and environmental factors influencing slope behavior, discusses conventional and numerical methods of analysis, and outlines the

consequences of failure. The chapter concludes with a transition to the modeling techniques that form the core of this study's methodology.

I.2. Ground Movements and Slope Failures

I.2.1 Overview of Ground Movements

Ground movements refer to the displacement or deformation of soil and rock masses due to gravity or external forces such as rainfall, earthquakes, or human activity. These movements can vary significantly in mechanism, speed, and impact. Understanding the nature and classification of ground movements is essential in geotechnical engineering to assess slope stability and prevent hazards (Cruden & Varnes, 1996; Wyllie & Mah, 2004).

I.2.2 Main Types of Ground Movements

Ground movements are generally classified into four principal types:

I.2.2.1 Landslides

Landslides are the general downslope movement of soil, rock, or debris under the influence of gravity. They are typically triggered by rainfall, seismic activity, or human-induced changes in slope geometry (Cruden & Varnes, 1996).

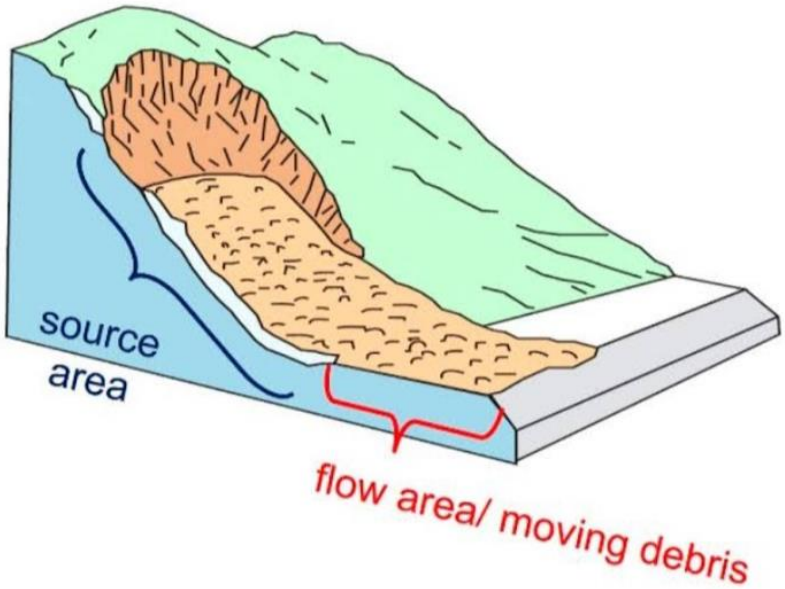


Fig I.1: Landslides movement detected using optical and radar imagery. (Peters et al ,2024).

I.2.2.2 Rockfalls

Rockfalls involve the sudden detachment and free fall of rock blocks from steep slopes or cliffs. They are usually associated with weathering, freeze-thaw cycles, or discontinuities in the rock mass (Wyllie & Mah, 2004).

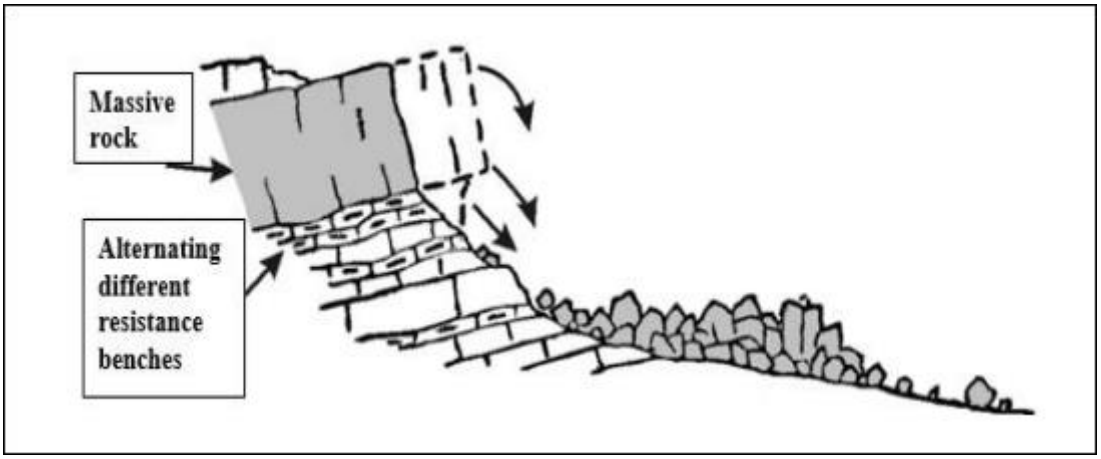


Fig I.2: Rockfall movement (Smith,J.;& Doe,A.2018).

I.2.2.3 Debris Flows

Debris flows are fast-moving mixtures of water, soil, rocks, and organic material. These flows commonly occur in mountainous terrain after intense rainfall and are considered highly destructive due to their speed and energy (Jakob &Hungr, 2005).



Fig I.3:Debri Flow movement.((Keefer, 2016)).

I.2.2.4 Soil Creep

Soil creep is a slow, imperceptible, and continuous downslope movement of soil. It occurs over long periods and is often detected by the tilting of trees, fence posts, or other surface features (Terzaghi et al., 1996).

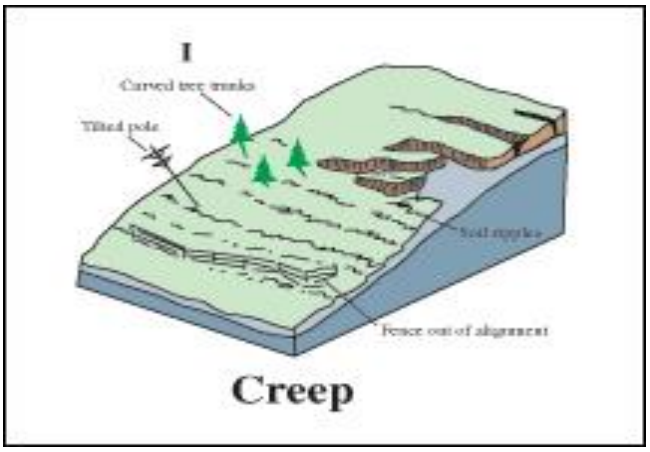


Fig I.4:Soil Creepmovement.(U.S. Geological Survey, (2004).

I.2.3 Causes of Ground Movements and Slope Failures

Ground movements and slope failures result from an imbalance between driving forces—such as gravity or external loadsand resisting forces that maintain slope stability. These imbalances may be triggered by a combination of natural and anthropogenic factors. Understanding these causes is fundamental for conducting hazard assessments and designing effective stabilization strategies (Fell et al., 2008; Duncan & Wright, 2005).

I.2.3.1 Natural Causes

a. Rainfall and Infiltration Intense or prolonged rainfall increases pore water pressure and decreases the effective stress in soil, thereby reducing its shear strength and increasing the likelihood of slope failure. This effect is particularly significant in unsaturated soils and steep terrain (Iverson, 2000).

b.Earthquakes and Seismic Vibrations Seismic activity can lead to sudden slope failure by inducing dynamic loading, shaking-induced pore pressure build-up, and in some cases, liquefaction of saturated granular soils (Seed & Idriss, 1982).

c.Weathering and Erosion Both physical and chemical weathering degrade the strength of rock and soil over time. Additionally, surface erosion caused by wind or water may remove support from the slope toe, ultimately leading to slope instability (Selby, 1993).

d.Geological Discontinuities Structural features such as joints, bedding planes, and faults serve as planes of weakness within rock masses, facilitating movement and contributing to slope failure under stress conditions (Wyllie & Mah, 2004).

I.2.3.2 Human-Induced Causes

a.Excavation and Loading Excavating slopes for construction—such as roads, railways, or foundations—alters the natural stress equilibrium and often leads to instability. Similarly, adding loads near the crest of a slope, such as buildings or heavy stockpiles, increases the driving forces acting on the slope (Duncan & Wright, 2005).

b.Deforestation and Vegetation Removal Vegetation plays a crucial role in stabilizing slopes by reinforcing the soil through root systems and reducing surface runoff. Deforestation removes this protective effect and accelerates erosion processes (Sidle & Ochiai, 2006).

c.Water Mismanagement Poor water management practices, such as inadequate drainage, leaking infrastructure, or excessive irrigation, can saturate soils and elevate pore pressures—reducing the effective strength and triggering slope movements (Fell et al., 2008).

d.Urbanization and Land Use Change Rapid urban development, especially in hilly or mountainous areas, often overlooks detailed geotechnical evaluation, thereby increasing the risk of slope instability (Glade et al., 2005).

Understanding the causes of ground movements and slope failures both natural and anthropogenic is essential for anticipating hazardous conditions and implementing mitigation measures. In practice, these causes often interact, creating complex failure scenarios that demand integrated analysis and modeling.

I.2.4 Engineering Hazards Associated with Ground Movements

Ground movements pose significant engineering hazards that threaten both human safety and structural integrity. These hazards manifest in various forms depending on the type, magnitude, and velocity of the movement. Rapid events such as landslides and debris flows can cause sudden infrastructure collapse, bury transportation routes, and damage buildings and utilities. Slower processes like soil creep lead to progressive deformation, resulting in cracks in foundations, misalignment of walls, and long-term structural deterioration. In geotechnical engineering, these effects are particularly critical for roads, railways, dams, and slope-adjacent constructions. Additionally, differential settlements caused by localized subsidence or lateral movement can compromise load-bearing capacity and serviceability (Duncan & Wright, 2005; Wyllie & Mah, 2004; Abramson et al., 2002). Understanding these

hazards enables engineers to implement appropriate mitigation measures, such as slope reinforcement, drainage control, or early warning systems.

I.2.5 Engineering Hazards Associated with Ground Movements

Ground movements and slope failures represent serious engineering hazards that compromise the integrity and safety of infrastructure and built environments. These phenomena can lead to structural damage, service interruptions, and even catastrophic failures with loss of life. The complexity of these hazards arises from the interaction between geotechnical conditions, loading factors, and environmental triggers (Lee et al., 2018).

Key engineering hazards include:

- **Structural Damage and Deformation:** Movements can cause cracks, tilting, and eventual failure of retaining walls, foundations, bridges, and tunnels (Zhou et al., 2021). For instance, differential settlement caused by slope creep can progressively undermine structural stability.
- **Transportation Disruptions:** Roads, railways, and pipelines traversing or adjacent to unstable slopes face risks of blockage, collapse, or distortion, which lead to costly repairs and delays (Hussain et al., 2019).
- **Sudden Slope Failures:** Landslides or debris flows may occur abruptly, damaging property and endangering human lives downstream (Fan et al., 2020). Early warning systems are critical but often challenged by unpredictable triggering factors.
- **Environmental and Socioeconomic Impacts:** Sedimentation from slope erosion affects water quality and aquatic habitats, while infrastructure damage disrupts communities and economies (Li et al., 2022).

Case studies in mountainous regions and urbanizing areas show how inadequate slope assessment and poor drainage design exacerbate these hazards (Singh & Kumar, 2021). Consequently, modern engineering practice emphasizes integrated hazard assessment, real-time monitoring, and adaptive management to mitigate risks associated with ground movements (Carrara et al., 2019).

This section highlights the critical need for comprehensive geotechnical investigations and slope stability analyses in infrastructure projects involving open trenches or cut slopes, especially for railway alignments.

I.3. Types of Slope Failures

I.3.1 Classificationof Slope Failures by Material Type

The classification of slope failures based on the material type is essential for understanding the failure mechanisms and designing effective mitigation measures. Slope failures can be broadly divided into soil slope failures and rock slope failures, reflecting the fundamental differences in material properties, mechanical behavior, and failure processes.

I.3.1.1 Soil Slope Failures

Soil slope failures occur in unconsolidated or weakly cemented earth materials such as clays, silts, sands, and weathered deposits. The stability of soil slopes is primarily governed by the soil's shear strength, pore water pressure, slope geometry, and external factors such as rainfall and human activities (Duncan & Wright, 2005).

I.3.1.1.1Rotational Slides

Rotational slides are characterized by a curved slip surface, typically circular or spoon-shaped, resulting in a rotational movement of the sliding mass. These slides commonly develop in homogeneous, cohesive soils with low permeability, where shear failure occurs along a well-defined concave surface. The mechanism involves soil mass rotating downward and outward, often causing slump blocks and scarps (Duncan & Wright, 2005; Kramer, 1996).

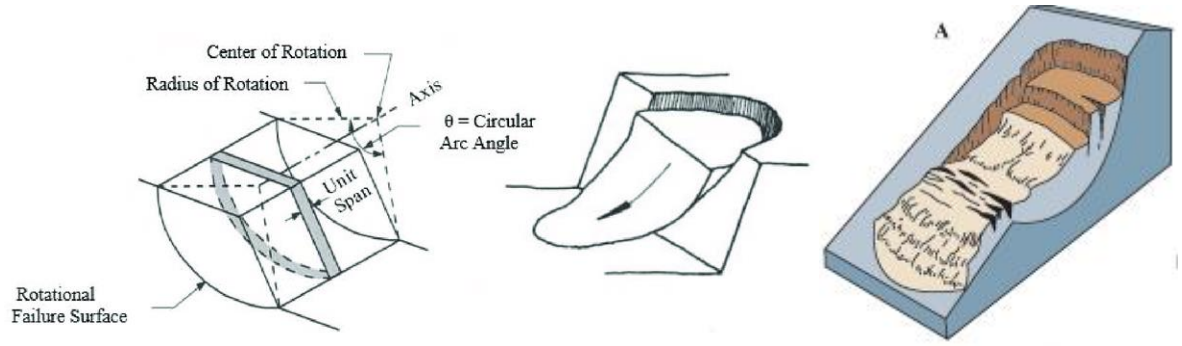


Fig I.5: Circular Failure (Kolapo et al., 2022/U.S. Geological Survey, (2004)).

I.3.1.1.2 Translational Slides

Translational slides involve movement along a planar or gently undulating slip surface, generally in stratified or fissured soils. The sliding mass tends to remain relatively intact, moving downslope without rotation. These slides frequently occur in layered soils or where weak bedding planes or discontinuities exist. External triggers include rainfall infiltration and seismic shaking (Das & Sobhan, 2017; Waltham, 2009).

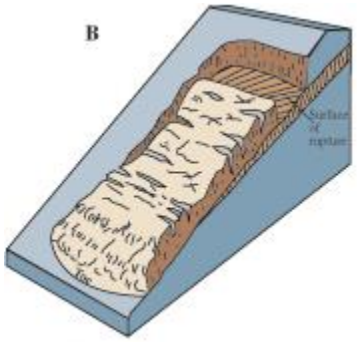


Fig I.6: Translational slide. (U.S. Geological Survey, (2004)).

I.3.1.1.3 Flows (Earthflows and Mudflows)

Flows are fluid-like movements of highly saturated soil masses that have lost internal cohesion. Earthflows typically involve slow to moderate movement of fine-grained materials like silts and clays, while mudflows are more rapid and consist of a mixture of water and soil debris. These failures often follow intense or prolonged rainfall events, leading to rapid mass wasting (Iverson, 2005; Kramer, 1996).



Fig I.7: Earthflow. (U.S. Geological Survey, 2004)).

I.3.1.1.4 Lateral Spreads

Lateral spreads occur when saturated soils lose shear strength due to liquefaction or strain-softening, causing large blocks of soil to move horizontally. These failures are commonly triggered by seismic events and are characterized by extensive horizontal displacement with minimal vertical subsidence (Idriss & Boulanger, 2008; Kramer, 1996).



Fig I.8:Lateral Spreads Niigata, Japan 1964 (U.S. Geological Survey (2023)).

I.3.1.1.5 Complex Failures

Complex failures represent combinations of two or more failure mechanisms, such as an initial rotational slide followed by a flow or lateral spread. These are typical in heterogeneous slopes with varying soil properties and multiple triggering factors, complicating the failure process (Cruden & Varnes, 1996).

I.3.1.2 Rock Slope Failures

Rock slope failures occur when blocks or masses of rock detach and move due to structural weaknesses like joints, bedding planes, or faults. These failures are commonly classified into rockfalls, topples, planar slides, wedge, circular, and bucking failures:

I.3.1.2.1 Rockfall

Rockfalls are sudden and rapid movements of detached rock fragments down a steep slope or cliff. These failures occur when weathering or structural weaknesses cause pieces to break off and fall freely under gravity. (Prasad Rayudu, 1997)

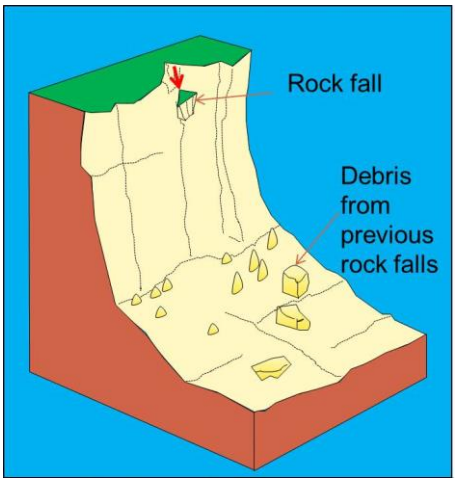


Fig I.9: Typical Rockfall Diagram. (InspiredPencil (2023)).

I.3.1.2.2Toppling

Toppling failures involve the forward rotation of rock blocks around a pivot point, usually occurring in rock slopes with steeply dipping discontinuities. The blocks rotate forward and detach due to gravity and structural instability. (Wyllie & Mah, 2004)

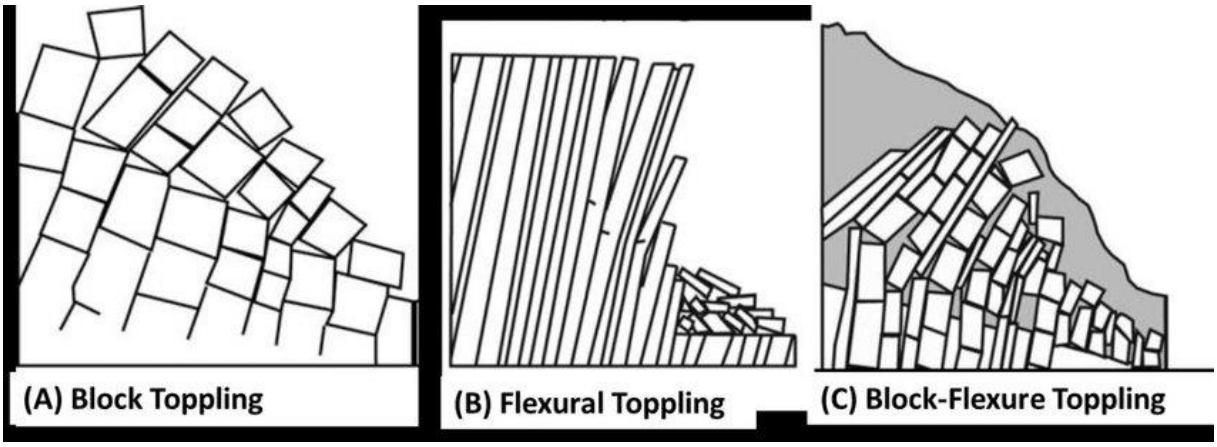


Fig I.10: Toppling Failure Schematic. (Wyllie, D. C., & Mah, C. W. (2004)).

I.3.1.2.3Planar Slide

Planar slides occur along a single planar surface of weakness such as bedding planes or joints. The rock mass slides downslope along this plane, typically in rock slopes with uniform layering. (Goodman, 1989)



Fig I.11: Planar Slide. (Acharya et al., 2017).

I.3.1.2.4 Wedge Failure

Wedge failures occur when two or more discontinuity planes intersect, creating a wedge-shaped block that can slide out of the rock mass. This type of failure depends heavily on the orientation of the intersecting planes relative to the slope face. (Hoek & Bray, 1981)

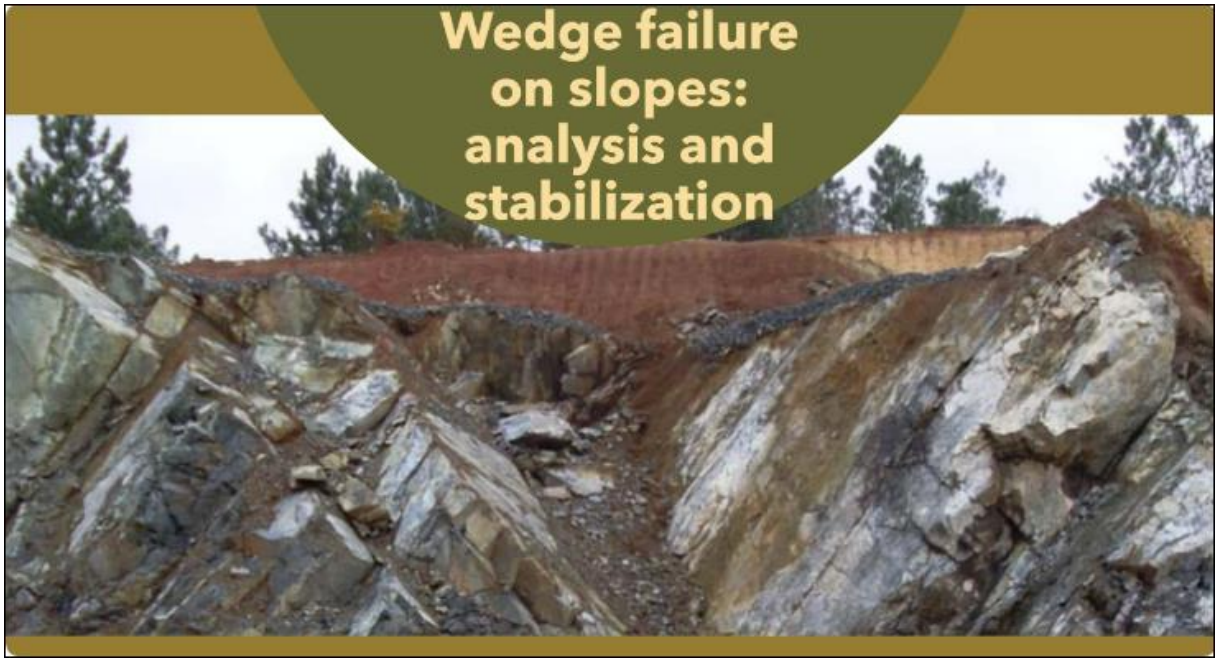


Fig I.12:Wedge Failure (CGI International Geotechnocal Center. (2024)) .

I.3.1.2.5Buckling Failure

Buckling failure occurs when rock layers are compressed and bend, leading to sudden collapse. This failure mode is common in layered rock slopes under compressive stress.

Reference: (Goodman, 1989)

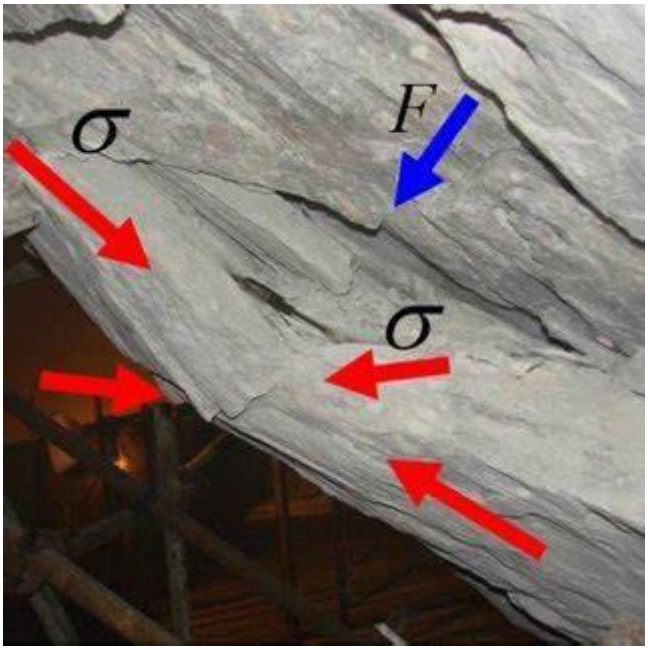


Fig I.13: Buckling Failure Schematic. (Cui et al., 2023).

I.3.2 Classification by Mechanism

Slope failures can be classified based on the dominant mechanism of movement. This classification aids in understanding the physical behavior of the failed mass, its interaction with the environment, and the appropriate mitigation approach. According to established geotechnical literature, five primary mechanisms are recognized: slides, flows, falls, topples, and creep (Varnes, 1978; Duncan & Wright, 2005; Das, 2010).

I.3.2.1 Slides

Slides involve the downslope movement of material along a distinct shear surface. They are subdivided into:

Rotational Slides: Occur when movement happens along a curved, concave-upward slip surface. These slides are common in homogeneous cohesive soils and exhibit a backward rotation of the sliding mass.

Translational Slides: Characterized by movement along a relatively planar surface, typically affecting stratified soil or rock layers. These slides are generally faster and more dangerous due to minimal internal deformation (Duncan & Wright, 2005; Das, 2010).

I.3.2.2 Flows

Flows resemble fluid movement, often involving saturated soils or debris. They occur when shear stresses exceed the soil strength in loose, fine-grained materials, particularly after heavy precipitation.

Debris Flows, Earth Flows, and Mudflows are subtypes based on the material composition. Flows are highly mobile and can cause severe destruction, especially in mountainous terrain (Iverson, 2000; Jakob &Hungr, 2005).

I.3.2.3 Falls

Falls involve the sudden detachment and free-fall of material from a steep face. Rockfalls are the most typical form, initiated by weathering, thermal expansion, or seismic activity. The material falls, bounces, or rolls downslope (Hoek & Bray, 1981; Wyllie & Mah, 2004).

I.3.2.4 Topples

Toppling is the forward rotation of blocks or columns of rock about a pivot point, often controlled by steeply dipping discontinuities. It may precede or evolve into a fall or slide depending on the geometry and loading (Hoek & Bray, 1981).

I.3.2.5 Creep

Creep is the slow, imperceptible downslope movement of soil or weak rock. It occurs due to repeated cycles of

expansion-contraction (e.g., freeze-thaw, wet-dry). Despite its low velocity, creep can severely damage infrastructure over time (Terzaghi, Peck &Mesri, 1996).

I.3.3 Classification by Movement Speed

An essential aspect of understanding slope failures lies in evaluating the rate at which movements occur, as it directly influences the associated risk level and the urgency of intervention. Therefore, slope failures are commonly categorized based on movement speed into slow and rapid types, each presenting distinct mechanisms, implications, and monitoring requirements (Duncan et al., 2014; Cornforth, 2005).

I.3.3.1 Slow Failures

Slow slope failures, commonly referred to as creep or progressive deformation, develop over long durations—ranging from months to several years—without sudden surface disruption. These failures predominantly occur in cohesive soils or weathered rock masses, where continuous strain accumulates under relatively stable or slowly varying stress conditions (Duncan et al., 2014; Wyllie & Mah, 2004). While their progression is gradual, they can induce long-term structural damage to infrastructure such as roads, pipelines, and retaining systems.

Such movements often go unnoticed until their effects become severe. Monitoring techniques such as inclinometers, extensometers, and surface markers are essential for early detection, especially when failure thresholds like excess pore water pressure or critical strain levels are approached (Chen & Lee, 2004; Sassa &Canuti, 2009). If unaddressed, slow failures may evolve into sudden catastrophic events.

I.3.3.2 Rapid Failures

Rapid failures are characterized by abrupt displacement occurring within seconds or minutes, typically involving high material velocity and significant volume. These include rockfalls, debris flows, and translational landslides triggered by intense precipitation, seismic activity, or anthropogenic excavation (Cornforth, 2005; Giani, 1992).

The velocities range from several meters per minute to over 100 km/h, depending on terrain slope, material saturation, and fragmentation (Wyllie & Mah, 2004). Loose, cohesionless soils and heavily jointed or fractured rocks are particularly susceptible. Due to their sudden and destructive nature, rapid failures demand robust preventive measures such as slope flattening, rockfall barriers, toe buttresses, and controlled drainage systems.

I.3.3.3 Engineering Implications

Understanding failure velocity is fundamental to engineering design and risk mitigation. Slow movements can often be managed with long-term interventions such as geosynthetic reinforcements, staged excavation, or drainage improvement. In contrast, rapid failures necessitate real-time monitoring systems, emergency protocols, and permanent structural defenses (Duncan et al., 2014; Wyllie & Mah, 2004). The classification by speed also informs monitoring strategies: while slow slopes allow periodic surveillance, rapid zones demand continuous observation and fast-response systems.

I.4 Causes of Slope Failures

Understanding the causes of slope failures is essential in geotechnical and geological engineering, as it enables accurate risk assessment and the implementation of effective mitigation strategies. Slope instability arises from a combination of natural and anthropogenic (human-induced) factors, often acting simultaneously or interactively.

I.4.1 Natural Causes

I.4.1.1 Heavy Rainfall

Intense and prolonged rainfall is one of the most common natural triggers of slope failure. Water infiltration reduces soil suction and increases pore water pressure, thereby decreasing

the effective stress and shear strength of slope materials (Cornforth, 2005; Duncan et al., 2014). Saturated soils, particularly in loose or clayey materials, may experience a loss of cohesion, leading to shallow landslides and debris flows.



Fig I.14:Bus trapped in floodwaters during heavy rainfall in Haldwani, India.(Kumari, 2022).

I.4.1.2 Seismic Activity

Earthquakes introduce sudden dynamic loading to slopes, often reducing interparticle friction and cohesion in both soil and rock masses. This seismic shaking may induce liquefaction in saturated granular soils or destabilize rock slopes through crack propagation and block detachment (Giani, 1992; Sassa &Canuti, 2009).

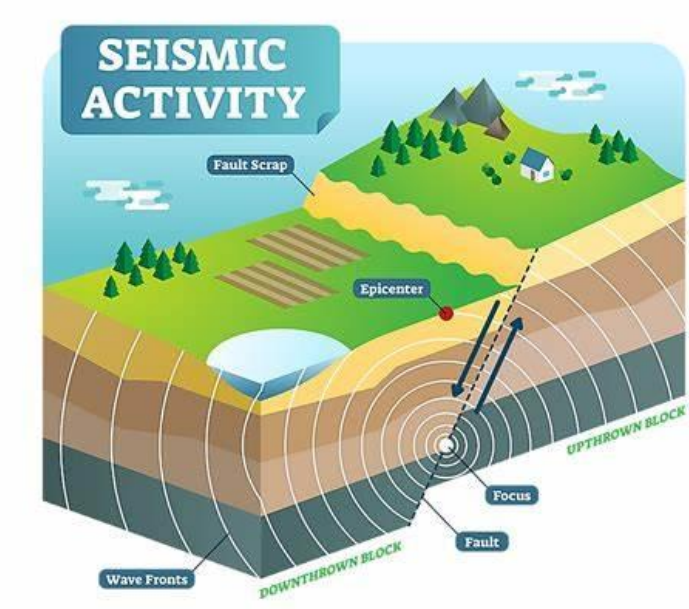


Fig I.15: Effects of Seismic Activity on Urban Areas. (Schematics Inkage, 2024).

I.4.1.3 Groundwater Fluctuations

Variations in groundwater levels due to seasonal changes or hydrological disturbances can drastically alter slope stability. Rising groundwater tables increase pore pressure and reduce effective stress, particularly in fine-grained soils and weathered rock formations (Duncan et

al., 2014). Conversely, a rapid drop in water levels may leave unsupported slope faces vulnerable to collapse.

I.4.1.4 Geological Structure

Slope geometry, bedding orientation, discontinuities (e.g., joints, faults, fractures), and lithological heterogeneity significantly influence failure mechanisms. Planes of weakness, such as stratification parallel to the slope face or highly fractured zones, often act as slip surfaces during failure (Giani, 1992; Wyllie & Mah, 2004).

I.4.2 Human-Induced Causes

I.4.2.1 Uncontrolled Excavation

Cutting into slopes for roadways, mining, or construction without proper engineering design can disturb the natural stress distribution and compromise slope stability. Removing toe support or oversteepening the slope face accelerates failure risks (Chen & Lee, 2004).

I.4.2.2 Overloading

Imposing excessive loads from buildings, storage, or embankments increases the driving forces acting on the slope. If not adequately accounted for in the design, such loads may surpass the shear strength of the materials, resulting in failure (Duncan et al., 2014).

I.4.2.3 Water Leakage and Poor Drainage

Unmanaged drainage systems, leaking pipelines, or irrigation can introduce uncontrolled water into slopes. This infiltration often leads to softening of clays, buildup of pore pressure, and internal erosion (Cornforth, 2005).

I.4.2.4 Urban Expansion and Vegetation Removal

Rapid urbanization often entails the removal of vegetation cover, which otherwise contributes to slope stability through root reinforcement and evapotranspiration. Bare slopes are more prone to erosion, runoff concentration, and shallow landslides, especially during storms (Wyllie & Mah, 2004).

I.4.3 Comparative Analysis of Natural and Human-Induced Causes

Table prepared by the author based on the synthesis of data and analyses from Cornforth (2005), Duncan et al. (2014), Giani (1992), and other referenced geotechnical literature.

Cause Category	Natural Causes	Human-Induced Causes
Triggering Factor	Heavy rainfall, earthquakes, groundwater fluctuations, geological structures (layer dip, faults)	Unplanned excavation, overload, water leakage, urban expansion, vegetation removal
	Increase in pore water	Disturbance of stress

Effect on Stability	pressure, seismic shaking, slope weakening	equilibrium, increase in load, water infiltration
Common Locations	Steep natural slopes, mountainous areas, fault zones	Construction sites, urban areas, cut slopes, embankments
Typical Examples	Rainfall-induced landslides, earthquake-triggered failures	Slope collapse due to excavation, failures from uncontrolled water drainage
Mitigation Measures	Drainage control, reforestation, seismic design	Proper excavation planning, load control, water management, land use regulation

TableI.1: Comparison between Natural and Human-Induced Causes of Slope Failures.

I.5 Parameters Influencing Slope Stability and Factor of Safety

I.5.1 Factor of Safety (FoS)

The Factor of Safety (FoS) is a numerical measure used to express the stability of a slope. It is defined as the ratio of resisting forces (shear strength of the soil or rock) to the driving forces (those promoting failure, such as gravity or water pressure):

FoS = (Shear Strength of Soil) / (Shear Stress acting on the failure surface)

I.5.1.1FoS for Soil Slopes

The stability of soil slopes is often evaluated using the Mohr-Coulomb failure criterion. The Factor of Safety (FoS) (Craig, 2004) can be expressed as:

$$FoS = (c' \cdot L + N' \cdot \tan(\varphi')) / T$$

Where:

• FoS: Factor of Safety – the ratio of resisting to driving forces.

• c′: Effective cohesion of the soil.

• L: Length of the potential slip surface.

• N′: Effective normal force acting on the slip surface.

• φ′: Effective internal friction angle of the soil.

• T: Driving shear force along the slip surface.

A FoS> 1 indicates a stable slope, while FoS< 1 signals potential failure. Design codes typically require FoS between 1.3 and 1.5 under static conditions (Budhu, 2011).

I.5.1.2FoS for Rock Slopes – Planar Sliding

For rock slopes exhibiting planar sliding failure, the FoS is calculated using the following expression:

$FoS = [c \cdot A + (W \cdot \cos(\beta) - u \cdot A) \cdot \tan(\varphi)] / (W \cdot \sin(\beta))$ (Hoek & Bray, 1981)Where:

• c: Cohesion along the failure plane.

• A: Area of the sliding surface.

• W: Weight of the sliding block.

• β: Dip angle of the failure plane.

• u: Pore water pressure acting on the plane.

• φ: Friction angle along the discontinuity.

• FoS: Factor of Safety – calculated based on force equilibrium.

FoS for Rock Slopes – Wedge Failure

In wedge-type rock failures, where two discontinuities intersect, the FoS can be calculated using either:

$FoS = [c \cdot A + (N - u \cdot A) \cdot \tan(\varphi)] / T$ or $FoS = R / D$ (Wyllie & Mah, 2004)Where:

• c: Cohesion along the failure surface.

• A: Area of the failure plane.

• N: Total normal force acting on the base.

• u: Pore water pressure.

• φ: Friction angle on the sliding surface.

• T: Driving shear force.

• R: Total resisting force.

• D: Total driving force.

For rock slopes, a Factor of Safety (FoS) greater than 1.0 generally indicates stability, whereas values below 1.0 suggest potential failure. However, due to the complex and discontinuous nature of rock masses, acceptable FoS thresholds may vary depending on the failure mechanism involvedsuch as planar, wedge, or toppling—and the specific design conditions. Design guidelines typically recommend FoS values ranging between 1.2 and 1.5 under static loading scenarios (Wyllie & Mah, 2004).

In general, the Factor of Safety is influenced by both material properties and external factors such as groundwater, loading, and geometry. It is commonly evaluated using analytical techniques like Limit Equilibrium Methods or advanced numerical simulations to ensure reliable and safe slope designs (Duncan & Wright, 2005; Wyllie & Mah, 2004).

I.5.2 Key Geotechnical Parameters Affecting Slope Stability

In slope stability assessments, several fundamental soil and rock properties must be evaluated to accurately estimate shear strength and predict failure conditions. These geotechnical parameters form the basis for both analytical and numerical modeling, influencing the Factor of Safety (FoS) and overall slope behavior. The most influential parameters are detailed below.

I.5.2.1 Cohesion (c)

Cohesion is the component of shear strength that exists independently of the applied normal stress. It arises from electrochemical attractions, cementation, or bonding between soil or rock particlesespecially in fine-grained materials such as clay.(Das, 2015)

Role in Slope Stability:

- Contributes to resisting forces in the slope.
- Essential for analyzing cohesive soils, particularly under short-term undrained conditions.
- Incorporated directly into the Mohr-Coulomb failure criterion.
- Higher cohesion values increase slope stability, especially when normal stress is low (e.g., near-surface failures). (Terzaghi et al., 1996)

I.5.2.2 Friction Angle (φ)

The internal friction angle (φ) represents shear strength due to interparticle friction and interlocking among soil grains. It measures material’s ability to resist sliding along internal surfaces.

Role in Slope Stability:

- Influences mobilized shear strength when normal stress is applied.
- Dominant in granular soils such as sand, gravel, and rock fill.
- Higher φ values enhance resistance against sliding, especially in dry, drained conditions.
- Expressed in Mohr-Coulomb equation

$$\tau = c + \sigma' \cdot \tan(\varphi') \quad \text{(Terzaghi et al., 1996)}$$

Where:

• τ: Shear strength (kPa)

• c: Cohesion (kPa)

• σ′: Effective normal stress (kPa)

• φ′: Effective internal friction angle (degrees)

I.5.2.3 Unit Weight (γ)

Unit weight (γ) is weight per unit volume of soil or rock, reflecting material density and moisture content. Typically measured in kN/m³.(Coduto et al., 2011)

Role in Slope Stability:

- Affects driving forces (gravity acting downslope) and resisting forces (normal stress on slip surface).
- Heavier soils may increase driving shear stress, especially on steep slopes.
- Accurate γ values essential in calculating slope self-weight, overburden pressure, and seepage forces.
- Varies with dry, moist, and saturated conditions; water content must be considered.

(Coduto et al., 201)

I.5.2.4 Pore Water Pressure (u)

Pore water pressure is pressure exerted by groundwater within soil or rock voids, directly influencing effective stress and shear strength.(Freeze & Cherry, 1979)

Role in Slope Stability:

- Reduces effective stress:

$$\sigma' = \sigma - u \quad \text{(Terzaghi, 1936)}$$

Where:

• σ′: Effective stress (kPa)
• σ: Total stress (kPa)
• u: Pore water pressure (kPa)

This principle is fundamental in geotechnical engineering and plays a critical role in slope stability, bearing capacity, and consolidation behavior.

- Time-dependent pore pressure changes critical in transient stability (storms, rapid drawdown)(Freeze & Cherry, 1979)

I.5.2.5 Effective Stress (σ′)

Effective stress is total stress minus pore water pressure, carried by soil skeleton, governing mechanical behavior and strength.(Terzaghi, 1943)

Role in Slope Stability:

- Governs all strength and deformation behavior, not total stress σ.
- Used in Mohr-Coulomb strength formula.
- Influenced by pore pressure, loading, and groundwater flow changes.
- Decrease in σ′ due to elevated u causes shear strength drop and possible instability.

(Terzaghi, 1943)

I.6 Methods of slope failure analysis

Analyzing slope stability is a core component of geotechnical engineering, aimed at evaluating the potential for ground failure and ensuring the safety of natural and engineered slopes. Over the decades, a range of analytical approaches has been developed to assess the risk of slope failure. These methods primarily focus on calculating the Factor of Safety (FS), identifying the most probable failure surface, and quantifying the stability margin under different loading and boundary conditions (Duncan & Wright, 2005; Budhu, 2011).

The various methods employed can be broadly classified into three categories: Limit Equilibrium Methods (LEM), Numerical Methods (such as Finite Element Method (FEM) and Finite Difference Method (FDM)), and Graphical (Abacus-based) Methods. Each of these

approaches differs in terms of theoretical assumptions, level of accuracy, data input requirements, and suitability for complex geometries or soil behaviors (Griffiths & Lane, 1999; Smith & Griffiths, 2004).

I.6.1 Limit Equilibrium Methods (LEM)

Limit equilibrium methods assume that slope failure occurs along a defined slip surface, and equilibrium conditions are used to compute the factor of safety (Duncan & Wright, 2005).

I.6.1.1 Method of Slices

This widely used method involves dividing the potential sliding mass into vertical slices.

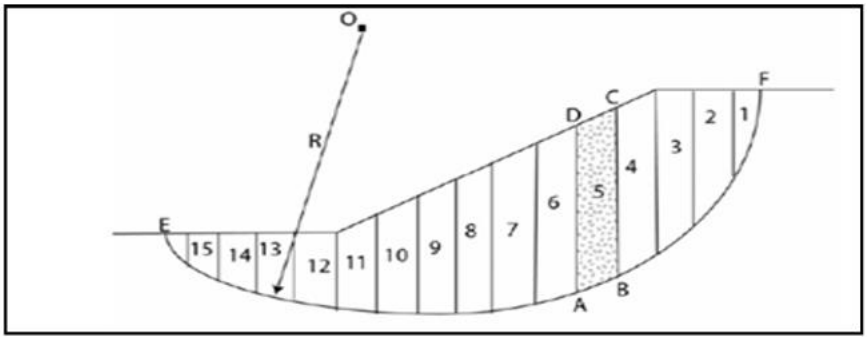


Fig I.16:Description of slicing with fracture surface.

Forces acting on each slice (weight, inter-slice forces, normal and shear reactions) are analyzed to compute FS. The general equation is:

$FS = \sum(c' \cdot l + (N - u \cdot l)\tan\varphi') / \sum(W \cdot \sin\alpha)$

Where:

- c' = effective cohesion
- φ' = effective internal friction angle
- N = effective normal force
- u = pore water pressure
- l = length of slice base
- α = base inclination angle
- W = slice weight

(Duncan & Wright, 2005)

I.6.1.2 Fellenius Method (1936)

Also known as the Swedish or Ordinary Method of Slices. It assumes a circular failure surface and neglects inter-slice forces. FS is calculated based on moment equilibrium around the center of the circular arc (Duncan & Wright, 2005).

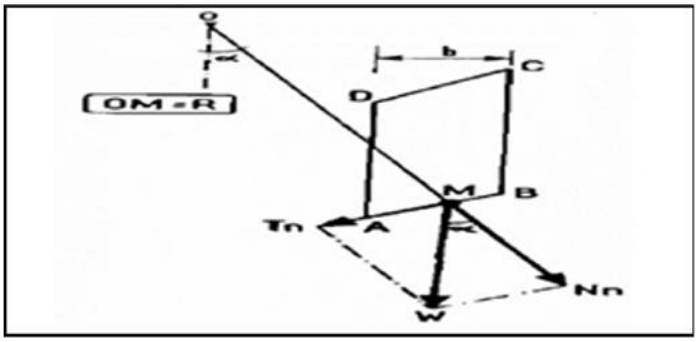


Figure I.17 The forces acting on a surface according to FELLENIUS

Rn= Cn × AB + Nn × tan ϕn AB=In=bn /cosαn

Rn= Cn × AB + Wn × cosαn × tan ϕnNn=Wn×cosαn

The sum of the maximum resisting moments is written as:

$\sum_1^m (Ci \frac{bn}{\cos \alpha n} + Wn \cos \alpha n tan\ \phi i)$ Tn = Wn sinαn

m is the number of slices C, ϕ are the mechanical characteristics in the layer in which arc AB is located the driving moment due to Tn is equal to Tn × R

$$\boldsymbol{Fs = \frac{\sum_1^m (\ Ci\ \frac{bn}{Cos\, \alpha n} + Wn\ Cos \alpha n\ \ tan \phi n\ )}{\sum_1^m Wn\ Sin\, \alpha n}}$$

I.6.1.3 Bishop Simplified Method (1955)

The simplified Bishop method also relies on a circular failure surface and the equilibrium of moments. It neglects horizontal inter-slice forces and requires an iterative approach. General formula for the safety factor (FS):

FS = ∑[c'·l + (W - u·l)·tanφ'·cosα] / ∑(W·sinα)
(Duncan & Wright, 2005)

This method requires successive iterations, starting with an initial estimate of the FS (often that of Fellenius).

I.6.1.4 Janbu Method (1956)

Allows non-circular slip surfaces and considers horizontal and vertical force equilibrium (but not moments). The calculated FS is corrected by an empirical factor f_0:

$FS = f_0 \cdot$ (Resisting Forces / Driving Forces)

(Janbu, 1956)

I.6.2 Numerical Methods (e.g., Finite Element Method - FEM)

Numerical methods provide a more realistic and detailed analysis by modeling the stress-strain behavior of soil. FEM simulates continuous media by discretizing the soil into finite elements and solving governing equations (e.g., Mohr-Coulomb model) numerically. It allows:

- Non-linear material behavior
- Complex geometries
- Time-dependent analysis (e.g., rainfall infiltration)

FEM does not yield an explicit FS but estimates slope performance through shear strain and deformation analysis (Smith & Griffiths, 2004).

I.6.3 Graphical Methods (Abacus-Based Methods)

Graphical methods estimate the FS using design charts based on empirical data and theoretical analyses. These charts relate FS to parameters such as:

- Slope height (H)
- Slope angle (β)
- Unit weight (γ)
- Cohesion (c)
- Friction angle (φ)

(Taylor, 1937; Biarez, as cited in Budhu, 2010)

I.6.3.1 Taylor-Biarez Chart

Developed by Taylor (1937) and refined by Biarez, this graphical tool estimates FS based on slope geometry and soil properties, especially for cohesive-frictional soils. It is simple and useful for preliminary design (Taylor, 1937; Budhu, 2010).

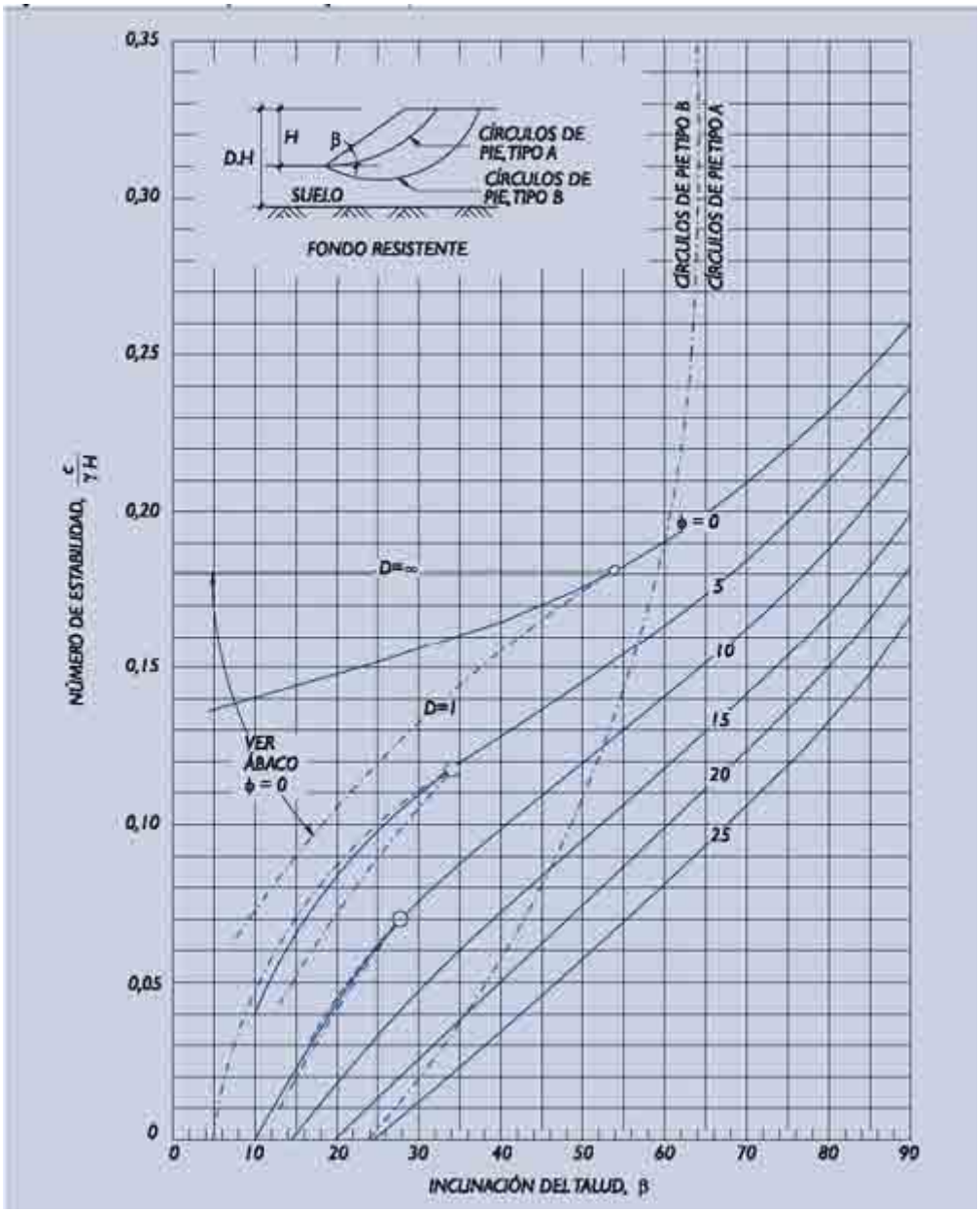


Figure I.18: Taylor's slope stability charts for homogeneous slopes under total stress conditions. (notasingenierocivil.blogspot.com, 2011; based on Taylor, 1937)

These methods are implemented in commercial software such as GeoStudio (SLOPE/W), Slide2, and STABL.

I.6.2 Numerical Methods

Numerical methods offer a more comprehensive and realistic approach to slope stability analysis by explicitly modeling stress-strain relationships, material nonlinearity, groundwater effects, and complex geometries. These methods are indispensable for projects where traditional Limit Equilibrium Methods (LEM) are insufficientparticularly when dealing with heterogeneous soil profiles, seismic loading, or time-dependent phenomena.

I.6.2.1 Finite Element Method (FEM)

The Finite Element Method divides the slope into a mesh of discrete elements and numerically solves the governing equations of equilibrium using constitutive models that describe material behavior. FEM can simulate:

- Stress and strain distributions.
- Pore water pressure variations.
- Progressive failure mechanisms.
- Seepage and consolidation effects.

This method is particularly suited for analyzing complex boundary conditions, unsaturated soils, seismic activity, and long-term slope behavior.

Software Example: In this study, FEM was implemented using PLAXIS 2D 2024, a powerful finite element software specialized for geotechnical problems. PLAXIS allows for staged construction modeling, advanced soil models (e.g., Mohr-Coulomb, Hardening Soil), and coupled flow-deformation analyses.

Advantages:

Realistic modeling of soil behavior.

Capable of predicting deformations and failure zones.

Handles complex geometries and loading scenarios.

Limitations:

Requires detailed soil parameters and calibration.

Computationally intensive.

Demands engineering judgment for mesh generation and model setup.

I.6.2.2 Finite Difference Method (FDM)

The Finite Difference Method approximates differential equations governing equilibrium by discretizing the soil domain into a grid and applying finite difference formulations. It uses time-stepping algorithms to simulate the evolution of stress, strain, and velocity fields over time.

Software: FDM is typically used in tools such as FLAC and FLAC3D, which are effective in simulating dynamic loading (e.g., earthquakes), large deformation, and plastic flow.

Advantages:

High adaptability to large strain and post-failure behavior.

Strong performance in dynamic and transient problems.

Suitable for problems involving strong plasticity or creep.

Limitations:

Simplified geometry handling compared to FEM.

Needs fine meshing for accuracy.

Sensitive to time step and boundary conditions.

I.6.3 Comparison between Limit Equilibrium Method (LEM) and Finite Element Method (FEM)

Aspect	Limit Equilibrium Method (LEM)	Finite Element Method (FEM)
Basic Principle	Based on static force and/or moment equilibrium of potential failure surfaces.	Based on discretization of the soil mass and solving continuum mechanics equations numerically.
Failure Surface	Pre-assumed (e.g., circular, non-circular); analysis searches for the critical one.	Not required; failure develops naturally based on stress–strain behavior.
Stress–Strain Relationship	Not considered (rigid–plastic assumption); does not model progressive failure.	Fully integrated; simulates stress–strain behavior and deformation response.
Pore Water Pressure	Can be incorporated using simplified models (e.g., Ru or pore pressure coefficients).	Allows for transient and steady-state seepage analysis; integrates pore pressures

		directly.
Inter-slice Forces	Often neglected or simplified (especially in simplified Bishop, Janbu methods).	Fully captured through stress tensor computation.
Soil Behavior	Requires input of shear strength parameters (c', φ'); no deformation prediction.	Requires full constitutive models (Mohr-Coulomb, Hardening Soil, etc.); predicts deformations.
Result	Factor of Safety (FoS) for assumed failure mechanism.	FoS + full stress, strain, displacement, plastic zones, and deformation fields.

TableI.2: Comparison between Limit Equilibrium Method (LEM) and Finite Element Method (FEM) (Duncan, J. M., & Wright, S. G. (2005).

I.6.4 Summary and Recommendations

In summary, the choice between analytical and numerical methods for slope stability analysis depends on the complexity of the slope conditions, the required level of precision, and the available data (Duncan & Wright, 2005). Limit Equilibrium Methods (LEM) remain practical and efficient for routine evaluations, preliminary design, and back-analysis of past failures (Duncan & Wright, 2005). However, their assumptions, particularly the predefined slip surface and rigid body behavior, limit their reliability in complex or heterogeneous settings (Griffiths & Lane, 1999).

On the other hand, Numerical Methods such as the Finite Element Method (FEM) and Finite Difference Method (FDM) offer significant advantages in modeling stress redistribution, progressive failure, groundwater interaction, and dynamic loading (Griffiths & Lane, 1999; Smith & Griffiths, 2004). Their ability to simulate real soil behavior and deformation makes them indispensable for high-risk projects and advanced research (Duncan & Wright, 2005).

In the present study, FEM was employed using PLAXIS 2D 2024 to model the slope behavior under site-specific geological and geotechnical conditions. This approach allowed for a detailed investigation of potential failure mechanisms and provided critical insights that would not be possible through conventional LEM alone (Duncan & Wright, 2005).

It is therefore recommended that LEM be used as a first-level screening tool, while numerical modeling should be adopted for final design validation, safety evaluation under dynamic conditions, and analysis of non-conventional slopes (Griffiths & Lane, 1999; Smith & Griffiths, 2004).

I.7 Importance of Modeling Slope Stability

Modeling slope stability is essential in geotechnical engineering as it offers a systematic framework to predict, analyze, and mitigate slope failures under diverse conditions. Geological materials and external forces such as water infiltration, seismic activity, and construction loads create complex scenarios that require precise analysis. Numerical modeling methods like the Finite Element Method (FEM) and Limit Equilibrium Method (LEM) simulate stress distribution, deformation, and failure mechanisms accurately (Duncan & Wright, 2005). This capability supports optimized design of stabilization measures, reliable risk assessment, and cost-effective decision-making. Without robust modeling, slopes risk being either over-engineeredresulting in unnecessary expense—or under-designed, which can lead to catastrophic failures.

I.8Consquences of Slope Failures

Slope failures are among the most hazardous geological events due to their sudden occurrence and devastating consequences. These failures can result in a wide range of human, economic, environmental, and social impacts depending on their scale, location, and the presence of infrastructure and communities in the affected area (Dikau et al., 1996).

I.8.1 Human Losses

Landslides can cause direct fatalities or injuries when they occur in populated areas. Entire communities may be buried under debris, especially in mountainous regions during intense rainfall or seismic events (Petley, 2012). Rescue operations are often difficult due to access constraints and continued instability.

I8.2 Economic and Infrastructural Losses

Slope failures can destroy roads, railways, buildings, and utilities. The cost of reconstruction and mitigation is often very high. In developing countries, where infrastructure investment is limited, these losses can be particularly severe (Dikau et al., 1996).

I.8.3 Environmental Impact

Landslides disturb natural vegetation, alter river courses, and lead to sedimentation in water bodies. This can degrade aquatic ecosystems, increase flood risk downstream, and contribute to long-term land degradation (Crosta et al., 2008).

I.8.4 Socioeconomic Impact

Beyond direct damage, landslides can displace families, disrupt livelihoods, and isolate communities. In rural areas, access to food, water, education, and healthcare can be severely

affected. The psychological toll and loss of cultural heritage are also significant (UNDRR, 2020).



Fig I.19: Structural damage caused by a man-made slope failure (Kolapo et al., 2022).

I.9Conclusion:

Slope failures represent a significant geotechnical challenge due to their complexity and potentially severe impacts on human safety, infrastructure, and the environment. Understanding the types of slope failures, their causes, and the key geotechnical parameters influencing stability is essential for effective risk management. Analytical and numerical methods, particularly Limit Equilibrium Methods (LEM) and Finite Element Methods (FEM), provide complementary tools for slope stability analysis, each with distinct advantages and limitations.

This study underlines the importance of integrating advanced modeling techniques with thorough field investigations to accurately predict slope behavior and design appropriate mitigation measures. Considering the consequences of slope failures, from human casualties to economic losses, prioritizing comprehensive analysis and proactive engineering solutions is

critical to safeguarding lives and assets. Future work should focus on enhancing modeling accuracy and incorporating real-time monitoring to improve early warning and response systems.

CHAPTER II: GEOLOGICAL,HYDROGEOLOGICAL AND GEOMORPHOLOGICAL CONDITION.

II.1.Introduction:

TheBekkaria region, situated in Tebessa Province of northeastern Algeria near the Algerian-Tunisian border, presents a unique convergence of geological, geomorphological, and climatic conditions that pose significant challenges for infrastructure development, particularly slope stability along critical railway projects (ANESRIF, 2022). This chapter synthesizes the multidisciplinary context of the area, integrating regional and local geographic, geological, tectonic, hydrogeological, and climatological frameworks to establish a foundation for assessing geotechnical risks.

Nestled within the Eastern High Plains (*Hauts PlateauxOrientaux*), the study area is characterized by a semi-arid climate (ONM, 2020), rugged topography, and complex geological structures shaped by Alpine orogenic processes (Vila, 1980; Bougherira et al., 2021). The juxtaposition of elevated plateaus, dissected hills, and karstified carbonate formations creates a dynamic landscape where natural processes such as erosion, tectonic activity, and groundwater fluctuations interact with anthropogenic interventions (Hadji et al., 2017; ANRH, 2018). Of particular focus is the Jebel Bekkaria mountain zone, where the proposed railway alignment traverses steep gradients and geotechnically unstable terrain (IGN, 2021; DTP Tébessa, 2020).

The region's geological history, spanning from Triassic evaporites to Quaternary alluvial deposits (Durozoy, 1956; Dubourdieu, 1956), reveals a stratigraphic record marked by tectonic upheavals, diapirism (Ghrieb, 2011), and sedimentary cycles (BRGM, 2000). These features are compounded by active geomorphological processes, including karstification and gully erosion, which are exacerbated by irregular but intense precipitation patterns (Legrioui et al., 2017; ONM, 2020). Hydrogeologically, shallow aquifers (e.g., the P1 aquifer) exhibit pronounced seasonal water table fluctuations (Ghrieb, 2010; Mrad et al., 2018), directly influencing pore pressures in slope-forming materials. Climatically, the semi-arid regime—with hot, dry summers and episodic heavy rainfall (Climate-Data.org, Tutiempo.net)—further amplifies the risk of slope destabilization through rapid infiltration and transient perched water tables (Fell & Fry, 2007; Boukerboub, 2020).

This chapter aims to provide an interdisciplinary synthesis of these factors, drawing on geological maps (Figs. 1–6; IGN, 2021; BRGM, 2000), stratigraphic data (Fig. 5; Durozoy,

1956; Smith et al., 2018), hydrogeological charts (Fig. 7; ANRH, 2018), and climatological trends (Fig. 8; ONM, 2020). By contextualizing the interplay of tectonic structures (Kowalski et al., 1997; Vila, 1980), lithological variability, climatic extremes, and hydrological dynamics, the analysis underscores the challenges inherent to slope stability in Bekkaria. Such insights are critical for informing engineering designs, risk mitigation strategies (Achour et al., 2012), and sustainable infrastructure planning in this geologically sensitive region (CRAAG, 2020; ANESRIF, 2022).

II.2. Location of the Study Area:

II.2.1.Regional Geographic Setting:

The study area, situated within the Tébessa Province (wilaya) of eastern Algeria, lies adjacent to the Algerian-Tunisian border. Geomorphologically, the region constitutes a collapsed basin surrounded by mountainous terrain with elevations ranging from 800 m to 1,600 m. Administratively, the province is bounded by Souk Ahras Province to the north, Oued Province to the south, the Algerian-Tunisian international border to the east, and the provinces of Oum El-Bouaghi and Khenchela to the west (Fig. 1). Spanning 21,000 km²**,**Tébessa Province is home to an estimated population of 700,000 inhabitants.

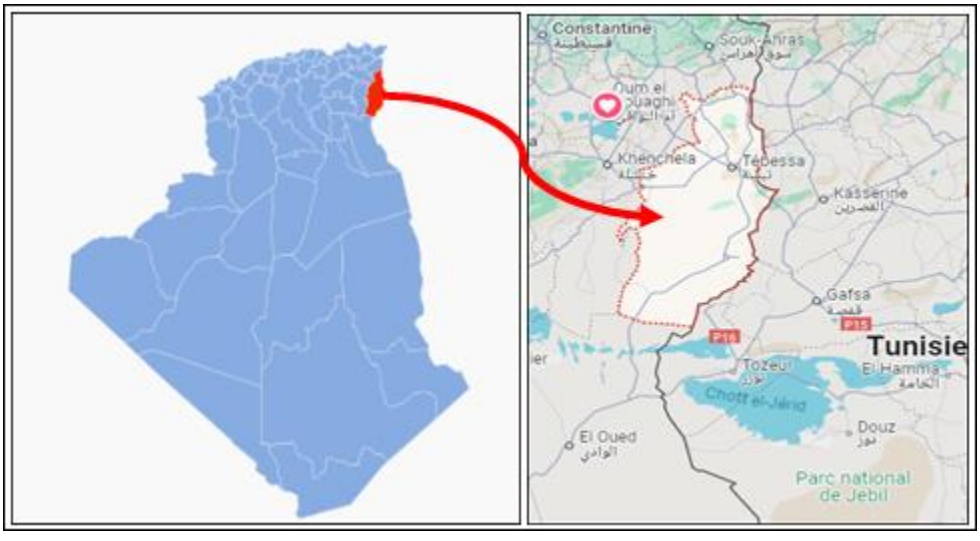


Fig II.1: Regional Geographic Location (Tebessa)(Google earth) .

II.2.2 Local Geographic Setting:

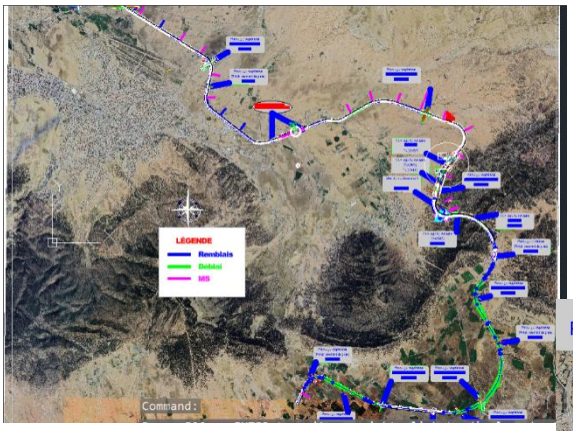
The study area is located in the commune of Bekkaria, situated in the eastern part of Tébessa Province, northeastern Algeria, near the Algerian-Tunisian border (ONS, 2020). Bekkaria lies approximately 20 km southeast of Tébessa city, and is part of the Eastern High Plains (Hauts PlateauxOrientaux) (ANRH, 2018).

Topographically, the region is characterized by moderately rugged terrain, with elevations varying between 800 m and 1200 m, and is surrounded by low hills and shallow valleys (IGN, 2021). The area has a semi-arid climate, marked by hot summers, cold winters, and relativellow annual precipitation (ONM, 2020).

Administratively, Bekkaria is bordered by:Tébessa municipality to the northwest, El Ma El Abiod to the south,and lies close to the Tunisian border to the east (Ministère de l'Intérieur, 2021).

The commune is accessible via National Road N10, which connects it to major regional centers (DTP Tébessa, 2020). The surrounding environment is predominantly agricultural and rural, with scattered settlements and limited urban infrastructure (ONS, 2020).

The project site is located within the mountainous zone east of Bekkaria, where the new railway alignment climbs Jebel Bekkaria. This topographical setting presents significant geotechnical challenges, making it a critical location for slope stability assessment (ANESRIF, 2022).



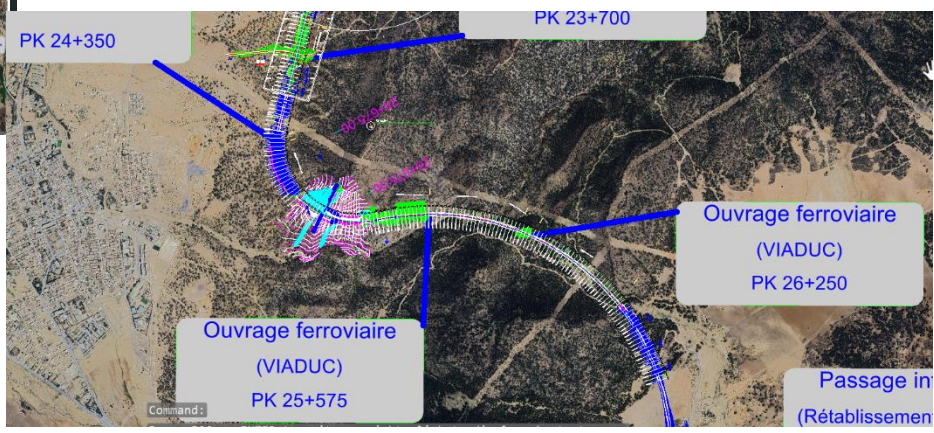


Fig II.2:Location of the railway crossing the study area and the project zone.

II.3. Geomorphological Setting of the Bekkaria Region (Tébessa, NE Algeria):

The Bekkaria region, located in the northeastern part of the Tébessa province near the Algerian-Tunisian border, belongs to the Eastern High Plains geomorphological unit. It is characterized by a heterogeneous relief shaped by the interplay of tectonic activity, lithological variability, and semi-arid climatic conditions (ANRH, 2018; ONM, 2020).

The topography consists of elevated plateaus, moderately dissected hills, and narrow valleys. The southern sector is marked by the presence of the Djebel Doukan, which reaches altitudes above 1600 meters, providing a significant contrast with the surrounding plains (\~770 m) (IGN, 2021). This altitudinal variation plays a key role in slope dynamics and water runoff.

Lithologically, the region is dominated by Upper Cretaceous and Paleogene carbonate formations (limestones and dolomites), prone to karstification. Karst landforms such as dolines, sinkholes, and underground drainage networks are common, particularly in the massive limestone blocks. These features influence groundwater flow and increase susceptibility to collapse or instability in certain zones (Hadji et al., 2017).

Structurally, the area lies within the Atlas Tellian domain, affected by Alpine compressive tectonics. Faulting and folding have contributed to the orientation and fragmentation of the terrain, controlling both surface hydrology and sediment redistribution (Bougherira et al., 2021).

The climatic context is semi-arid with irregular but intense precipitation events. These conditions favor active geomorphic processes such as gully erosion, sheet wash, and slope failures. In addition, the combination of steep gradients, weathered materials, and anthropogenic pressure (agriculture and road cuts) enhances geomorphological hazards (ONM, 2020; ANRH, 2018).

II.4. Geological Context

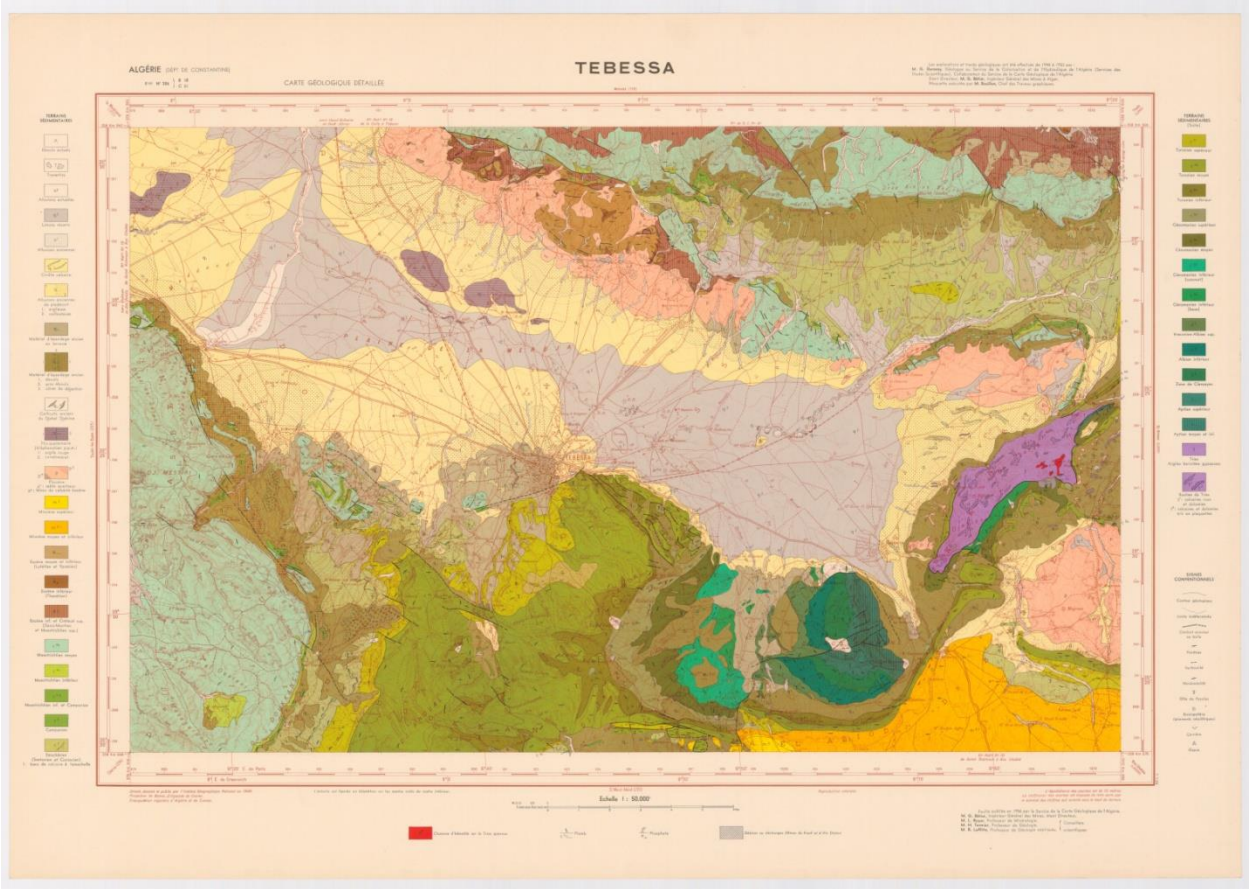
II.4.1. RegionalGeologie:

The Tébessa region is part of the autochthonous North Aurelian structure (AurèsNememcha) of the Saharan Atlas (Durozoy 1956; Blès 1969; Vila 1974; Kowalski et al. 1997). The geological map (Fig03) at a scale of 1:50,000 shows the distribution and structure of the different lithologies in the region. It is essentially composed of:

- A diapiric Triassic formation dislocating overlying formations at the level of Djebel Djebissa.

- Carbonate formations represented by significant layers of marly limestone and marl of Cretaceous to Tertiary age. Some of these formations can be observed at the edges of the Tébessa plain. - A large Mio-Plio-Quaternary alluvial deposit which lies unconformably on the preceding formations and thus forms the filling of the depression, currently the plain. This formation is observed especially at the foot of the rugged terrain.

II.4.2Geological map:



FigII.3: Geological Map of Tebessa.

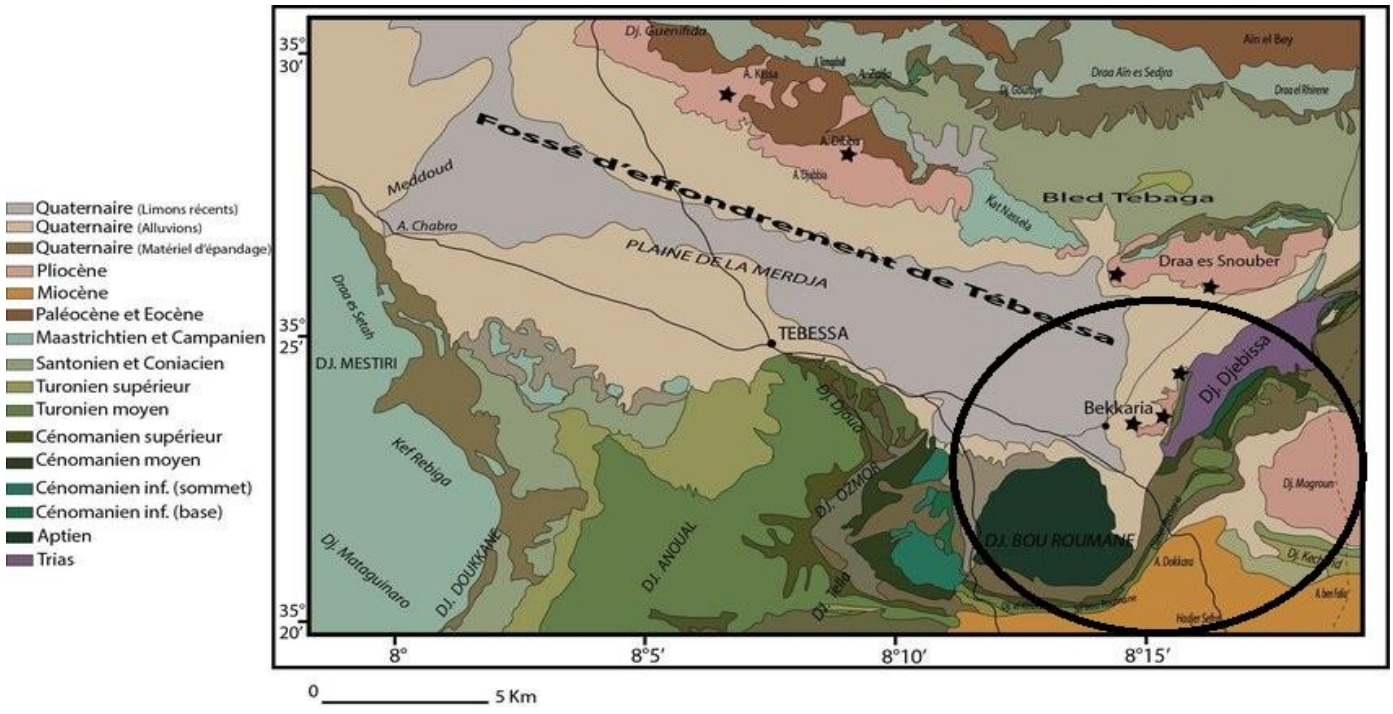
II.4.3 Local Geology

The Bekkaria region is situated within the Tellian domain of the Atlas Mountains, which forms an integral part of the Alpine orogenic belt resulting from Cenozoic compressional tectonic phases (Maáfat& Slimani, 2005). The geological structure of the area is shaped by a complex interplay of tectonic activity and lithological diversity.

The local stratigraphy is predominantly composed of carbonate formations, specifically limestones and dolomites, dating from the Upper Cretaceous to the Paleogene period. These formations are particularly prone to karstification processes, which have led to the widespread development of typical karst landforms such as sinkholes, dolines, and subterranean drainage

systems (Legrioui et al., 2017). Such features significantly influence both surface morphology and the behavior of groundwater flow within the region.

Post-Cretaceous tectonic activity has resulted in a network of folds and thrust faults that structurally control the geometry of aquifers and dictate the dynamics of groundwater movement (Maáfat& Slimani, 2005). These structural deformations have also played a critical role in fragmenting the carbonate units and enhancing their permeability.



FigII.04: Geological Map of Study Area (Bekkaria).

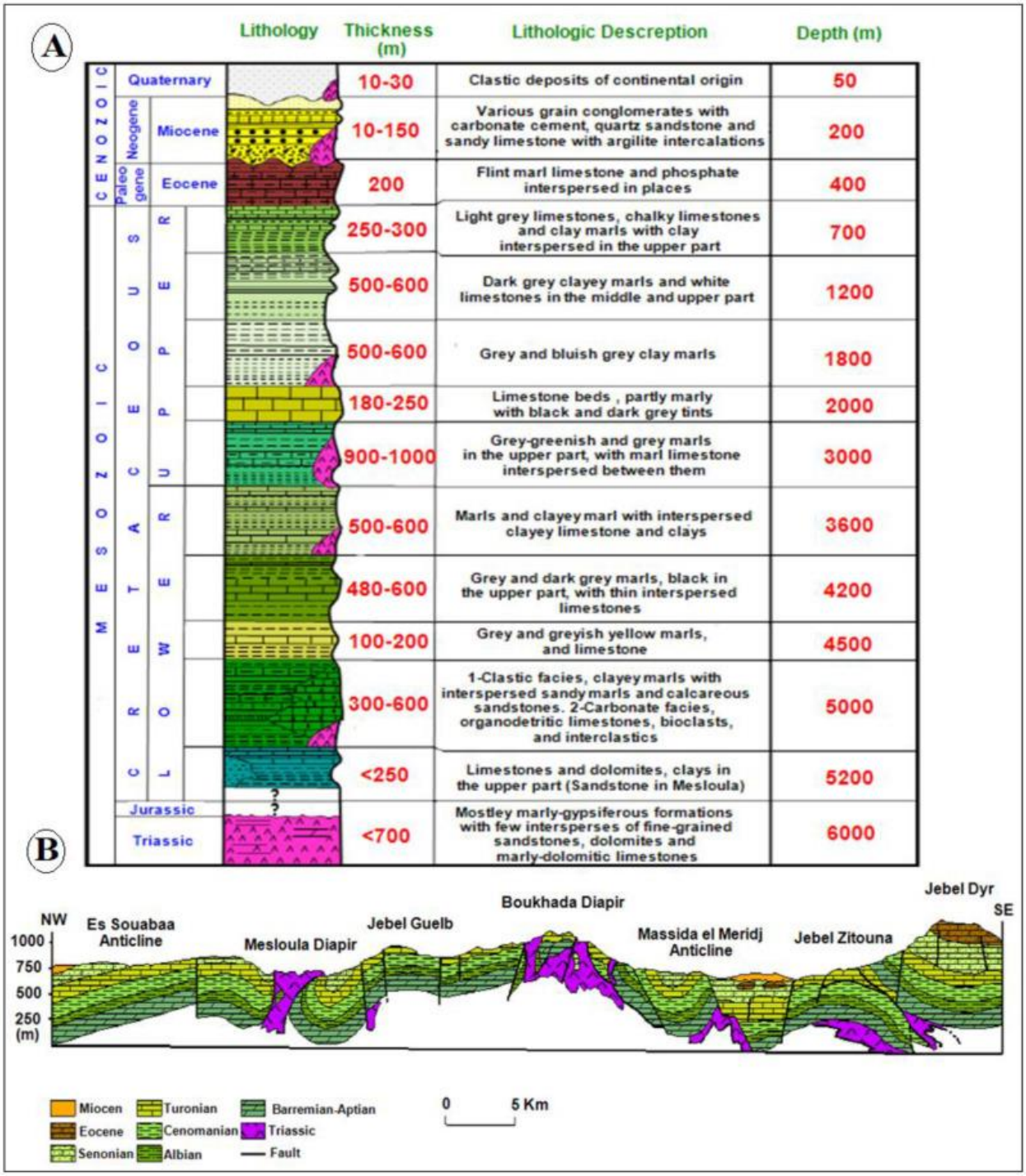
II.5. Stratigraphic Summary of the Tébessa

The stratigraphic sequence of the Tébessa region presents a complete geological history ranging from the Triassic to the Quaternary. This succession reflects a dynamic interplay of depositional environments, tectonic activity, and diachronous erosional processes that have shaped the geological framework.*(Durozoy, 1956)*

Lithology varies from clayey-gypsiferous-dolomitic facies in the Triassic to marl-limestone alternations in the Cretaceous, phosphatic micritic limestones in the Paleogene, and continental

detrital deposits in the Neogene and Quaternary. The absence of Jurassic deposits and the presence of diapiric structures emphasize significant tectonic movements.*(Dubourdieu, 1956)*

This synthesis is based on foundational works by Durozoy (1956) and Dubourdieu (1956), supplemented by recent studies on the paleogeographic evolution and tectono-sedimentary dynamics of the eastern Saharan Atlas.*(BRGM, 2000; Smith et al., 2018)*



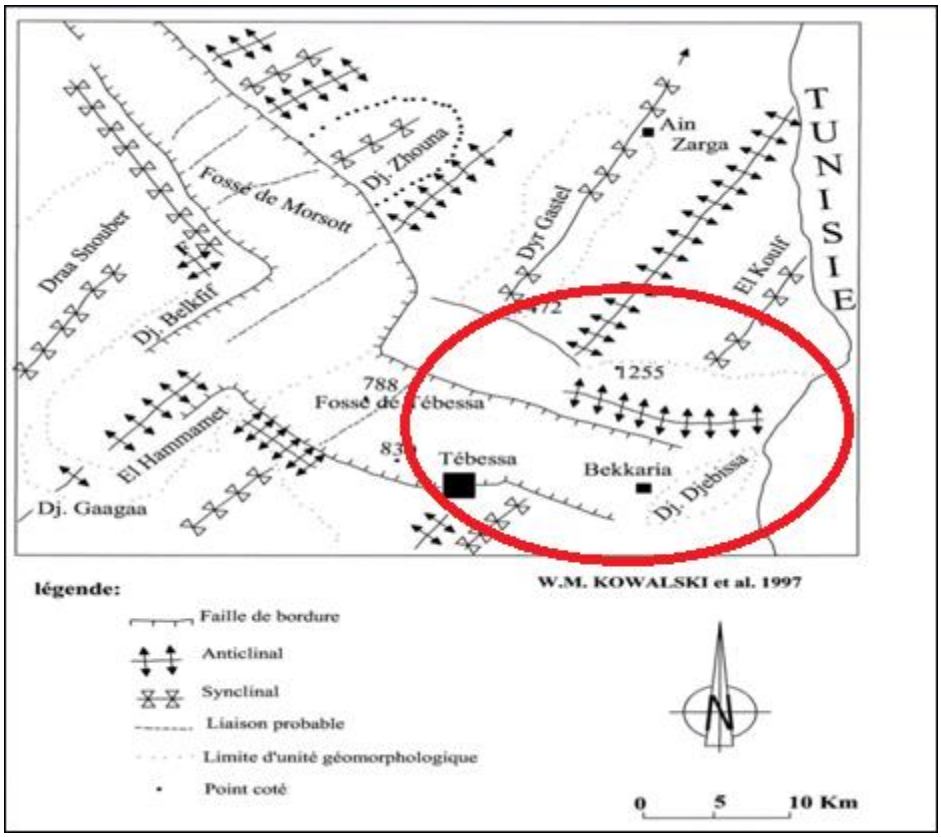
FigII.05: Complete Stratigraphic Column of the Tebessa Region: Lithostratigraphic Sequence from the Triassic to the Quaternary(Durozoy, J. P. (1956)).

Synthetic stratigraphic column of the Tébessa region.

(From: Dubourdieu 1956; David 1956; Madre 1969; Fleury 1969)

II.6. Tectonic Features in the Tebessa Region:

The tectonic map of the Tebessa region shows that it is located within the Eastern Saharan Atlas tectonic belt, which is the result of the collision between the African and Eurasian plates, leading to the formation of complex geological structures (Vila, 1980). One of the most prominent features of these structures are the folds, which are bends in the rock layers formed by lateral compressional forces. These folds are clearly visible in the folds of Jebel Meria and Wadi al-Rabi, which extend from northwest to southeast, where they take the shape of both anticlinal (upward) and synclinal (downward) folds (Ghrieb, 2011).



FigII.06. Tectonic sketch of the Tébessa region (Kowalski et al. 1997)

The region is also characterized by fault systems, which are fractures in the Earth's crust accompanied by the movement of rock blocks. These faults reflect different stages of extensional and compressional tectonic activity. Among the most significant of these faults is the Merssout-Tébessa fault, which cuts the structure almost vertically in a N–S direction and is considered one of the geomechanically active faults in the region (Mebrouk, 2014). Additionally, diapirism is a

distinctive structural feature, where rock masses, often salt-rich from the Triassic period, rise through the overlying layers. A clear example of this is the Djebel Djebissa diapir, which is composed of evaporites such as gypsum and halite that penetrate the younger rocks due to density differences (Ghrieb, 2011).

In terms of basins, the region contains several grabens, such as the Merssout-Tébessa-Yokous graben, which is a longitudinal depression resulting from extensional forces during the Miocene. It is surrounded by faults that define its structural boundaries and has since been filled with Pliocene deposits (Zerrouki et al., 2013). These deposits are now used as indicators of the crustal evolution in the region and help identify stages of later tectonic activity.

The geological foundation of Tébessa primarily dates back to the Mesozoic era, consisting of limestone and marl layers from the Upper Cretaceous period. These layers form the base upon which the Neogene rocks were deposited (Perrodon, 1957). As for the more recent geological periods, post-Miocene structures—such as the recent compressional folds—demonstrate that tectonic activity in the region has not ceased but has continued in new forms, affecting land stability, as seen in the Wadi al-Rabi area (Vila, 1980).

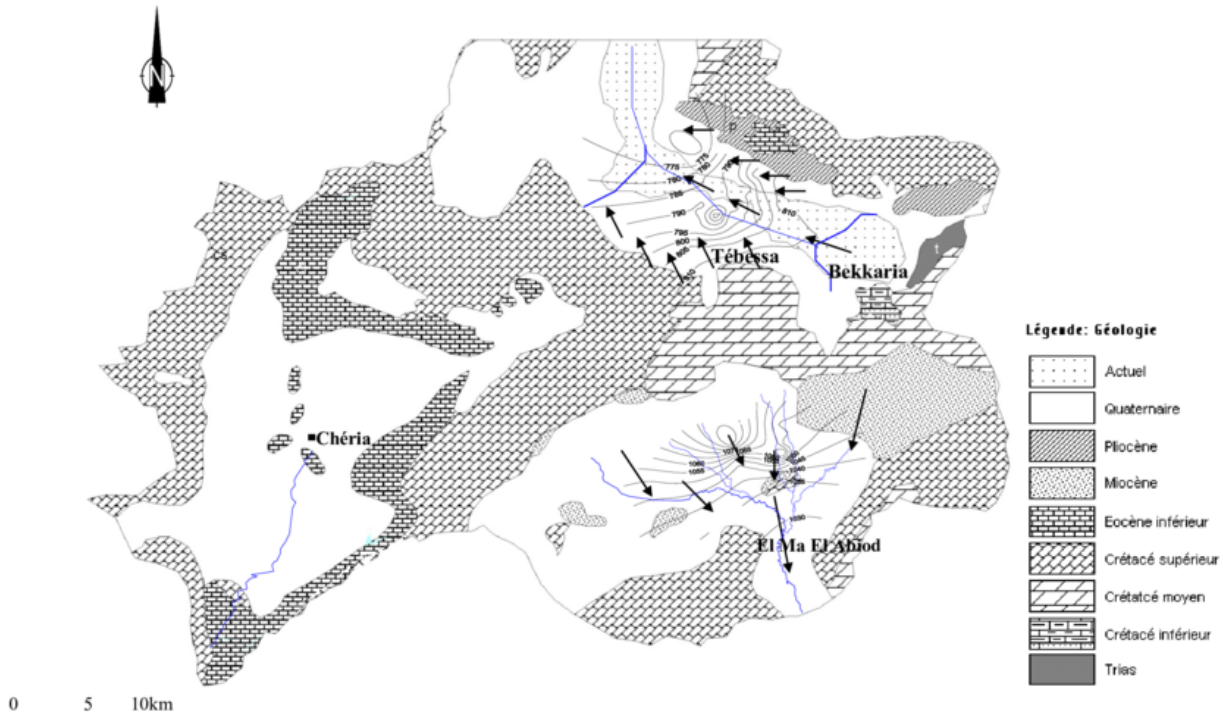
Although Tébessa is not classified as a high seismic hazard area, seismic activity in the region requires caution. Studies indicate low but noticeable seismic activity in areas like Bakkaria, necessitating consideration of the tectonic structure in geotechnical projects (CRAAG, 2020).

II.7. Hydrogeological and Climatological Conditions of the Bekkaria Region:

The Bekkaria area sits atop a multilayered aquifer system whose shallow horizon (P1) exhibits pronounced seasonal water-table fluctuations that directly affect slope stability in open trenches (Lallemand & Roux, 1989; Gogu &Dassargues, 1998). The climate is semi-arid (BSh), with hot, dry summers and mild, wetter winters; annual rainfall averages 300–500 mm, concentrated between October and March (Climate-Charts.com; ClimateKnowledgePortal), and mean temperatures range from 5 °C in winter to 35 °C in summer (Weatherspark; Tutiempo). These hydro-climatic dynamics drive pore-pressure changes in clayey soils, reducing shear strength during wet periods and thus increasing the risk of slope failure.

II.7.1. Piezometry and Groundwater Levels

- The **P1 aquifer** in the Bekkaria area is unconfined and closely follows seasonal precipitation, showing wet-season rises up to 4 m in piezometric head (Ghrieb, 2010).
- Two deeper, confined horizons (P2 and P3) lie beneath impermeable marl and limestone; over the last decade their heads have declined by 1–2 m due to abstraction and reduced recharge (Drias et al., 2022).
- Transient perched water tables often form within clayey layers above P1 during heavy rains, elevating pore pressures and weakening trench sidewalls (Mrad et al., 2018).



FigII. 07 :Carte-piezometrique-El-Ma-El-Abiod-et-Tebessa-janv-2009

II.7.2. Climate Classification, Precipitation, and Temperature

- According to Köppen–Geiger, the region is **BSh** (hot semi-arid steppe) with >30 °C summers and mild winters (Nomadseason, n.d.).
- **Annual rainfall** averages **300–500 mm**, ~70% falling October–March; interannual variability is high owing to orographic effects from the Tell Atlas (Climate-Charts.com, n.d.).

- **Mean monthly temperatures** range from ~5 °C in January to ~35 °C in July, with daily lows near 1 °C and highs above 33 °C in peak summer (Climate-Charts.com, n.d.).

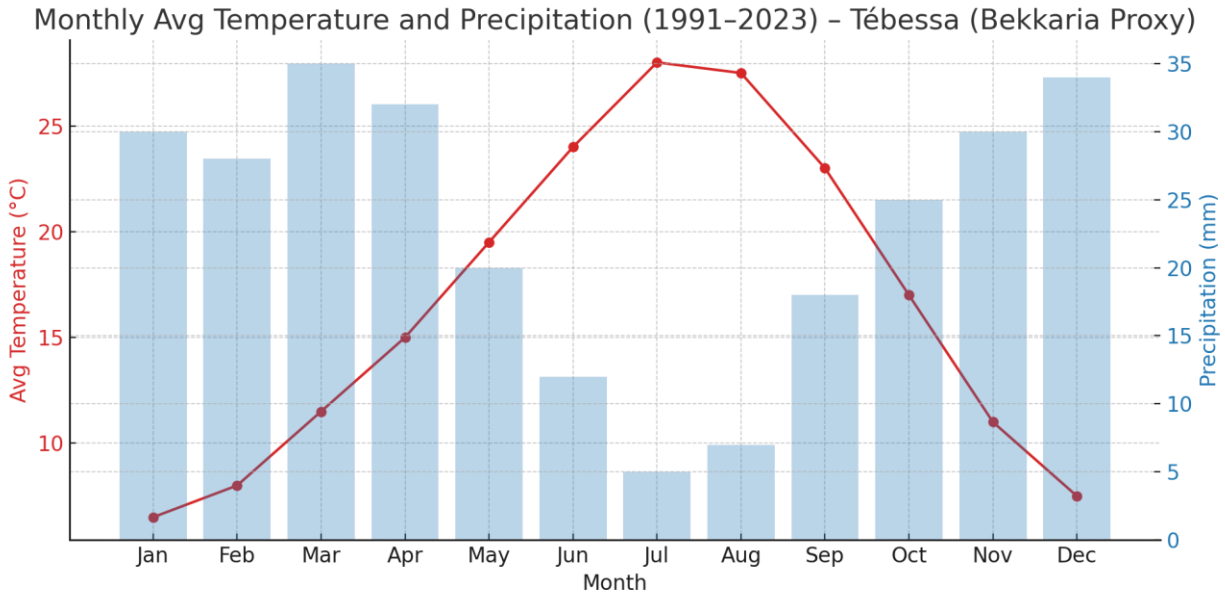


Figure II.8: Monthly Average Temperature and Precipitation (1991–2023) – Tébessa (Climate Proxy for Bekkaria) (Adapted from Climate-Data.org, Tutiempo.net, and Climate-Charts.com)

II.7.3. Implications for Open-Trench Slope Stability

- Seasonal P1 rises increase pore pressures in clayey marls, reducing effective stress and thus shear strength, which can trigger circular or planar failures in trench walls (Fell & Fry, 2007).
- Sporadic heavy storms produce rapid infiltration and perched tables above impermeable beds, causing sudden loss of support at slope faces (Boukerboub, 2020).
- Effective mitigation requires drainage measures (e.g., relief wells, horizontal drains) and continuous piezometric monitoring to track transient water-table behavior (Achour et al., 2012).

II.7.4. Impact of These Factors on Slope Stability

- **Pore water pressure increase**: Heavy rainfall and flooding saturate the soil, increasing pore pressure and reducing shear strength, which promotes soil and rock slides.

- **Fluctuating groundwater levels**: Post-winter rise weakens the p_1 layer and increases short-term slide risk; summer drops cause cracking and internal erosion.
- **Contamination and soil property alteration**: Pollution from iron mine runoff alters soil chemistry and reduces cohesion, decreasing slope stability.
- **Future changes**: Climate models predict recurring intense rainfall and extreme droughts, necessitating improved runoff management and slope drainage designs.

II.7.5. Recommendations for Data Collection and Stability Management

1. **Rainfall and groundwater monitoring stations**: Expand the local station network and integrate real-time flow and level monitoring systems.
2. **Periodic geotechnical surveys**: Assess soil saturation and pore pressure during critical seasons.
3. **Wadi management**: Construct drains and retention structures along main wadis (Kebir and Djebissa) to reduce flow velocity and erosion.
4. **Pollution monitoring**: Regularly test wadi and groundwater chemistry to assess effects on soil behavior.
5. **Modeling and prediction**:

II.8Conclution:

The Bekkaria region of Tébessa Province, northeastern Algeria, represents a geologically dynamic and environmentally sensitive area where natural processes and anthropogenic activities intersect. The synthesis of geographic, geological, tectonic, hydrogeological, and climatological data reveals a landscape shaped by:

1. **Complex Geology**: Dominated by Upper Cretaceous to Paleogene carbonate formations prone to karstification (Hadji et al., 2017) and Triassic evaporitic diapirism (Ghrieb, 2011), the lithological heterogeneity amplifies slope instability risks, particularly in mechanically weak zones such as marl-limestone interfaces and fractured karst terrains.
2. **Active Tectonics**: The region's position within the Tellian Atlas domain, influenced by Alpine compressive stresses (Vila, 1980; Bougherira et al., 2021), has produced folds,

thrust faults (e.g., Merssout-Tébessa fault), and diapiric structures that fragment the terrain, control groundwater pathways, and enhance slope susceptibility to failure.

3. **Semi-Arid Climatic Extremes**: Characterized by hot summers (up to 35°C) and episodic heavy rainfall (300–500 mm annually), the climate drives rapid pore pressure fluctuations in slope materials (ONM, 2020), triggering gully erosion, sheet wash, and transient perched water tables that weaken soil cohesion (Boukerboub, 2020).
4. **Hydrogeological Dynamics**: Shallow aquifers (e.g., P1) exhibit seasonal water table variations of up to 4 m (Ghrieb, 2010), while deeper confined aquifers (P2, P3) show declining heads due to over-extraction. These fluctuations critically influence slope stability by altering effective stress in clay-rich soils (Mrad et al., 2018).

The proposed railway alignment across Jebel Bekkaria's steep gradients faces compounded challenges from these factors. Karst-induced subsidence, tectonic fault reactivation, and hydro-climatically driven erosion pose significant geotechnical hazards. Mitigation demands:

- **Integrated Drainage Systems** to manage rapid infiltration and perched water tables (Achour et al., 2012).
- **Real-Time Monitoring** of piezometric levels and rainfall patterns to anticipate pore pressure spikes.
- **Adaptive Engineering Designs** accounting for lithological variability (e.g., reinforced cut slopes in marls, grouting of karst voids).

In conclusion, the Bekkaria region exemplifies the critical need for multidisciplinary risk assessment in infrastructure projects within tectonically active, semi-arid environments. Future work must prioritize predictive modeling of slope behavior under climate change scenarios (e.g., intensified rainfall extremes) and integrate local geological knowledge into sustainable engineering solutions (CRAAG, 2020; ANESRIF, 2022).

CHAPTER III:

GEOTECHNICAL INVESTIGATION AND DATA COLLECTION.

Chapitre III: Geotechnical Investigation and Data Collection

III.1. Introduction:

The geotechnical assessment of infrastructure projects is an essential component in ensuring structural safety, particularly in regions marked by complex geomorphological and geological conditions. Such investigations provide a scientific basis for understanding the mechanical behavior of soils and rocks, evaluating slope stability, and designing appropriate mitigation strategies to address potential geohazards.

This study focuses on a critical segment of the Tanokla bypass, a key element in the modernization project of the mineral railway line linking Oued Kebrit to Jebel Onk. The section under investigation, extending from PK 24+700 to PK 25+078, traverses steep terrain with slope heights reaching up to 40 meters and is characterized by significant subsurface heterogeneity. These conditions necessitate a comprehensive geotechnical investigation to evaluate the risks of slope instability and inform engineering decision-making.

The adopted methodology integrates field reconnaissance, subsurface exploration through borehole drilling, and systematic sampling. Laboratory testing programs include physical, mechanical, and chemical analyses to determine the geotechnical parameters governing soil and rock behavior.

The findings from this study aim to support the design of effective stabilization measures and contribute to the safe and sustainable development of the railway infrastructure in the Tébessa region.

III.2. Geotechnical investigation:

III.2.1 Boreholes and drill cores

As part of the geotechnical investigation, a total of eight (8) boreholes were drilled across the project site. The depths of these boreholes ranged from 20 meters to 60 meters. Both vertical and inclined boreholes were performed, depending on the local terrain and the geotechnical objectives of the study.

The drilling was carried out using core drilling, which allows continuous extraction of cylindrical samples (cores) from the ground. This method was chosen to obtain high-quality, undisturbed samples necessary for precise lithological and structural analysis.

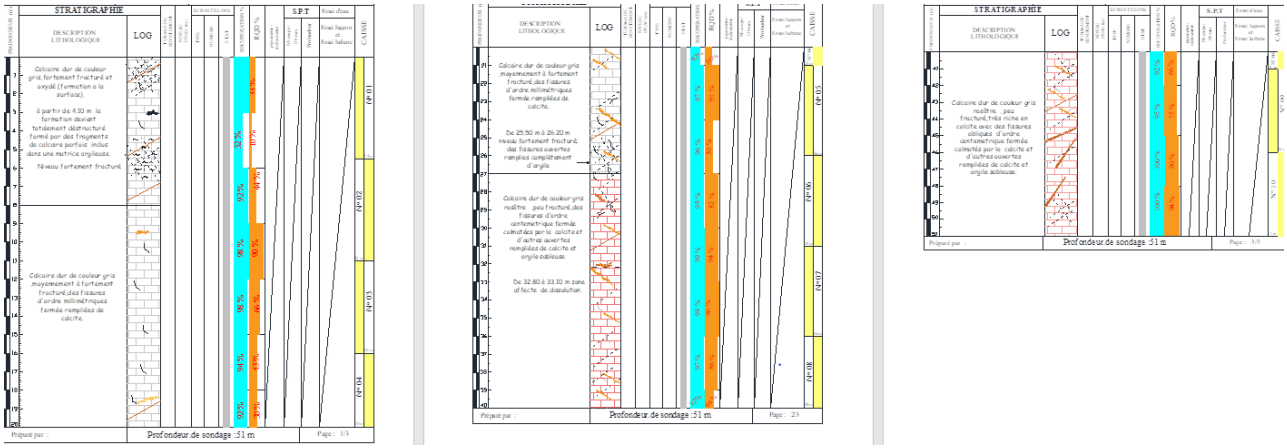


Fig III.1: An example of borehole drilled in the limestone facies.

The cores retrieved from each borehole were carefully logged and visually described to identify the nature and sequence of the subsurface materials.The formations encountered consist primarily of clay, limestone, and geological units belonging to the Triassic period. The use of core drilling enabled accurate identification of material transitions, stratification, discontinuities, and any signs of weathering or structural weakness.

Inclination and azimuth were recorded for the inclined boreholes to assess subsurface conditions in targeted slope zones. Groundwater levels were also observed during drilling and used for hydrogeological interpretation.

A summary of borehole characteristics including coordinates, depth, inclination, azimuth, and general lithology is presented in Table III.1. Detailed borehole logs are provided in the following section.

N°	Denomination	Inclination	Depth (m)	Description
1	SCD-01	Inclined 30°	51	Limestone
2	SCD-02	Vertical	50	Trias
3	SCD-03	Vertical	60	Clay
4	SCD-04	Vertical	60	Clay-Limestone
5	SCD-05	Vertical	60	Limestone
6	SCD-06	Vertical	40	Clay
7	SCD-07	Inclined 30°	53	Clay-Limestone
8	SCD-08	Vertical	20	Limestone-Trias

Table III.1: Summary of Boreholes Location and Cracteristics.

III.2.2Detailed Lithological Description of Boreholes:

BH 01: Inclined 30° downstream. Depth = 51 m (Annex 1)

X = 432,766.75 Y = 3,914,747.39 Z = 1018.37

This borehole, located along the track axis in the central part of the trench alignment, encountered:

From 0 to 8.0 m, hard, highly weathered limestones, fragmented at the surface, with a low RQD from 8 to 51 m, compact and hard limestones with oblique fissures, with a generally high RQD. Fractured and certified zones were observed at depths of: 15 to 15.50; 18.80 to 21; 25-20 to 26.50; 39.70 to 40.70;

BH 02: Vertical, depth = 50 m (Annex)

X = 432,931.16 Y = 3,914,669.00

Located downstream in the Triassic facies zone. It contains:

From 0 to 14.5 limestone fragments embedded in a clay matrix leached by drilling water. From 14.5 to 20.5 m variegated clay rich in gypsum

From 20.5 to 50 m Compact gray marl clay with a rocky appearance with a reddish passage from 43 to 44.10

BH 03: Vertical, depth = 60 m

X = 432,711.892 Y = 3,914,782.07 Z = 1003.98

Along its entire length, this borehole crosses reddish indurated clays with some centimeter-sized gravelly passages, particularly over the first 3 meters

BH 04: Vertical, depth = 60 m

X = 432,769.69 Y = 3,914,720.018 Z = 1015.95

This borehole crosses hard, compact karstified limestones on several levels, particularly at depths 6.40 _ 6.60 and 8.0 – 8.90.; 16.0-16.40 with loss of the tool. The infill is often clayey-pebbly. The RQD is often low in these areas.

There is a highly tectonized zone between 52 and 57m,

BH 05: Vertical, depth = 60 ml

X = 432,841.85 Y = 3,914,700.54 Z = 1009.86

This drill hole, like the previous one, encounters compact and hard limestones with several karstified levels; notably from 32.80 to 34.20 and 52.70 to 54.70 with a clayey infill.

The core is heavily oxidized over a large portion of its length.

BH 06: Vertical, depth = 40 m (Annex 3)

X = 432,741.7 Y = 3,914,836.9

Like SD3, the reddish clays of the Mio Pliocene with gravelly layers are encountered along its entire length.

BH 07: Vertical, depth = 53 ml

X = 432,754.37 Y = 3,914,789.04

The purpose of this survey was to identify the contact between the Mio-Pliocene clays and the Turonian limestones. These appear to have been reached at a depth of 44 m; in a zone likely uralitized with clay infill.

BH 08: Vertical, depth = 20 m

X = 432,920.49 Y = 3,914,719.54

This survey encountered compact and hard limestones, often fractured, over the first 13 meters, followed by healthier limestones with a high RQD.

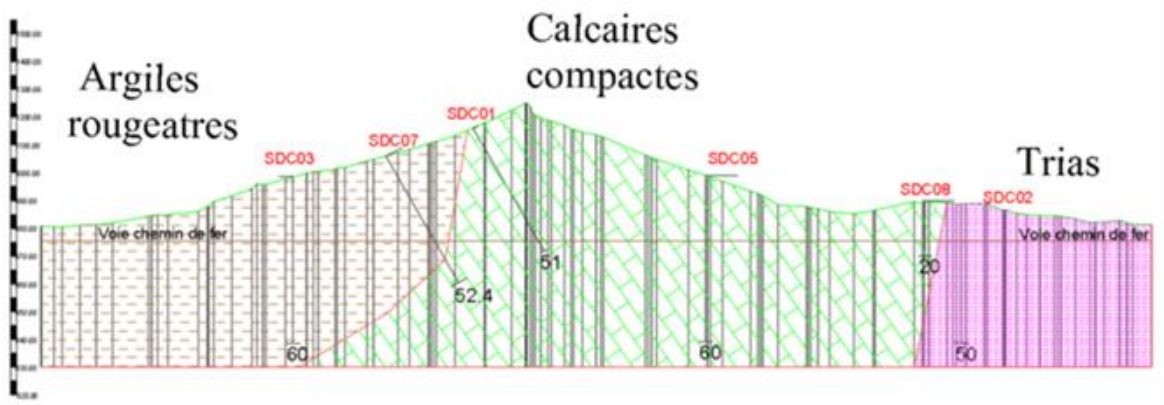


Fig III-2: Preliminary geological section along the axis of the track.

III.2.3Water Table:

No groundwater table was encountered in any of the eight (8) boreholes. This absence is likely due to the prolonged drought affecting the region in recent years.

III.3 Geophysics:

III.3.1Description:

To delineate the contact boundaries between the Mio-Pliocene clays and the underlying Turonian limestone, a combined geological and geophysical approach was implemented. Lithological and stratigraphic information was obtained through in-situ core drilling, supported by visual analysis of the extracted cores. These geological observations were complemented by seismic refraction surveys aimed at characterizing subsurface discontinuities and defining the geometry of the interface.

Three seismic refraction profiles (PS1, PS2, PS3) were carried out along 120-meter lines. Multiple shot configurations—including peripheral, central, and offset positions—were used to optimize ray coverage and improve the resolution of subsurface layers.

Figure (III-3) illustrates the spatial distribution of the geophysical profiles and borehole locations on satellite imagery, providing a georeferenced overview of the study area. This integration of surface and subsurface data helped establish a coherent interpretation of the lithological transitions.

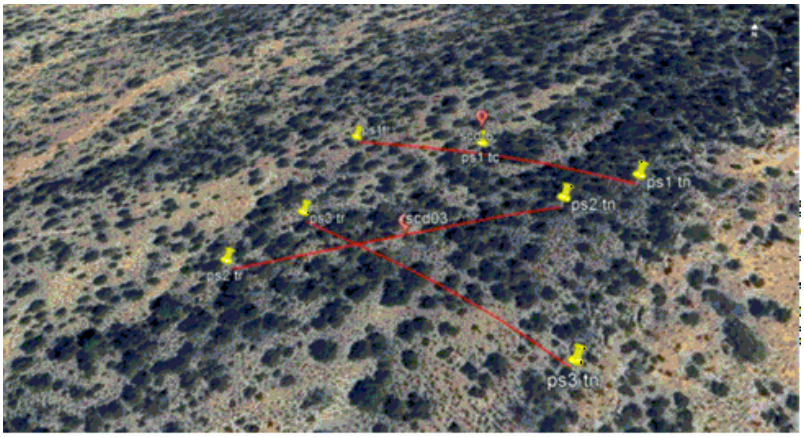


Fig III-3: Mapping of Geophysical Investigation Points and Boreholes on Satellite Imagery.

III.3.2 Seismic Refraction Results (Vp Profiles) :

The recordings allowed the construction of travel-time curves (dromotropes) based on the first arrivals of P-waves. The interpreted velocity profiles reveal three main subsurface layers across the study site:

Layer 1: Unconsolidated near-surface deposits with seismic velocities ranging from 300 to 3530 m/s, and thicknesses between 1 and 3 meters. Notably, PS3 begins with a very high velocity value (3530 m/s), indicating the presence of hard rock at the surface, unlike PS1 and PS2 which show loose or weathered material.

Layer 2: Transition zone with Vp = 800–1319 m/s, and thicknesses of 3 to 5 meters. This layer is interpreted as compacted clay or alluvial deposits.

Layer 3: Deeper, competent units with velocities between 1640 and 1770 m/s, of undefined thickness. These are likely consolidated sediments or bedrock (possibly Turonian limestone).

The interpreted results of the three seismic refraction profiles—PS1, PS2, and PS3—are presented in Figures III-8 through III-10, respectively. These visualizations illustrate the spatial layout of each profile and their corresponding velocity models, highlighting the identified stratigraphic layers and supporting the described interpretations. The interpreted results of the three seismic refraction profiles PS1, PS2, and PS3 are presented in Figures III-8 through III-10, respectively. These visualizations illustrate the spatial layout of each profile and their

corresponding velocity models, highlighting the identified stratigraphic layers and supporting the described interpretations.



Fig III -4: Location of Geophysical Profile PS1 on the Study Site.

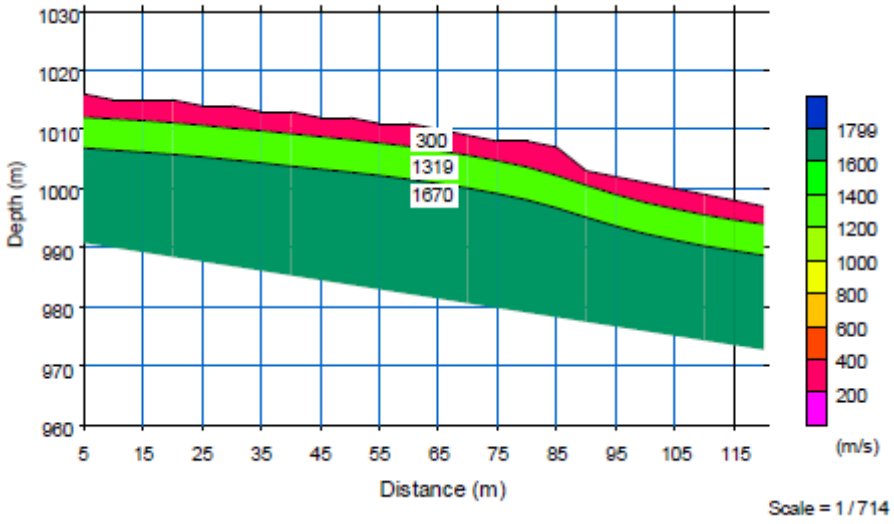


Fig III- 5: Interpritation Results of PS1 Geophisical Profile .



Fig III-6 : Location of Geophysical Profile PS2 on the Study Site .

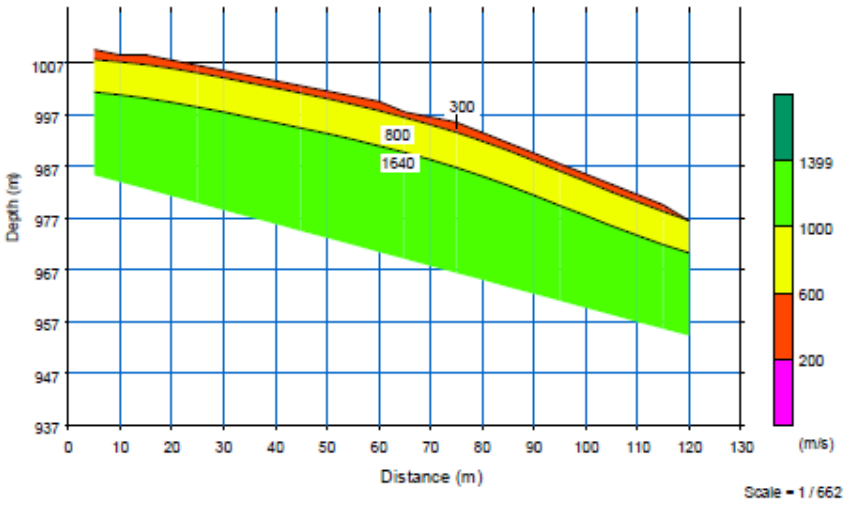


Fig III-7 : Interpritation Results of PS1 Geophisical Profile .



Fig III- 8: Location of Geophysical Pro

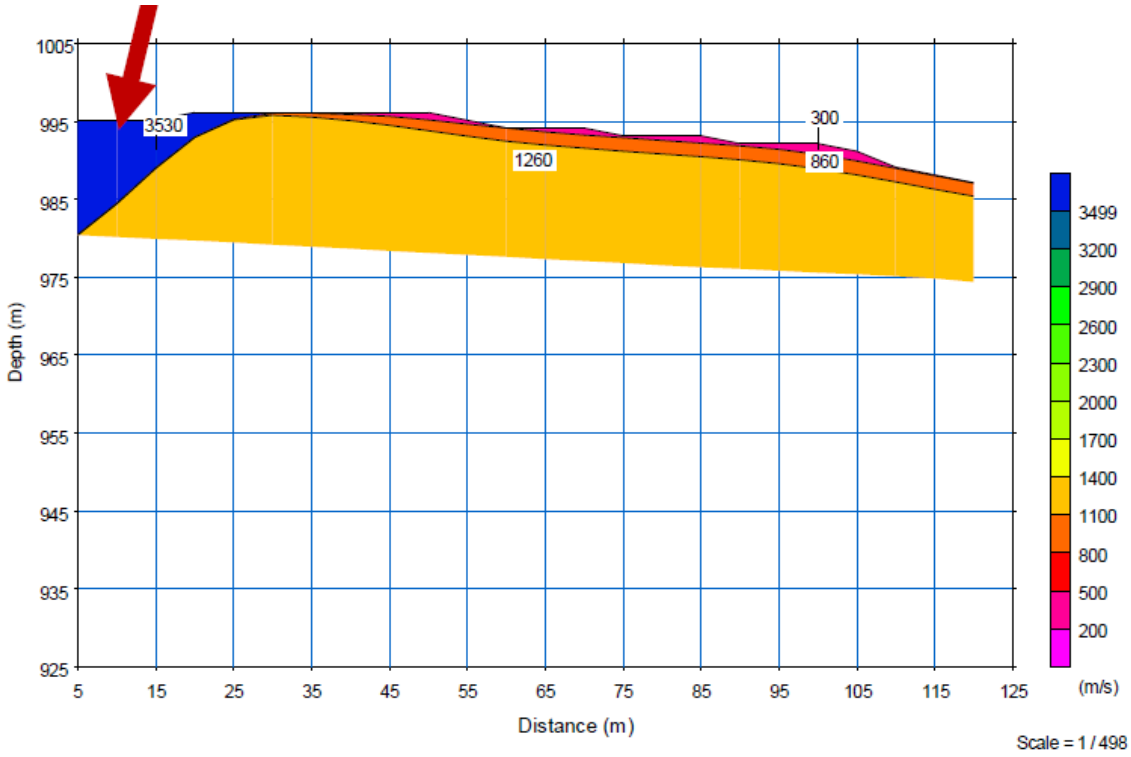


Fig III- 9: Interpritation Results of PS3 Geophisical Profile .

Here's a concise summary of the findings from the seismic profiles (**PS1**, **PS2**, **PS3**) and their correlation with core drilling data (**SC6**, **SCD06**):

III.3.3 Profile Comparisons:

PS1 and **PS2** share near-identical layering and velocity gradients, suggesting uniform lithology across the study area.

PS3 diverges in its shallow section (high-Vp surface layer) but aligns with PS1/PS2 at depth.

III.3.4 Core Data Validation :

Data from boreholes SC6 and SCD03 provide direct confirmation of the seismic interpretation**:**

- Alluvial deposits (thickness 3–5 m) observed in the cores correspond to Layer 2's velocity range (800–1300 m/s).
- Cohesive clays and competent formations deeper in the cores match Layer 3 velocities (1640–1770 m/s), confirming the presence of denser, consolidated material.

III.3.5 Implications:

The presence of a high-velocity surface layer in PS3 suggests localized Turonian limestone outcrops, which are crucial for understanding the contact with the overlying Mio-Pliocene clays. These transitions influence subsurface stability, and recognizing them accurately is vital in the context of slope stability studies.

III.4Presentation of Project :

III.4.1 Site Overview and Field Observations:

The slope stability assessment constitutes a fundamental phase in the planning and design of major infrastructure projects, especially in regions characterized by rugged topography and complex geological structures. This study focuses on a sensitive segment of the **Tenoukla deviation**, which is part of the **mineral railway modernization project** led by the **National Railway Transport Company (SNTF)**. The project aims to enhance the efficiency of mineral transport between **Oued Kebrit and Jebel Onk** in northeastern Algeria.

The new railway alignment follows the existing line for the most part but includes a significant deviation between **Boulhaf El Dir and El Maa El Abiadh**, bypassing the densely populated city of **Tébessa** and cutting across mountainous areas. The new route traverses the **Bakaria region**, climbs **Jebel Bakaria**, crosses **El Houijbat**, and continues to **El Maa El Abiadh**, over a distance of approximately **43 km**.

This study specifically targets the section between **PK 24+700 and PK 25+078**, a **378-meter-long segment** situated on the **right bank of Wadi Djebissa**, a tributary of **Wadi Bekkaria**. The site lies in close proximity to the urban edge of Tébessa and is characterized by **steep, irregular slopes exceeding 35°**, presenting substantial challenges in excavation planning and long-term stability.

Field reconnaissance revealed a **highly heterogeneous lithology**. Moving from east to west, the stratigraphy includes:

- Reddish clays (argile),
- Compact and hard limestones,
- Variegated Triassic clays.

These formations are interbedded with **metric-scale limestone layers**, oriented **N35°** with a dip of about **70° southeast**. Borehole **SDC08** revealed signs of **karstification** near the contact with the Triassic series, suggesting possible structural weaknesses in depth. Surface access to the area was achieved via **unpaved tracks** along the **northern bank of Wadi Djebissa**, enabling the execution of boreholes and geotechnical tests.

III.4.2 Geological and Topographic Mapping:

The geological and topographic characterization of the study area is based on maps and data provided by KOSIDAR Company (2024) (Fig 01), complemented by field observations and photographic documentation ,also in site visites and geological cross section effectuated along the project.

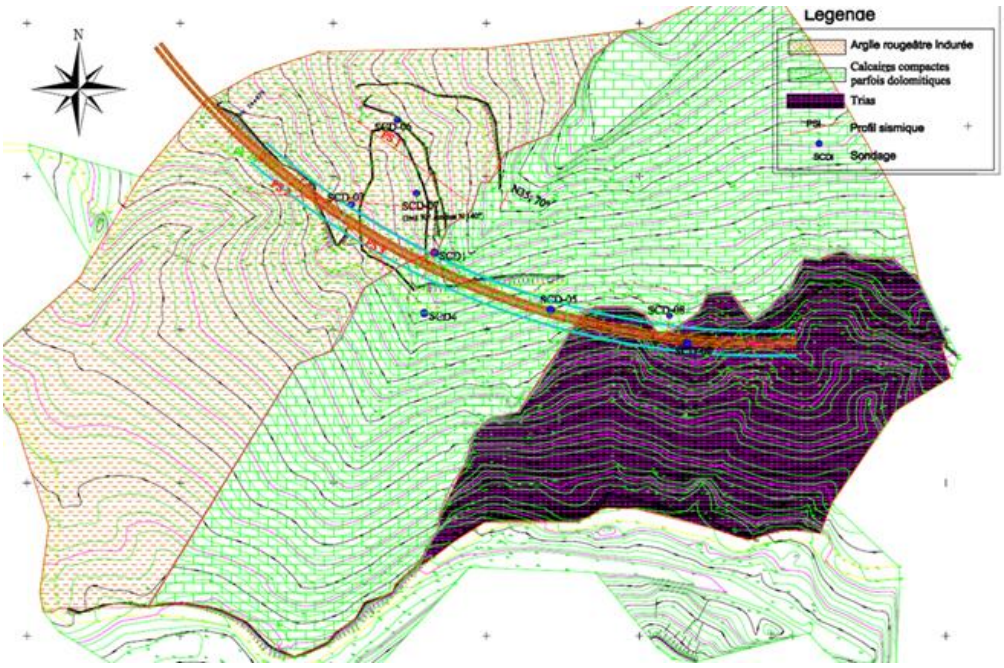


Fig III- 10: Geo Map View in Topographic Plan (COSIDER 2024) .

Field investigations and mapping enabled the identification and documentation of the **main geological formations** exposed at the surface, as well as their structural and lithological characteristics. These include:

- Mio-Pliocene clays (soft and plastic),
- Turonian limestones, characterized by well-stratified beds dipping toward the southeast**,**
- Fractured rocky zones located at the upper portions of the relief, showing instability,
- Variegated Triassic clays, typically altered and sensitive to water.

III.4.3Representative Field Photos:

The following field photographs illustrate representative outcrops of the main geological formations identified in the study area. They highlight the lithological and structural characteristics observed in the field, including: Mio-Pliocene clays, Turonian limestones dipping towards the southeast, unstable rocky zones at the top of the hill, and the variegated clays of the Triassic:



Fig III.11: Outcrop of Pliocene Moi clays



Fig III.12: Turonien Limestones Dipping Towards The SE



Fig III.13: Unstable rocky area at the top of the hill.



Fig III.14: Variegated Triassic Clays.

III.4.4Geological Observations and Geotechnical Stability Implications

Field investigations identified intensely fractured limestone ridges at higher elevations, forming overhanging rock masses that may represent potential geohazards under dynamic conditions such as seismic loading or extreme precipitation events. Although no active signs of slope movement were documented during the site reconnaissance, the structural discontinuities observed in these elevated zones necessitate cautious consideration in slope stability assessments.

At the surface, the limestone units appeared structurally competent, with no visible signs of fracturing or karstification. However, subsurface exploration, particularly data from borehole SDC08 near the Triassic stratigraphic contact, revealed localized karst development at depth. This subsurface karstification suggests the presence of concealed hydrogeological pathways that may influence groundwater flow dynamics and, consequently, the mechanical behavior of the slope under variable loading conditions.

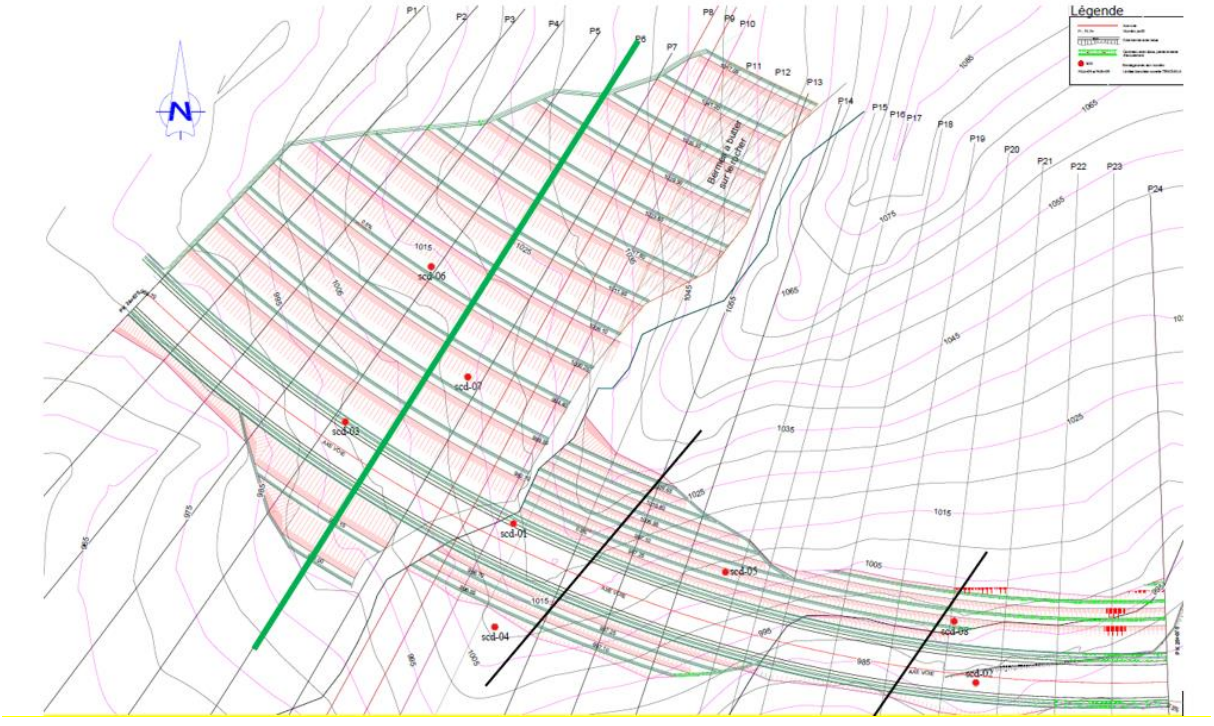


Fig III.15: Excavation Work Plan View (COSIDER 2024)

III.4.5 Project Description

The selected segment under investigation is a **strategic component** of the new railway deviation designed to optimize mineral transport across the **Tébessa region**. The project forms part of a **major infrastructure initiative** to construct a **double-track railway line** that circumvents the urban center of **Tébessa**, thereby reducing congestion and enhancing logistic efficiency.

III.4.5.1Location and Scope

The trench excavation studied in this report extends from **PK 24+700 to PK 25+078**, covering a **total length of 378 meters**. It is located on the **right bank of Wadi Djebissa**, a **tributary of Wadi Bekkaria**, and represents a **critical crossing point** characterized by **steep and unstable terrain**, with slopes exceeding **35°**. This topographic complexity necessitated detailed geotechnical and geological investigation to assess excavation feasibility and slope stability.

III.4.5.2Geological Profile of the Trench

The excavation crosses three distinct geological formations identified via borehole logging, topographic profiling, and geophysical surveying:

- **Eastern Zone – Reddish Clays (Argiles Rouges)**

Maximum height: 1010m

Minimum height: 980m

- **Central Zone – Compact Hard Limestone (Calcaire Dur)**

Maximum height:1025 m

Minimum height:993 m

- **Western Zone – Variegated Triassic Clays (Argiles Triasiques)**

Maximum height:993 m

Minimum height:980 m

These lithologies were confirmed by eight geotechnical boreholes**,** longitudinal profiles**,** and geophysical techniques such as seismic refraction .

III.4.5.3Technical Survey and Excavation Data

High-precision instruments including **total stations** and **geodetic GPS** were employed to establish accurate **topographic baselines**. The data were processed using **AutoCAD** to trace the trench alignment, define geological contacts, and guide borehole positioning along **accessible field paths**.

The estimated excavation volumes are as follows:

- **Total excavation volume**: 547,168 m³
  - **69%** soft soil (terrain meuble)
  - **31%** rock (roche dure)

III.5 Geotechnical Tests and data extraction

III.5.1 Results of Physical, Mechanical, and Chemical Analyses

The physical, mechanical, and chemical analyses performed on core samples (carottes) extracted from the various geological formations provided essential and reliable data to understand the behavior and properties of each soil and rock type within the excavation zone. These core samples, obtained through borehole drilling, offer an accurate representation of subsurface conditions. The results highlight significant variability in strength, permeability, and composition, which are critical factors for slope stability assessment and excavation design. The following section summarizes the key findings from laboratory tests conducted on samples from the reddish clay, compact limestone, and Triassic

III.5.1.1Turonian Limestones:

Laboratory Tests:

The following tables summarize the results for samples from drill holes SDC-04 and SDC-05

Survery		Wet density	Compressive strength	Tensile strength
		γ_h (t/m3)	R_C (MPa)	R_T (MPa)
SCD 04	max	2,69	140,50	6,70
	min	2,32	19,90	2,40
	avg	2,51	61,98	5,22
SCD05	max	2,78	108,70	7,50
	min	2,36	57,30	2,50
	avg	2,62	79,98	5,40

Table III.2: Results of mechanical tests SDC-04 / SDC-05.

Both measurements give values of Rc and Rt of equal magnitude.

On average, Rc is high and Rt is medium.

III.5.1.2Mio Pliocene clays:

Laboratory Tests

The results of physical tests conducted on the Mio-Pliocene clays of SD3 and SD6areshown

in the table below.

Survery		Water contant	Wet density	Dry density	Grain Size (%)						Atterberg limits		
					Stones	Gravel	Sand	Silts	Clays	< 80µ			
		(%)	h (t/m3)	s (t/m3)							WL(%)	Wp(%)	IP(%)
SCD 03	max	15.57	2.22	1.96	-	-	10.00	40.00	64.00	98.59	53.00	27.67	26.96
	min	13.37	2.16	1.87	-	-	4.00	32.00	50.00	92.38	45.00	23.04	17.33
	avg	14.55	2.19	1.91	-	-	6.80	36.40	56.80	96.13	49.70	26.24	23.46
SCD06	max	2.78	2.78	7.50	-	-	18.00	35.00	64.00	98.26	-	-	-
	min	2.36	2.36	2.50	-	-	6.00	30.00	50.00	84.90	-	-	-
	avg	2.62	2.62	5.40	-	-	10.00	31.75	57.75	94.75	-	-	-

Table III.3: Results of the physical tests SDC-03/ SDC-06.

These materials are silty, slightly sandy, inorganic, plastic to highly plastic clays (Category CL to CH) with a relatively low water content (average of 13.37); with a high dry density.

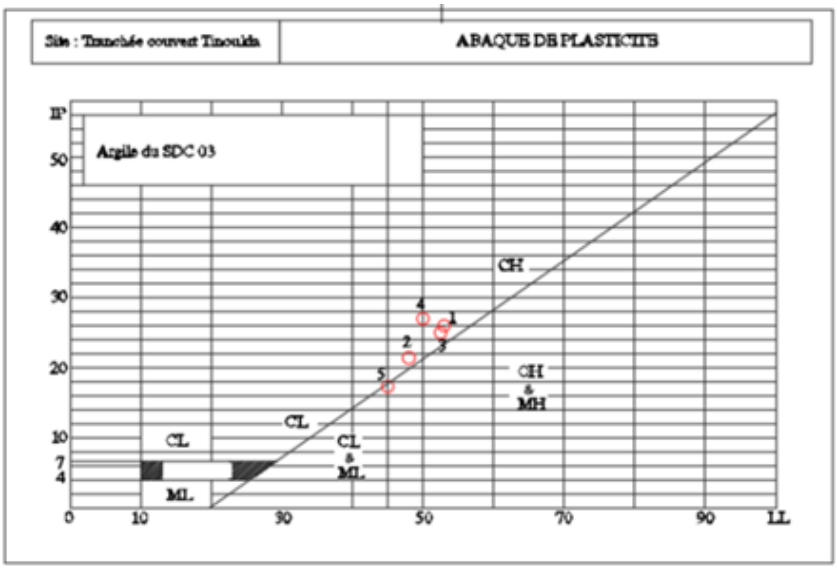


Fig III.16: Casagrande SDC-03 clay classification chart.

Mechanical Tests:

The results of the mechanical tests are shown below. The values obtained are average to high.

Survery		Shear CD	
		C (KPa)	Ø(°)
SCD 03	Max	320,00	24,03
	Min	210,00	17,47
	avg	275,00	20,98
SCD06	max	270,00	16,70
	min	180,00	9,12
	avg	227,50	13,66

Table III.4: Results ofthemecanical tests SDC-03/ SDC-06.

The shear test values for SDC-06 are significantly lower than those

for SDC-03, while the identification tests show almost identical soils,

slightly sandier.

In-situ testing (SPT)

Boreholes SD3 and SD6 underwent SPT testing, the results of which are summarized in the tables below.

The average number of blows corresponds to stiff to very stiff clays for SD3.

For SD6, the recorded values correspond to stiff clays, with a number of blows (cps) >50.

The large difference in values obtained between SDC 03 and SDC 06 is difficult to explain given formations that appear identical at outcrop and in boreholes. However, the SD6 log appears more indurated and locally more gravelly.

SDC 03				SDC 06			
Profondeur	Nombre de coups			Profondeur	Nombre de coups		
(m)	15 cm	30 cm	45 cm	(m)	15 cm	30 cm	45 cm
3	6	12	15	3	>50		
6	5	24	>50	6	>50		
9	5	12	>50	9	>50		
12	10	18	20	12	>50		
15	9	11	13	15	>50		
18	12	15	25	18	>50		
21	10	14	21	21	>50		
24	14	20	27	24	>50		
27	10	16	25	27	>50		
30	6	17	23	30	>50		
33	>50			33	>50		
36	11	19	27	36	>50		
39	15	30	37	39	>50		
42	14	21	32				
45	15	23	35				
48	15	25	37				
51	12	25	39				
54	9	20	36				
57	15	26	39				
60	24	39	45				
Maximum		39	45				
Minimum		11	13				
Moyenne		**20,37**	**30,06**				

Table III.5: Results of SPT SDC-03 and SDC-06 tests.

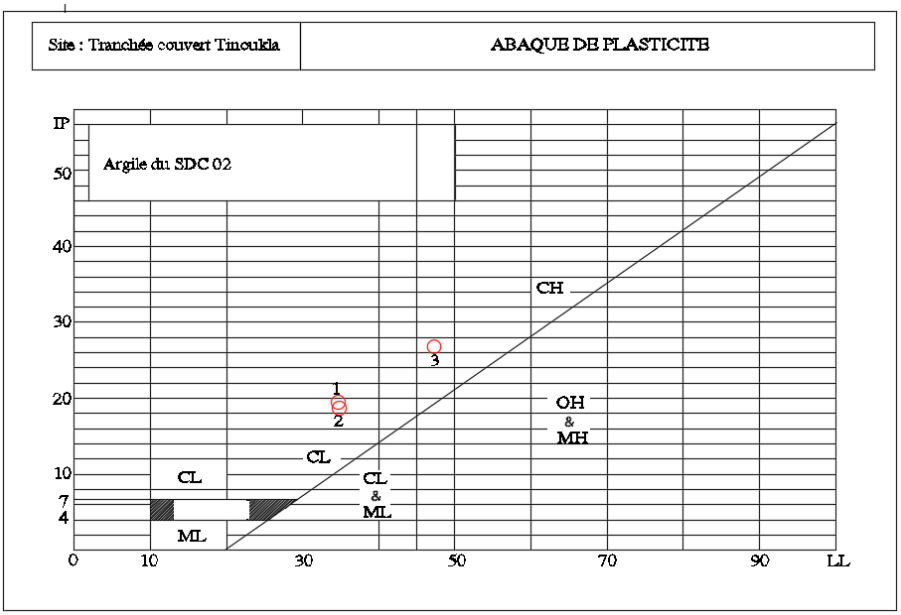
III.5.1.3Triassic Clays

Samples collected from drill hole SDC02 in the Triassic formations were subjected to identification tests and chemical analyses. The table below summarizes the results obtained for the three samples analyzed.

Particle size analyses show quite different soils, the first sample corresponds to slightly pebbly sandy silty clays, the other two correspond to more gravelly silty clay sands for the last sample. All three samples are dense with medium water contents. In terms of plasticity, these materials are classified as CL (inorganic, moderately plastic).

Survery		**Water contant**	**Wet density**	**Dry density**	**Grain Size (%)**						**Atterberg limits**		
					Stones	**Gravel**	**Sand**	**Silts**	**Clays**	**< 80µ**			
		(%)	**h (t/m3)**	**s (t/m3)**							WL(%)	Wp(%)	IP(%)
SCD 02	**max**	12,21	2,23	2,10	-	-	48,00	40,00	46,00	88,92	48,00	26,66	21,34
	min	6,02	2,14	1,91	-	-	10,00	11,00	29,00	48,56	35,00	18,26	16,35
	avg	9,60	2,18	1,99	-	-	33,00	24,67	37,33	63,72	39,60	21,46	18,14

TableIII.6: Results of physical tests of the SDC 02 survey.



FigIII.17: Casagrande SDC-02 clay classification chart.

Chemical Analysis:

Chemical analyses show traces of gypsum and SO4 in the first sample, while in the other two samples located beyond 18 m depth, gypsum is present with an appreciable percentage of 8 to 12.35% and high SO4 percentages, making them aggressive soils.

Survey	Depth	Chemical Analysis					
		gypse	SO4	SO4	Chlorides	Caco3	CO2
(N°)	(m)	%	%	Mg/kg	%	%	%
SCD-02	6,45-7,00	Traces			0,57	5,75	2,5
	18,00-18,35	12,35	6,89	68919,04	0,71	5,83	2,54
	21,00-21,35	8,91	4,97	49773,58	0,53	5,37	2,34

Table III.7: Results of chemical analyses of the SDC 02 survey.

III.6Conlusion:

The geotechnical investigation conducted along the segment PK 24+700 to PK 25+078 of the Tanokla bypass provided a comprehensive understanding of the site's subsurface conditions, essential for evaluating slope stability and informing safe excavation practices. Through a multidisciplinary approach involving borehole drilling, core sampling, geophysical surveys, and laboratory analyses, the study successfully characterized the geological complexity of the region marked by steep slopes, heterogeneous formations, and structural discontinuities.

The borehole data revealed a stratigraphy dominated by Mio-Pliocene clays, compact Turonian limestones, and variegated Triassic clays, each with distinct geotechnical behaviors. Core logging identified key features such as karstification, weathering, and fracturing—factors that influence the mechanical integrity of the slope. No groundwater was detected during drilling, though signs of subsurface karst suggest potential hydrogeological activity under variable climatic conditions.

Seismic refraction profiles complemented the lithological findings, confirming the presence of competent bedrock beneath softer surface layers and enabling the delineation of critical interfaces between clay and limestone units. These profiles validated the geological model developed from borehole and field observations.

Topographic mapping, field reconnaissance, and photographic documentation enriched the contextual understanding of surface geology and geomorphology. The project segment lies in a geologically sensitive area, with slopes exceeding 35°, necessitating careful consideration of slope geometry, material strength, and structural defects during excavation and stabilization planning.

Finally, laboratory tests on core samples provided quantitative parameters essential for slope stability analysis, such as unit weight, cohesion, internal friction angle, and permeability. The variability in these properties across formations underscores the importance of tailored engineering solutions.

In conclusion, the findings from this chapter form the geotechnical foundation for the design and execution of safe, effective slope stabilization and excavation strategies. This detailed understanding of subsurface conditions is critical to ensuring the long-term stability and operational safety of the railway infrastructure in the Tebessa region.

CHAPTRE IV:
CASE STUDY, RESULTES AND DISCUSSION.

IV.1 Introduction:

As part of the geotechnical assessment for the realignment of the mining railway track, a numerical analysis was conducted to evaluate the stability of the proposed open trench (tranchée ouverte). This trench is a key component of the earthworks required for the new railway path, and its behavior under excavation-induced stress conditions must be thoroughly understood to ensure long-term stability and operational safety.

The finite element software PLAXIS 2D was employed to simulate the mechanical response of the slope associated with the trench excavation. The model incorporates three representative geological formations encountered on site: Miopliocene clay, Triassic clay, and Turonian limestone. Each unit was analyzed individually through staged construction (mobilisation phases) to capture the progressive development of deformation and safety factor reduction throughout the excavation process.

This chapter presents the full modeling approach, including geometry, boundary conditions, mesh generation, and material parameters. The results are discussed in terms of deformation patterns, mesh distortion, and safety factor evolution (FS curves) for each scenario. By comparing the performance of different geological units, zones of potential instability are identified, providing critical insights for design optimization and risk mitigation in the proposed realignment project.

IV .2Geotechnical Molding:

At this stage of investigation, it has been used to achieve the whole stability of the project, different geometrical and geotechnical models along the railway project crossing the Bekkaria mountain are used as 2D numerical models in Plaxis 2D. Three cross section from all the geological facies composed the studied section from PK24 to PK25 (about 378m) this cross section areas follow:

IV.2.1 Clayey soil formation (MIOPLIOCEN):

A Define the Geometry: from the cross section imported as DXF AutoCAD file sheet and Material properties has been introduced

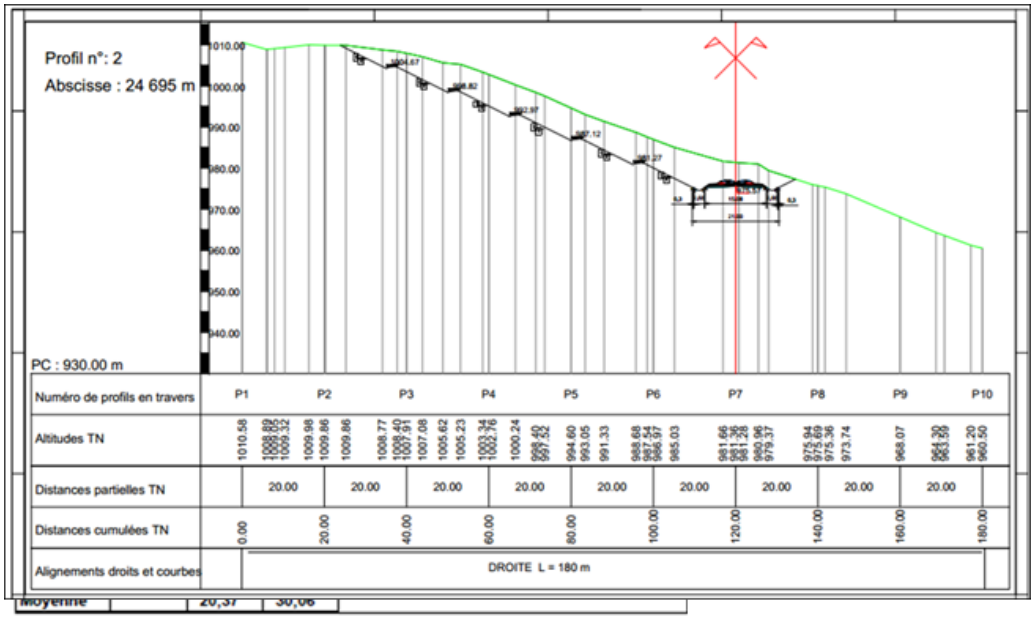


Fig IV.1: The Cross section of clayey soil.

B) Geometrical Molding of the Clayey Layer:

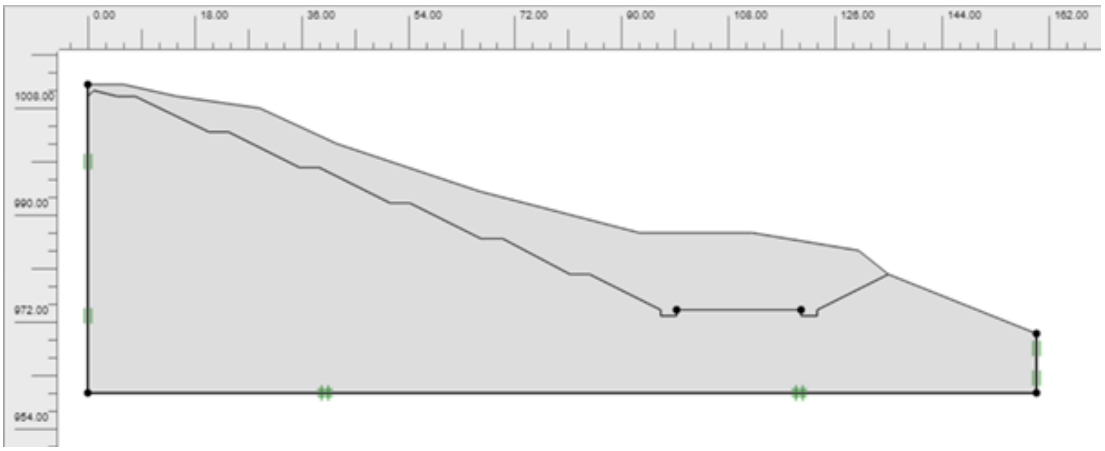


Fig IV.2: The Geometry Clayey Layer.

C Material Properties:

Parameter	Name	Value	Unit
Material model	Model	Mohr-Coulomb	-
Type of material behavior	Type	Drained	-
Saturated Unit Weight	γ_{sat}	21.5	KN/m^3
Unsaturated Unit Weight	γ_{unsat}	19	KN/m^3
Young's modulus	E'	30000	KN/m^2
Poisson's ratio	**ν**	0.35	-

Table IV.1:Clay layer properties.

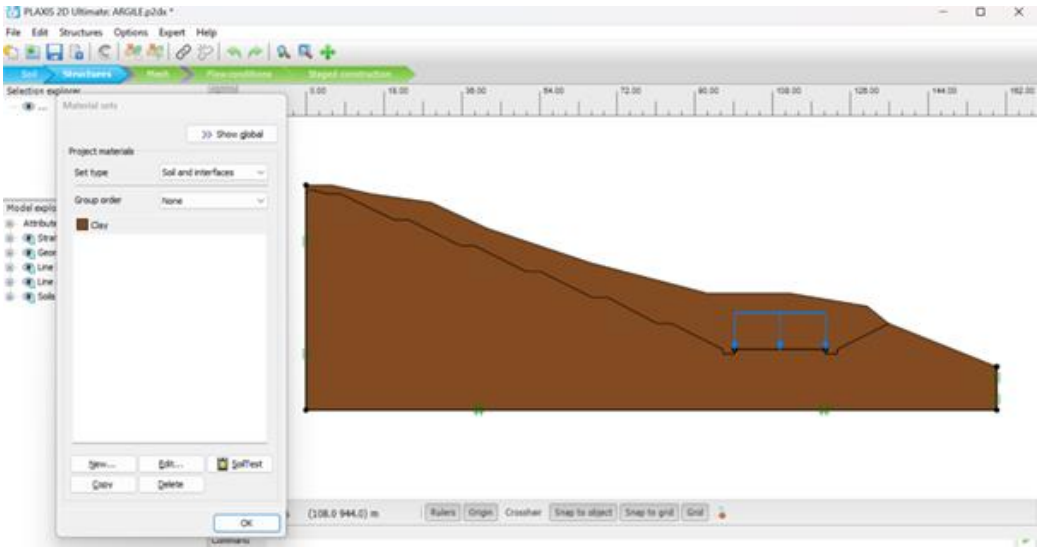


Fig IV.3: Input material.

D). Boundaries Conditions:

To simulate realistic mechanical behavior of the slope, appropriate boundary conditions were applied to the numerical model. The bottom boundary was fully fixed in both horizontal and vertical directions, preventing any displacement. The lateral boundaries were treated with standard constraints: the left and right sides were restricted in the horizontal direction only (no

horizontal displacement), while the top surface remained free to move and deform naturally. These conditions ensure numerical stability and reflect field constraints, avoiding unrealistic edge effects during calculation.

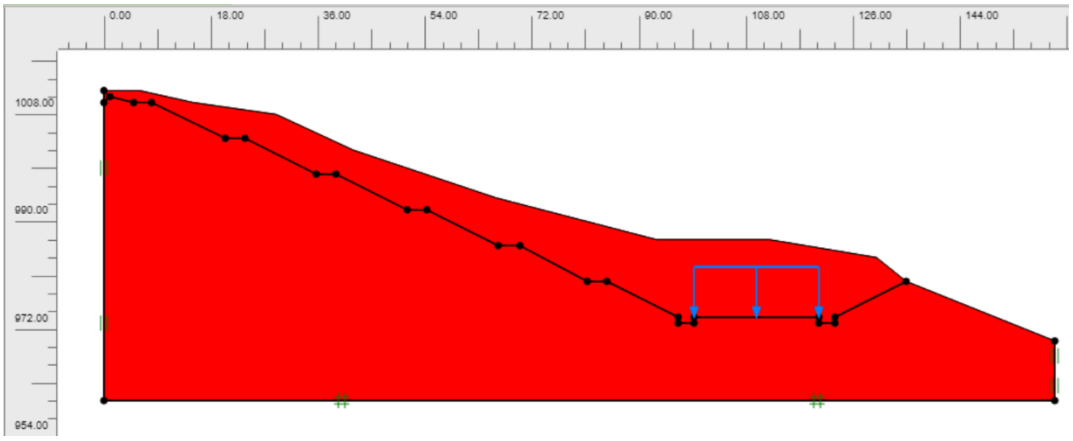


Fig IV.4: Boundaries Conditions.

E. Mesh generation:

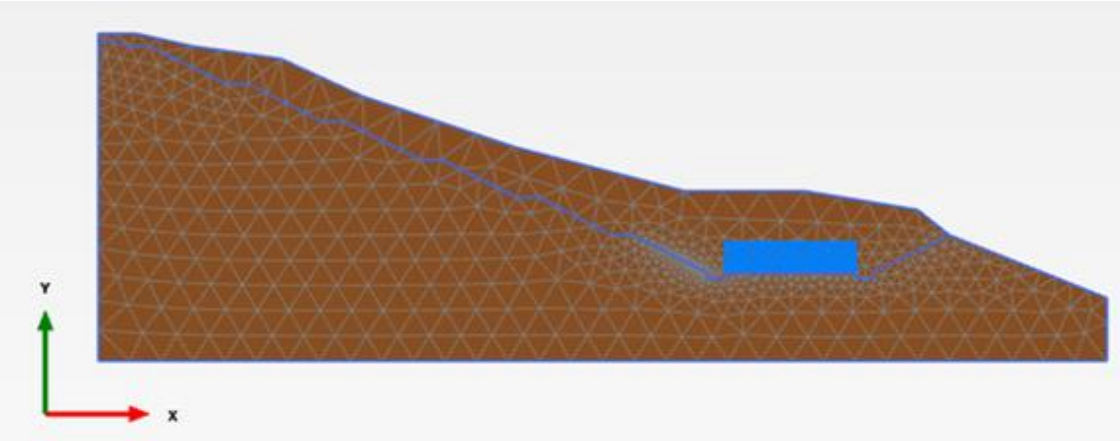


Fig IV.5: Generate Mesh.

F).Flow conditions:

According to site investigations and borehole data, no permanent groundwater table was observed within the studied area. Therefore, a dry condition was assumed for the initial state of the model. To account for possible infiltration scenarios during rainfall events, an infiltration boundary was defined at the slope surface. The lateral and bottom boundaries were considered impermeable (closed), representing no water flow across these edges. This hydraulic configuration allows evaluation of transient pore pressure development in response to surface water infiltration.

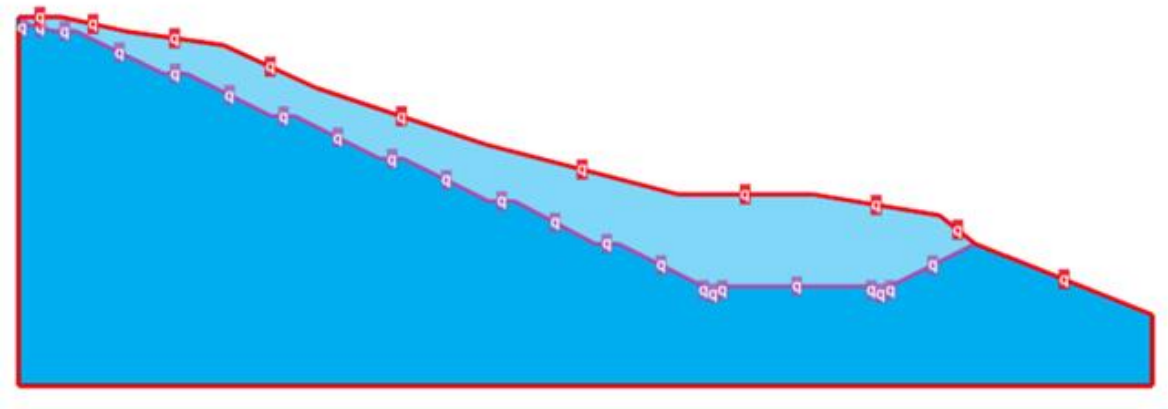


Fig IV.6: Flow condition.

G) Construction Stages and Calculation Types:

In this numerical model, four main types of calculations were employed to simulate the slope behavior under different loading conditions: K_0 procedure, Plastic, Safety, and Dynamic analysis.

The initial stress state was generated using the K_0 procedure, which ensures geostatic equilibrium based on the in-situ earth pressure conditions. This was followed by sequential construction and loading phases using the Plastic calculation type, which allows simulation of long-term drained behavior, plastic deformation, and progressive failure mechanisms.

To evaluate the global stability of the slope, a Safety analysis was conducted by incrementally increasing the load until failure, allowing for the calculation of the Factor of Safety (FoS).

Additionally, a Dynamic analysis was performed to simulate the effects of seismic loading and train-induced vibrations. A time-dependent acceleration input was applied at the model base to represent ground motion due to earthquakes and traffic loads. This phase is critical for assessing the slope's response to transient dynamic forces, particularly in zones affected by nearby railways or seismic activity.

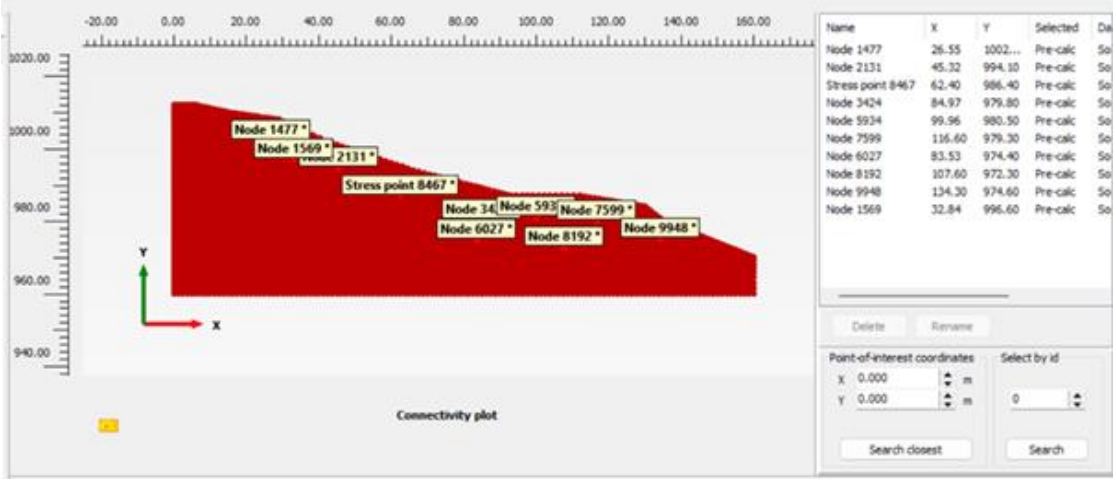


Fig IV.7: the nodes of calculation phases in PLAXIS.

Sequence of Calculation Phases:

- Initial phase: using K_0 Procedure calculation type.

- Phase 01: the safety factor of the initial phase.

- Phase 02: Excavation phase:plastic phase calculation type.

- Phase 03: the safety factor of excavation phase.

-Phase04 :Railway phase: plastic phase calculation type.

- Phase 05: The safety factor of the railway phase.

- Phase 06: Dynamic phase:dynamics phase calculation type.

-Phase 07 :Rainfall phase (0.01m/day): fully coupled flow-deformation calculation type.

-Phase 08 :The safety factor of the rainfall phase.

This step-by-step procedure allows for a comprehensive understanding of slope behavior under both static and dynamic loads, capturing the key deformation and failure mechanisms that may occur.



Fig IV.8: Configuration of calculation phases in PLAXIS.

Once the model setup was completed, the numerical calculation was executed using PLAXIS 2D. This step involves solving the finite element equations for each defined phase in order to simulate the behavior of the clayey formation under various mechanical and hydraulic

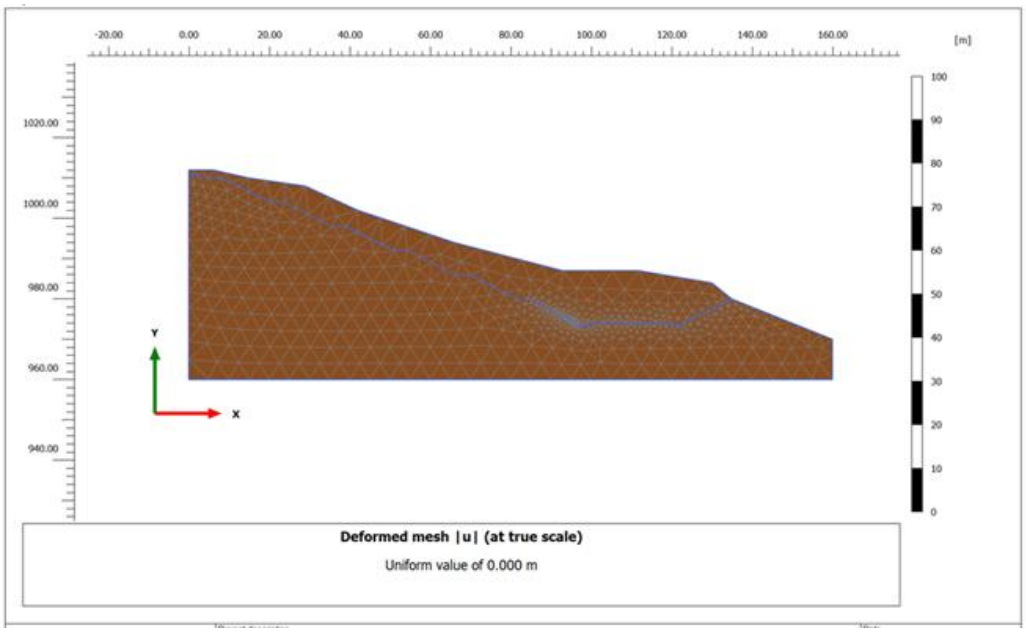
conditions. The calculation process was performed with the Plastic analysis option for all stages

The following image illustrates the execution of the calculation process:

IV.2.2 Results and discussion of Clayey

This section presents and interprets the simulation results of all phases:

Initial phase: using calculation type:



FigIV.9 :Mesh Deformation during Initial Phases

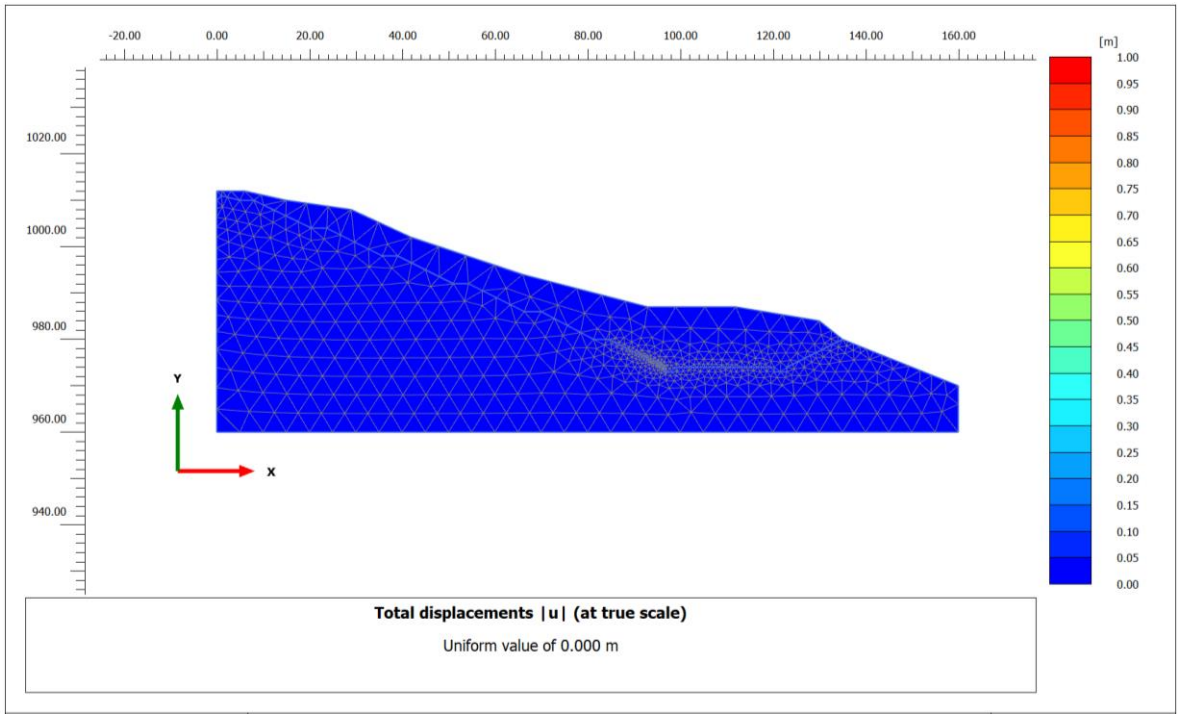


Fig IV.10 :Total Deformation during Initial Phases

Phase 01: the safety factor of the inial phase.

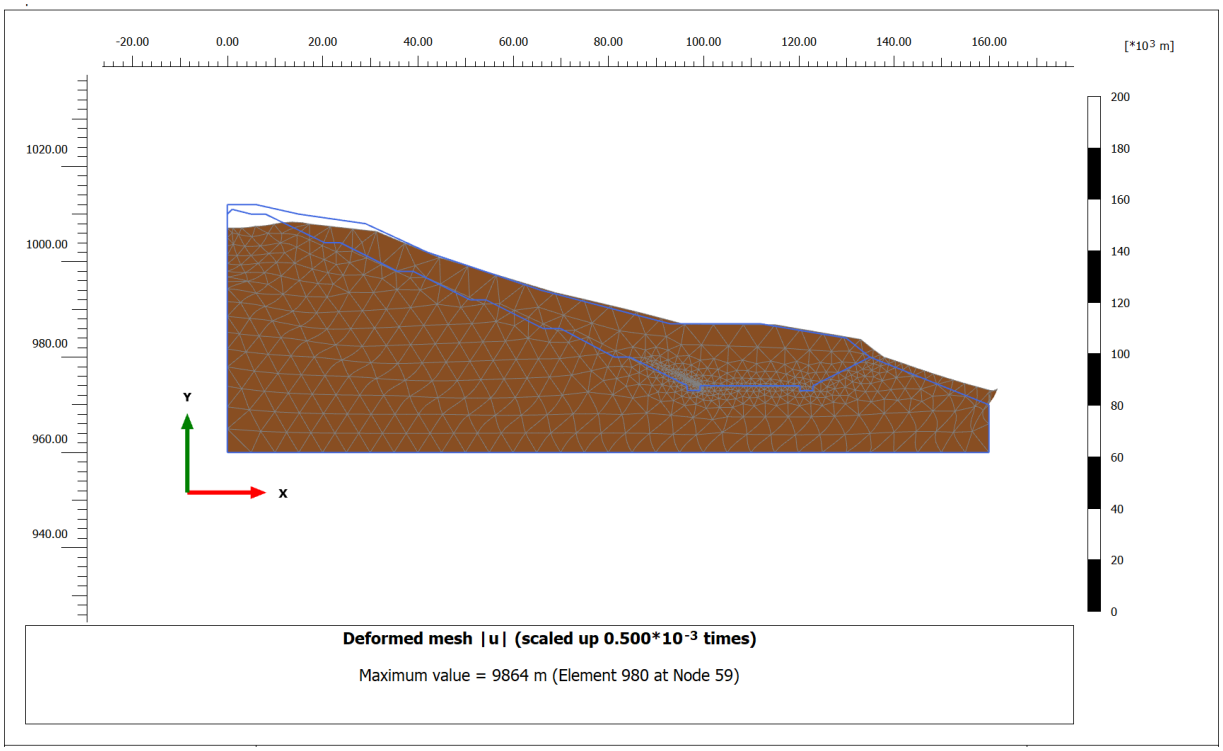
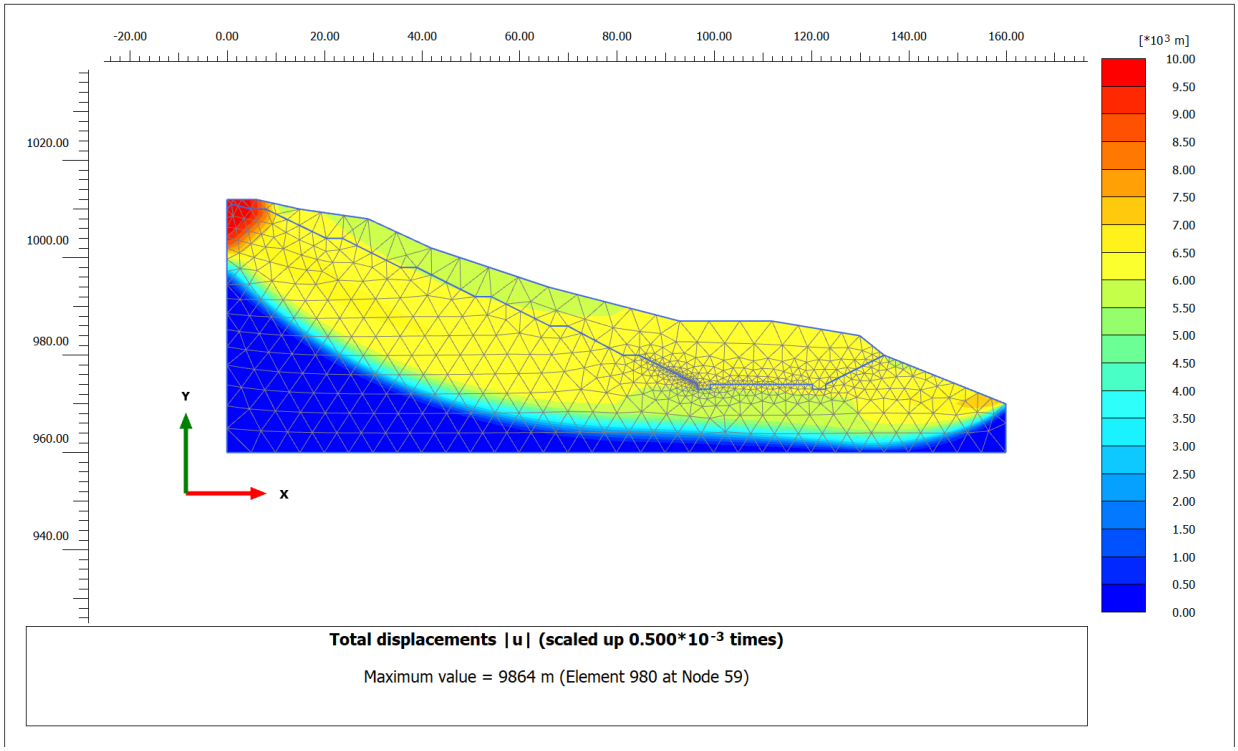


Fig IV.11 :Mesh Deformation during Phase 01



FigIV.12:Total Deformation during Phase 01

Phase 02: Excavation phase:plastic phase calculation type.

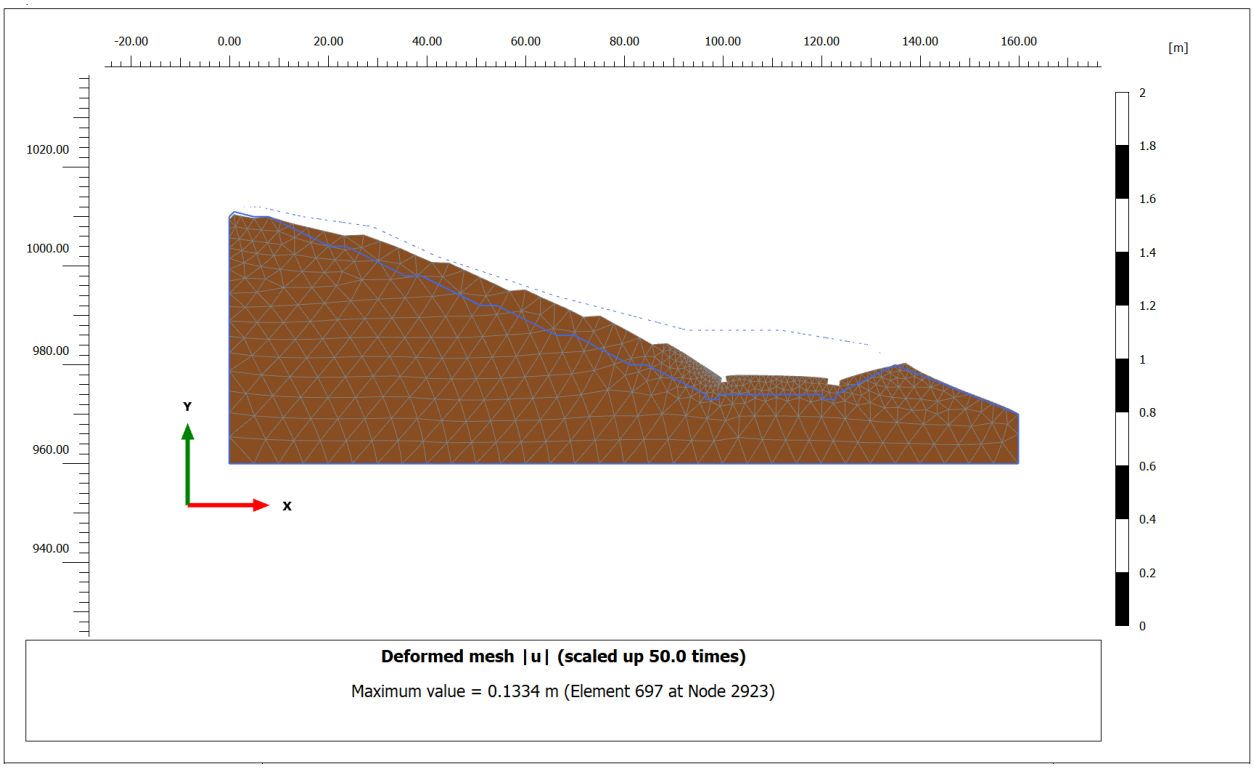


Fig IV.13:Mesh Deformation during Excavation Phase

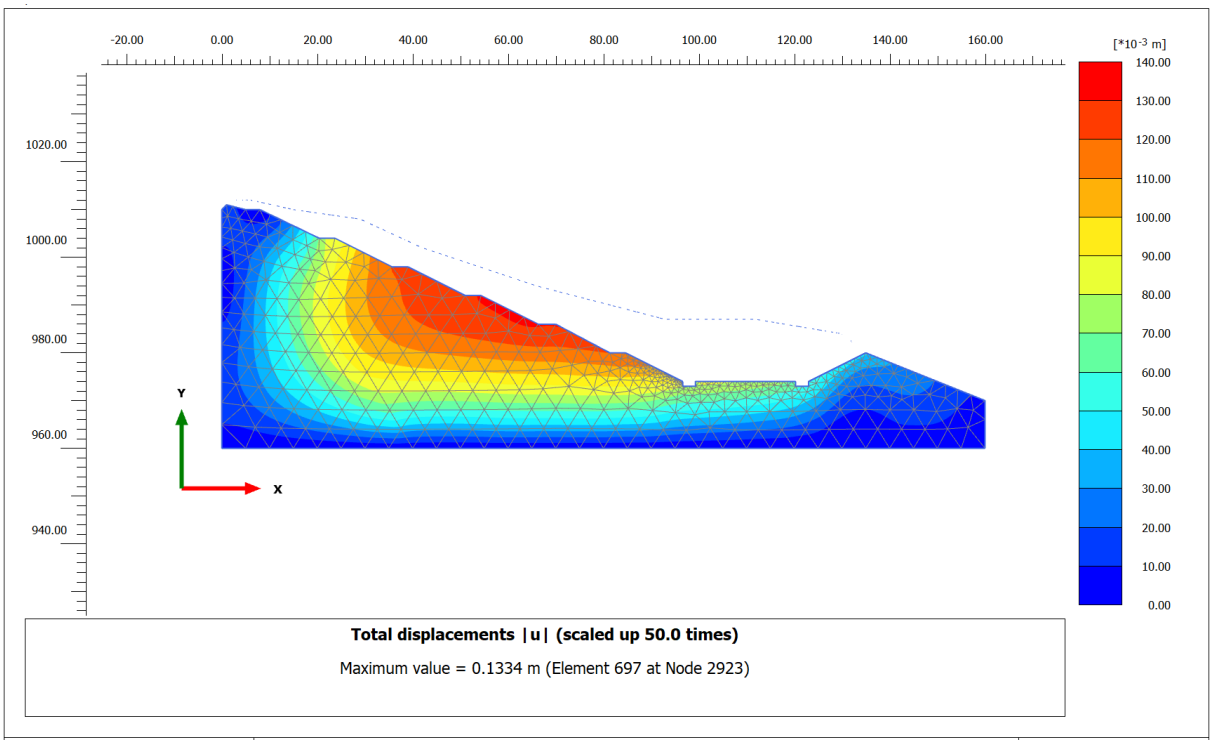


Fig IV.14: Total Deformation during Excavation Phase.

Phase 03: The safety factor of the Excavation phase.

Fig IV.15 :The safety factor of the Excavation phase.

Phase 04: Railway phase: plastic phase calculation type.

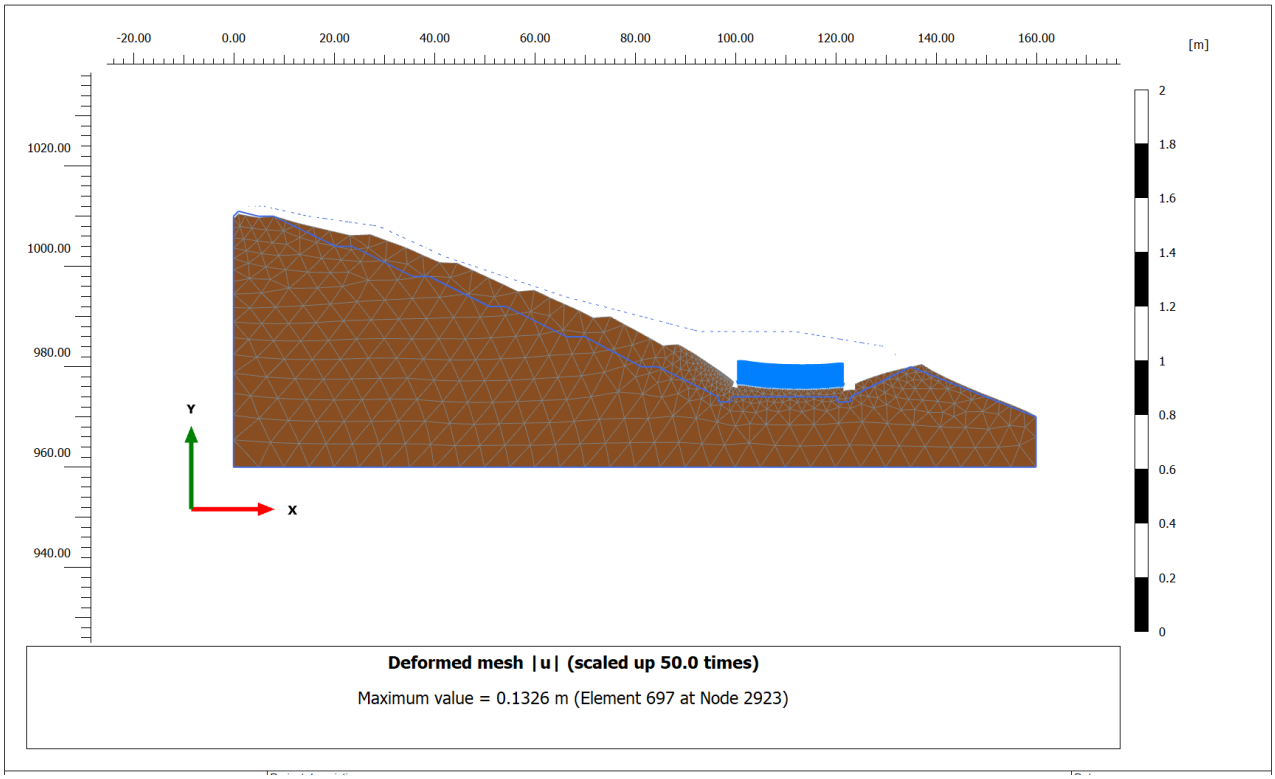


Fig IV.16:Mesh Deformation during Phase 04

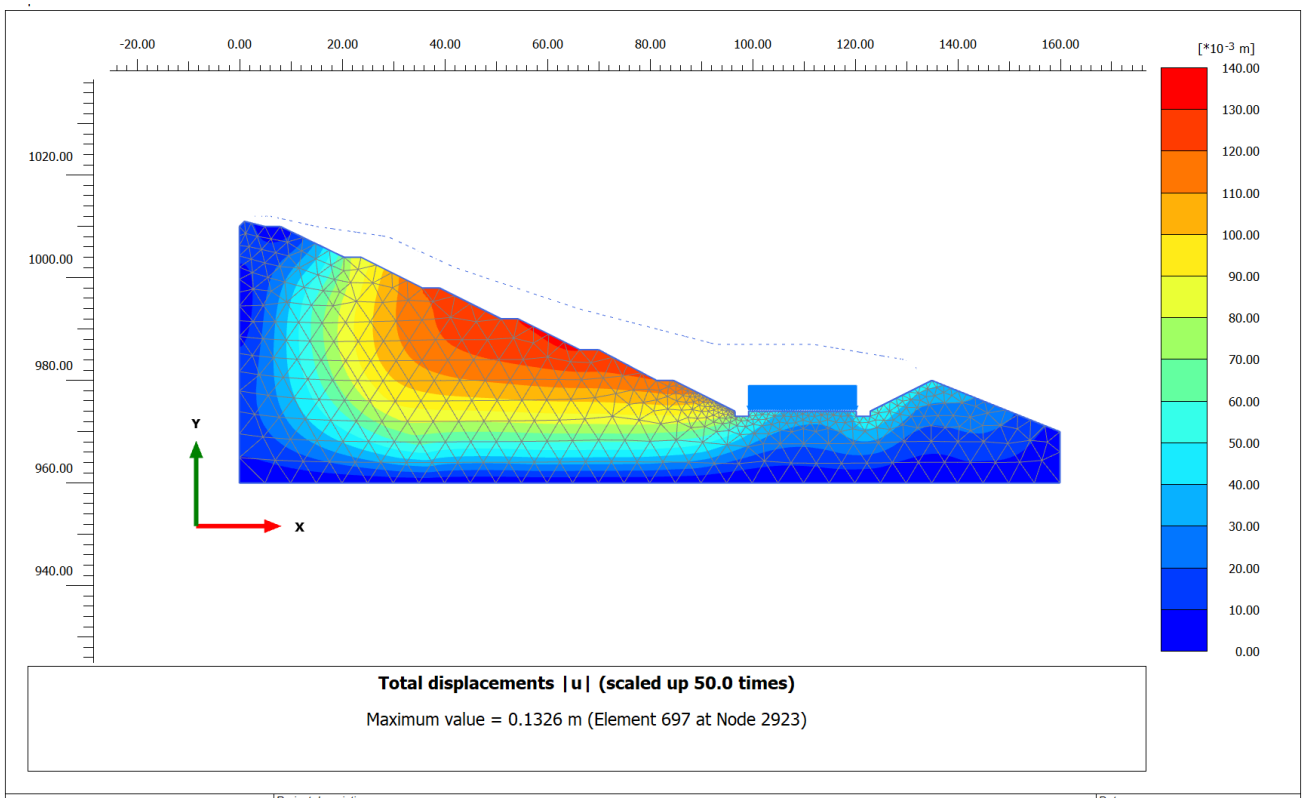
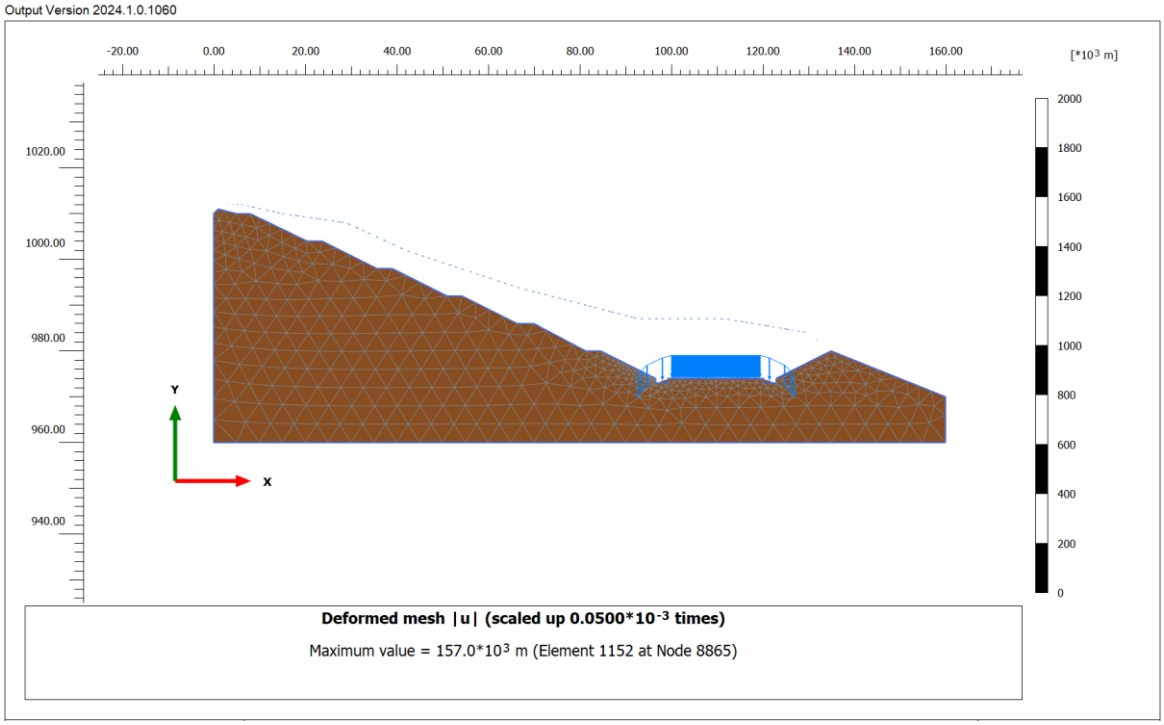


Fig IV.17:Total Deformation during Phase 04

Phase 05: The safety factor of the fourth phase.



FigIV.18:Mesh Deformation during Phase 05

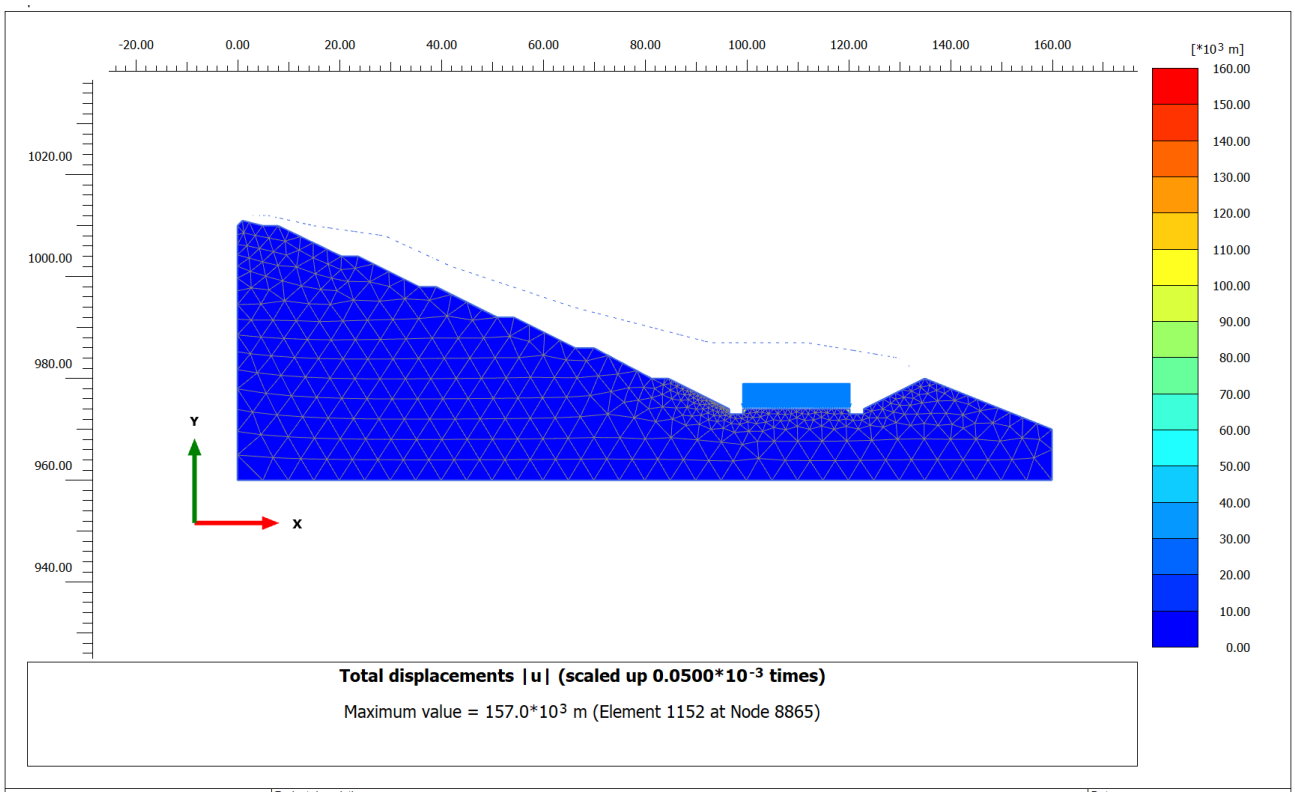


Fig IV.19**:** TotalDeformation during Phase 05.

Fs railway [Phase_5]

Initial

Classical mode

Safety

False

Picos

64 bit

0.5000

-0.01900E-9

		ΣM_{Weight}	1.000
M_{sf}	0.6018E-3	ΣM_{sf}	1.130

Fig IV.20:The safety factor of phase 05.

Phase 06: Dynamic phase:dynamics phase calculation type.

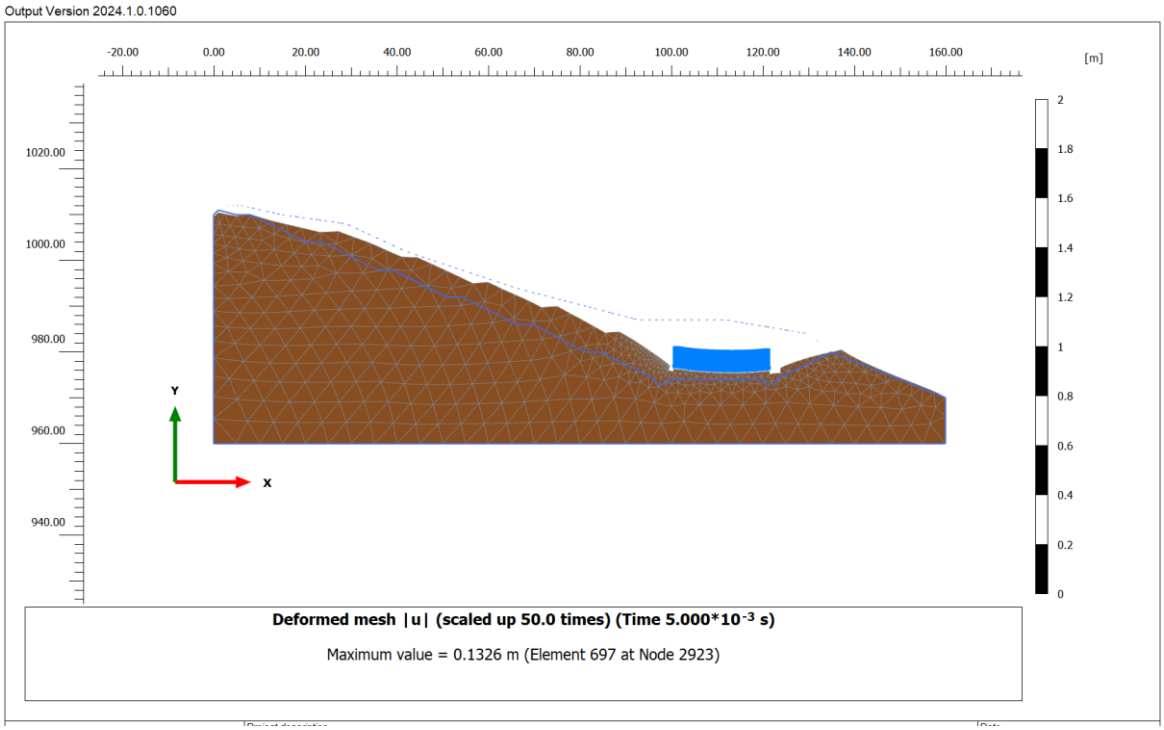


Fig IV.21:Mesh Deformation duringPhase 06(dynamic)

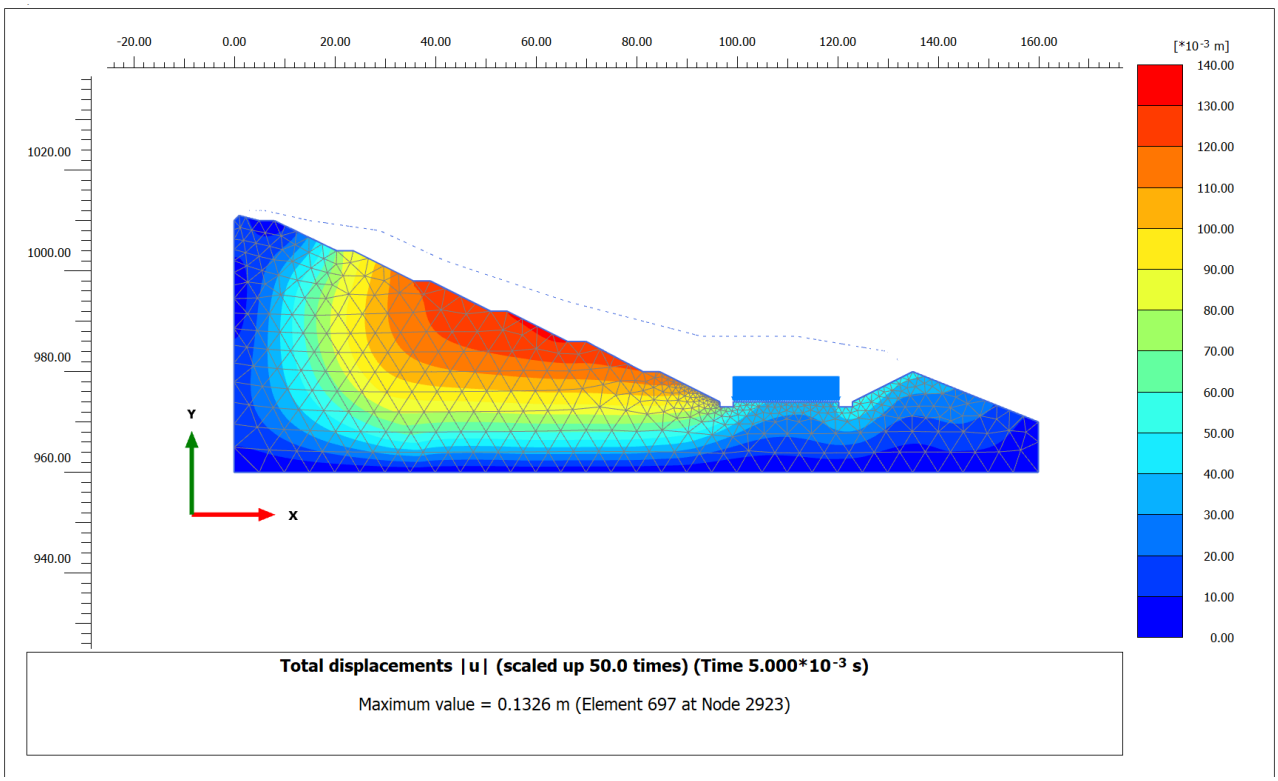


Fig IV.22:Total displacement during phase 06 (dynamic)

Dynamic [Phase_6]			
Initial			
Classical mode			
Dynamics analysis			
False			
Picos			
64 bit			
0.000			
0.06102			
		ΣM_{Weight}	1.000
M_{sf}	0.000	ΣM_{sf}	1.000

Fig IV.23:The safety factor of phase06 (Dynamic).

Phase 07: Rainfall phase (0.01m/day): fully coupled flow-deformation calculation type.

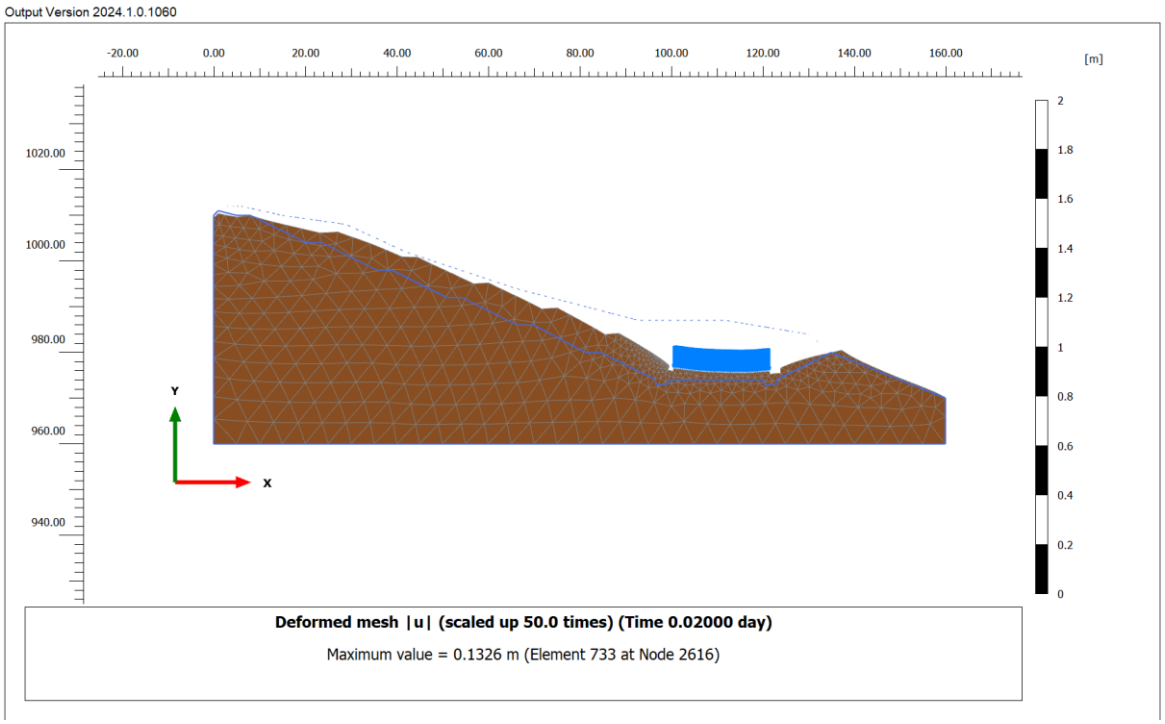
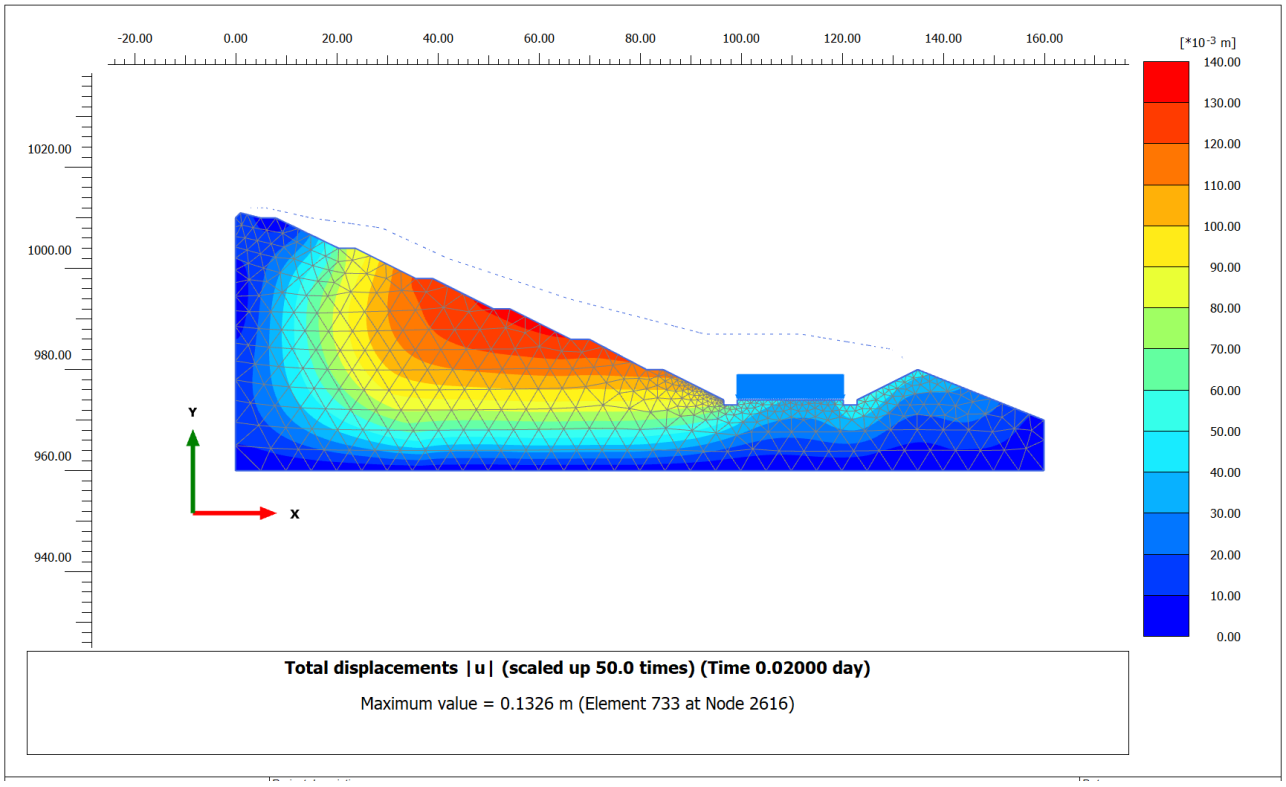


Fig IV.24:Mesh Deformation during Phase 07(rainfall).



FigIV.25:Total displacement during phase 07(rainfall).

Phase 08: The safety factor of the phase07.

Fs rain fall [Phase_9]

Initial

Classical mode

Safety

False

Picos

64 bit

0.5000

0.03493E-9

		ΣM_{Weight}	1.000
M_{sf}	5.000E-3	ΣM_{sf}	1.121

Fig IV.26:The safety factor of the phase07

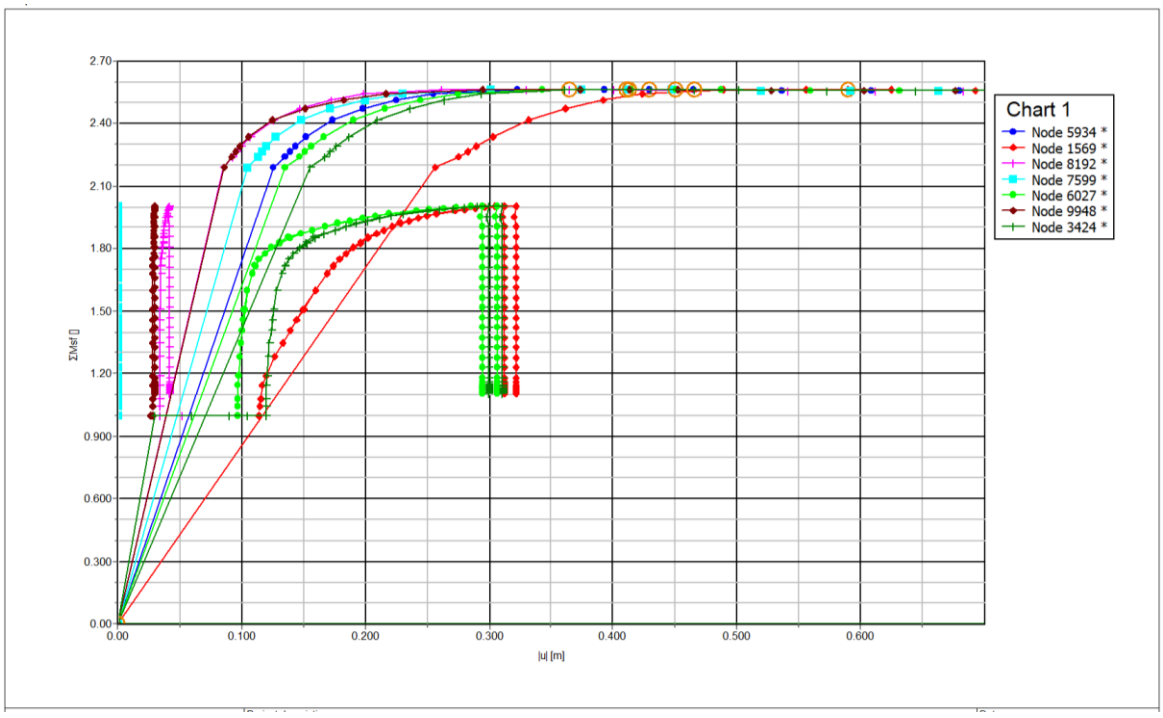


Fig IV.27 :Displacement versus Strngth Reduction Factor (Msf)

IV.2.3 Interpretation:

The Clayey facies exhibits concerning stability behavior throughout all calculation phases, with safety factors consistently dropping to critical levels particularly under rainfall infiltration. Water saturation drastically reduces shear strength, leading to progressive softening, increased pore pressure, and eventual slope failure. Unlike the resilient Limestone facies, this material shows no stable phases when subjected to hydraulic loading. The persistent low safety factors, exacerbated by wet conditions, demonstrate an urgent need for comprehensive stabilization measures, such as improved drainage systems, slope reinforcement, or even material replacement in high-risk zones to prevent catastrophic slope deformations.

IV.2.4 Limestone Layer facies (Turonian) :

A Define the Geometry: from the cross section imported as DXF AutoCAD file sheet and Material properties has been introduced

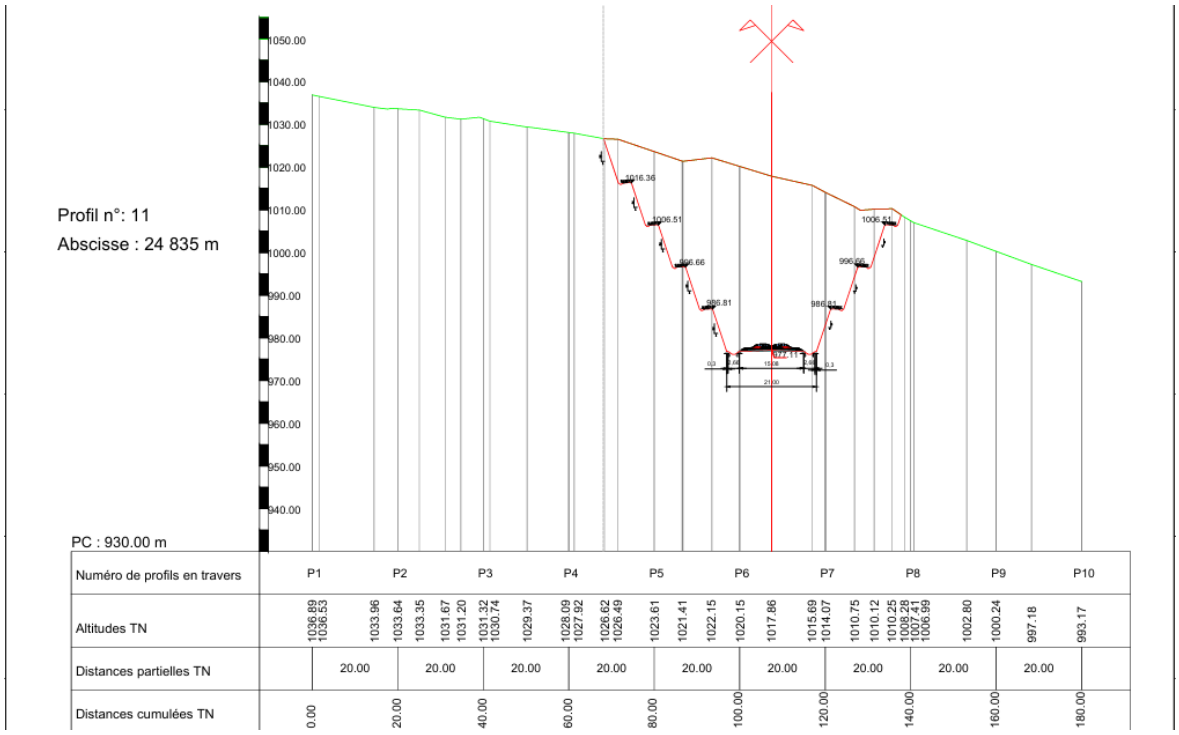
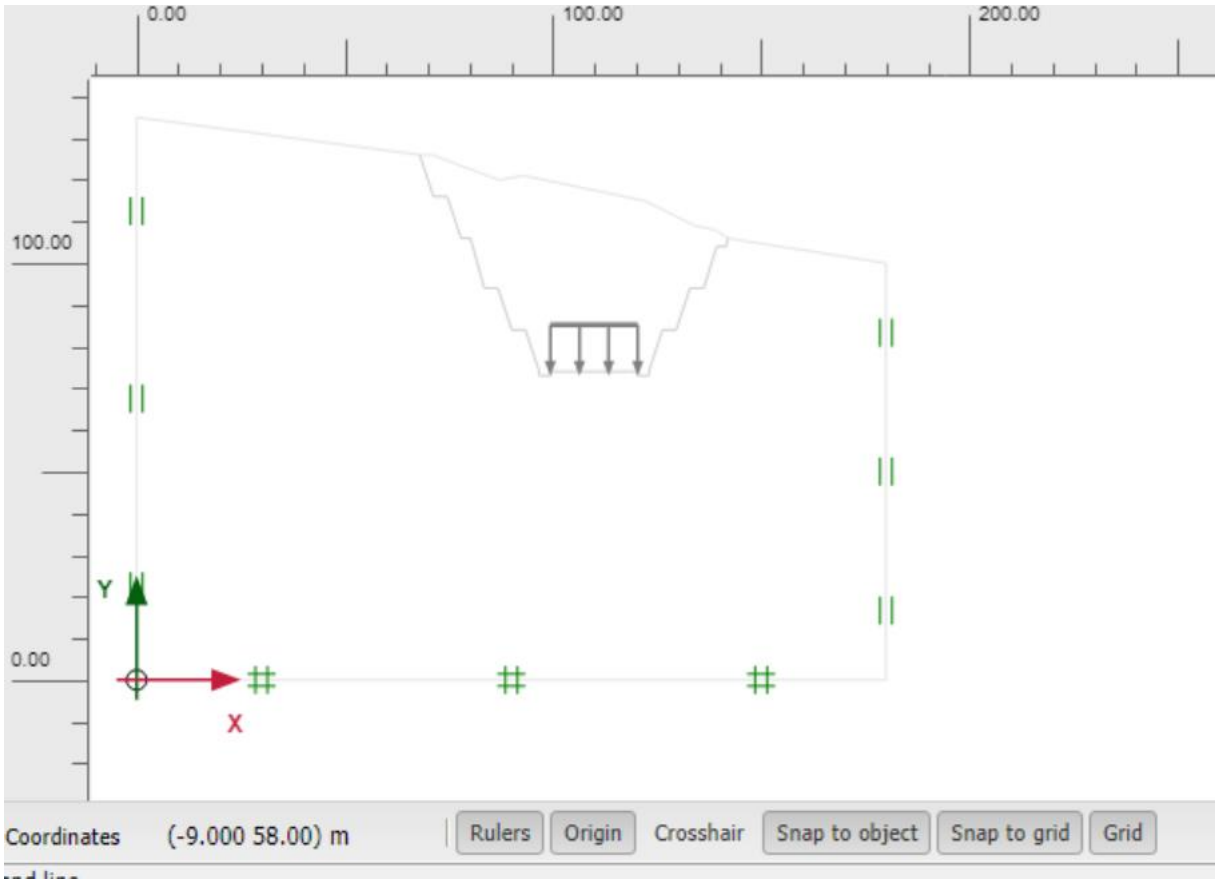


Fig IV.28: The Cross section of clayey soil.

B) Geometrical Molding of the Limestone Layer:



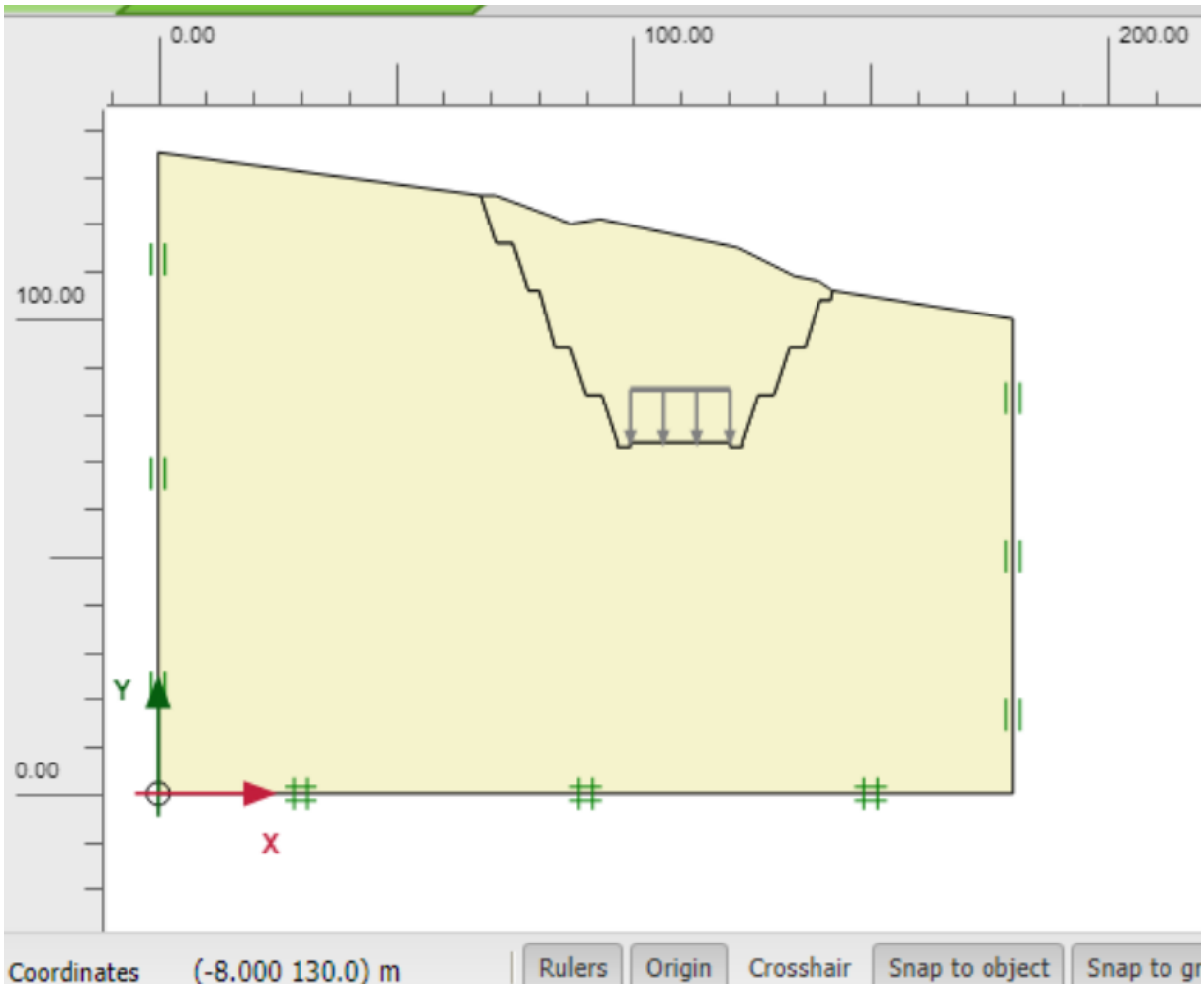


Fig IV.29: The Geometry Limestone Layer.

C) Material Properties and boundaries Conditions:

Parameter	Name	Value	Unit
Material model	Model	Jointed Rock	-
Type of material behavior	Type	Non-porous	-
Saturated Unit Weight	γ_{sat}	-	KN/m^3
Unsaturated Unit Weight	γ_{unsat}	23	KN/m^3
Young's modulus	E'	30000000	KN/m^2
Poisson's ratio	ν	0.21	-

Table IV.1: Limestone layer properties.

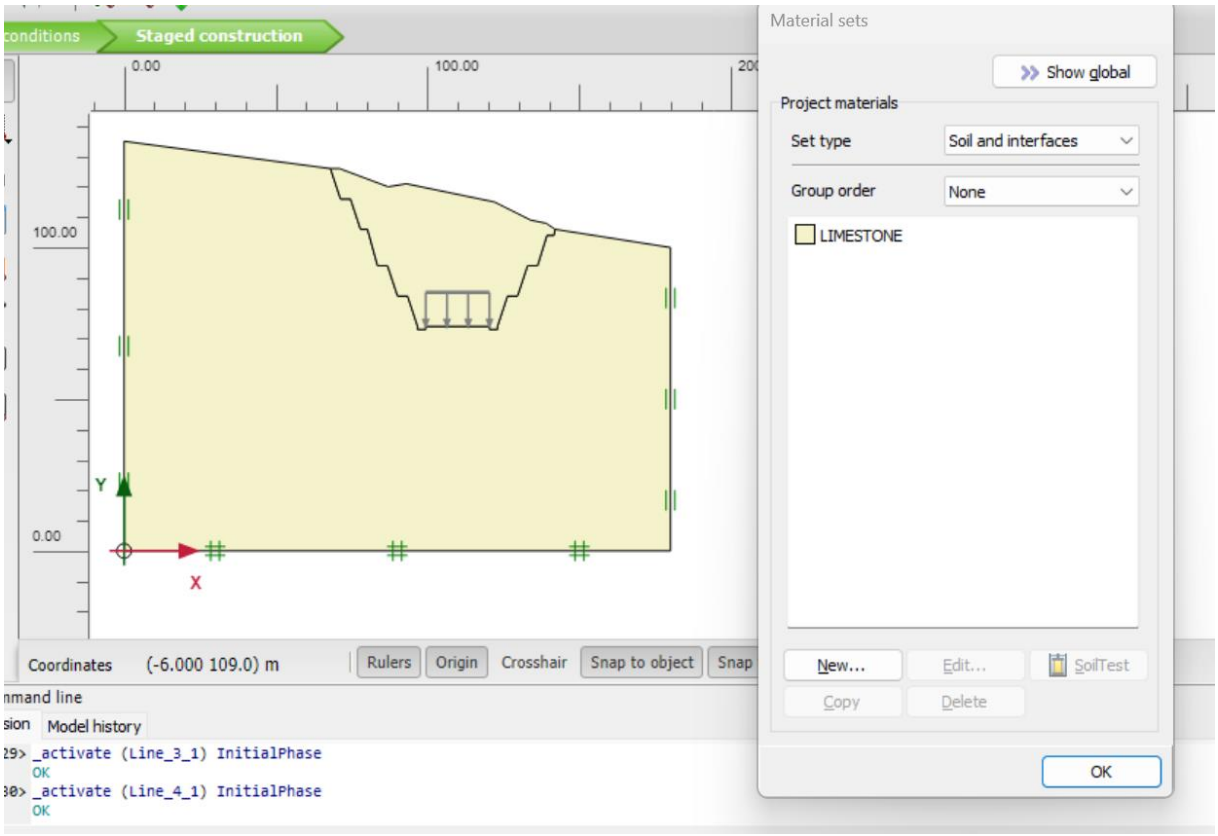


Fig IV.30:Input material.

D. Mesh generation:

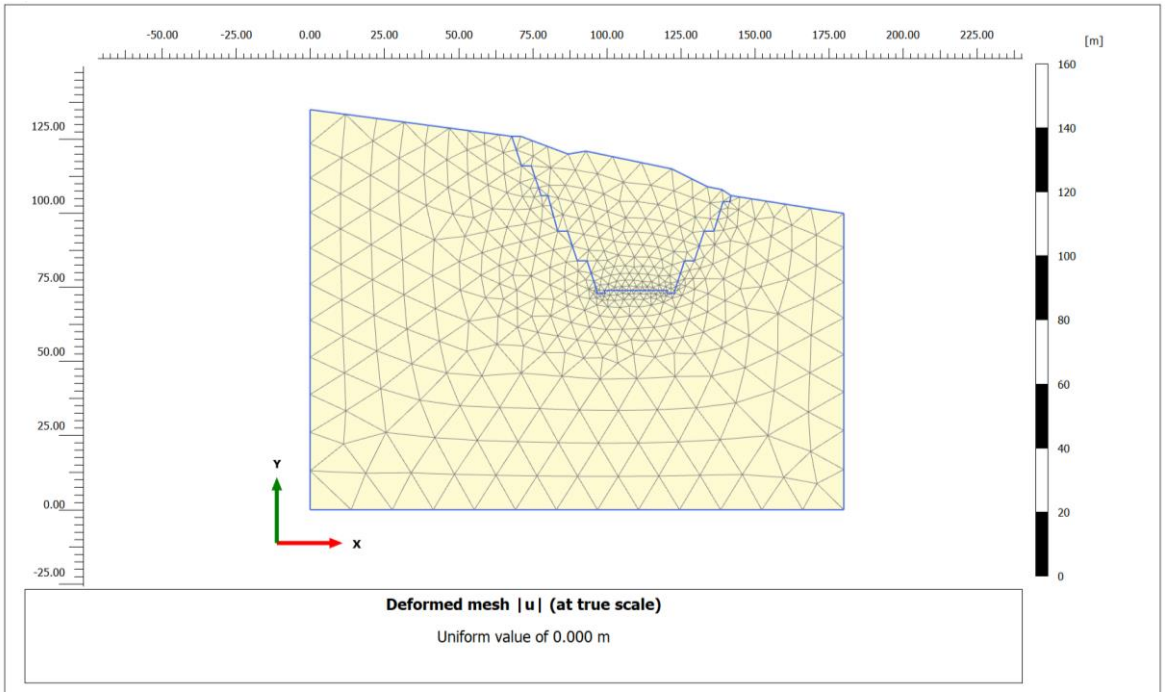


Fig IV.31: Generate Mesh.

F).Flow conditions:

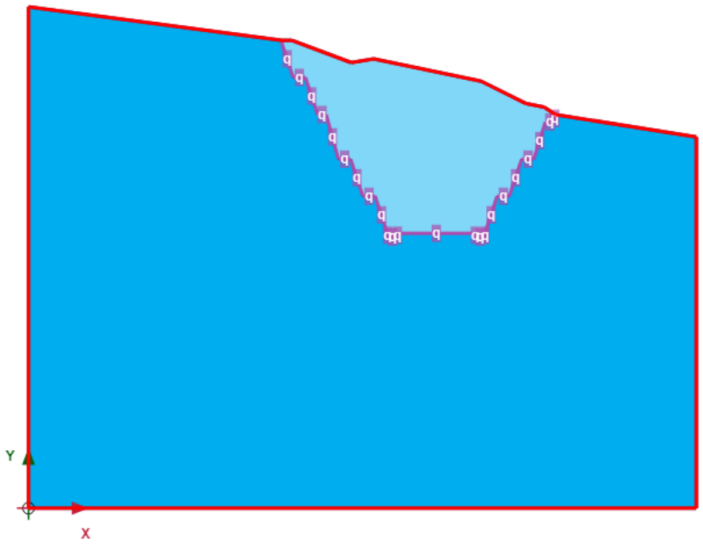


Fig IV.32: Flow condition.

G) Construction Stages and Calculation Types:

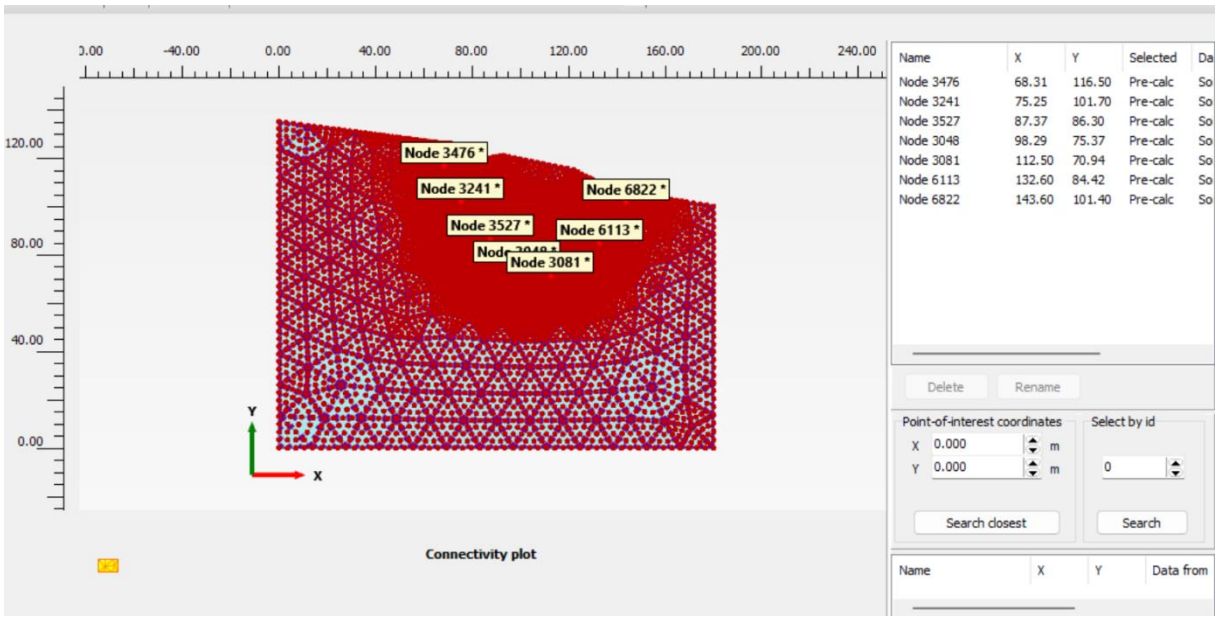


Fig IV.33: the nodes of calculation phases .

Sequence of Calculation Phases:

- Initial phase: using K_0 Procedure calculation type.

- Phase 01: the safety factor of the initial phase.

- Phase 02: Excavation phase :plastic phase calculation type.

- Phase 03: the safety factor of excavation phase.

-Phase04 :Railway phase: plastic phase calculation type.

- Phase 05: The safety factor of the railway phase.

- Phase 06: Dynamic phase:dynamics phase calculation type.

-Phase 07 :Rainfall phase (0.01m/day): fully coupled flow-deformation calculation type.

-Phase 08 :The safety factor of the rainfall phase.

This step-by-step procedure allows for a comprehensive understanding of slope behavior under both static and dynamic loads, capturing the key deformation and failure mechanisms that may occur.

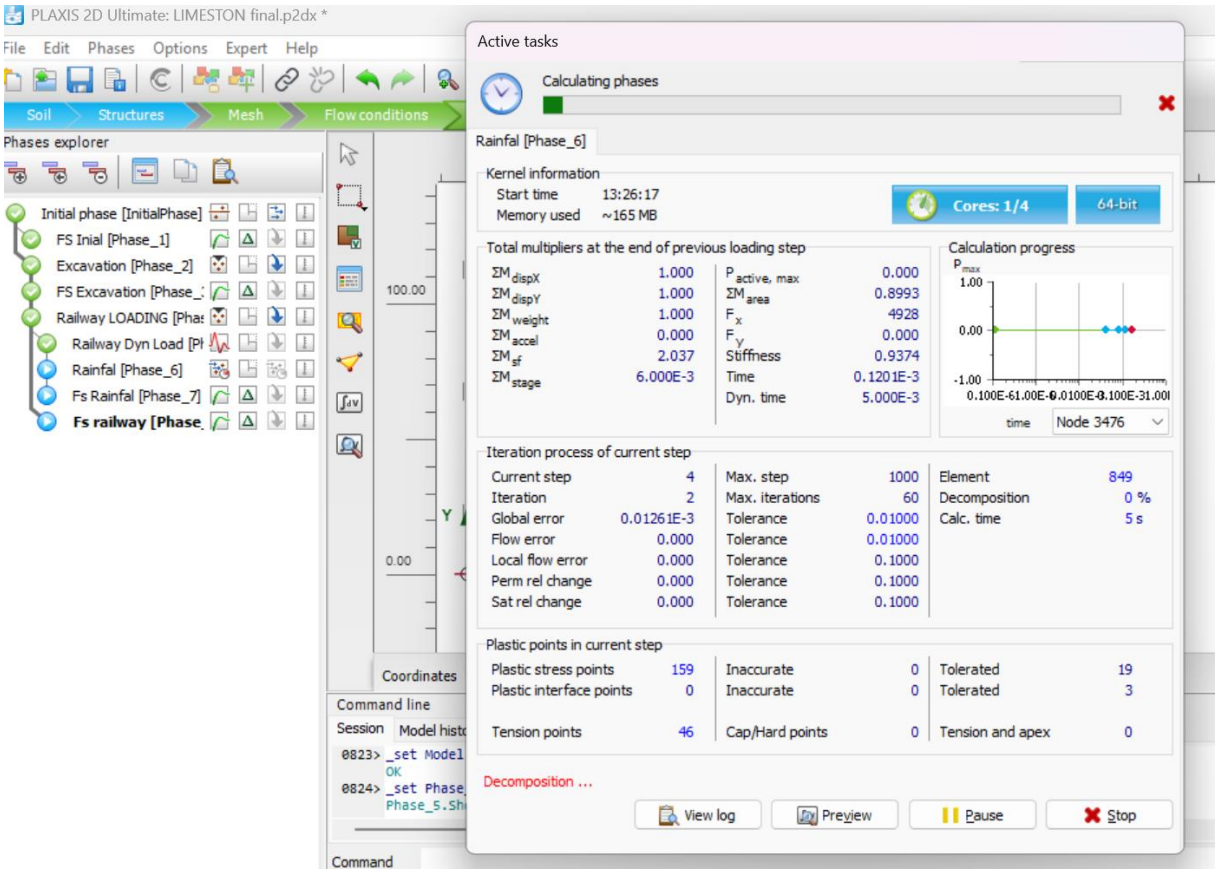


Fig IV.34: Configuration of calculation phases in PLAXIS 2D.

IV.2.5Results and discussion of Limestone

This section presents and interprets the simulation results of all phases:

Initial phase: using calculation K_0 poceduretype:

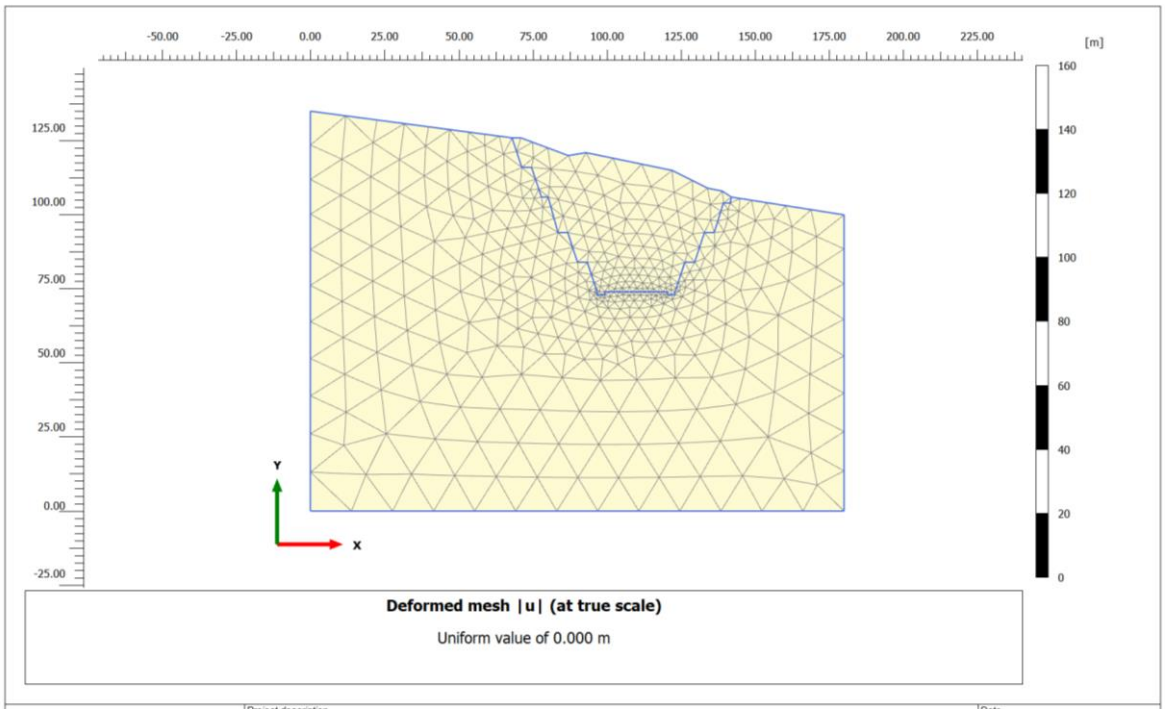


Fig IV.35 :Mesh Deformation during Initial Phases

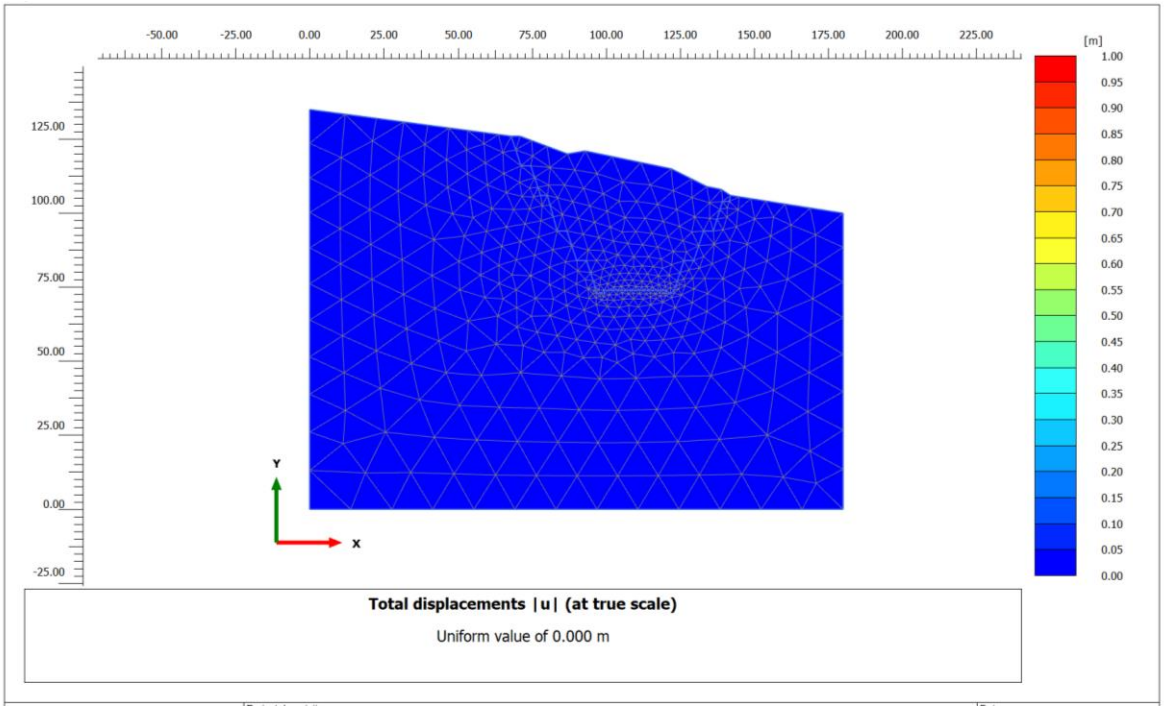


Fig IV.36 :Total Deformation during Initial Phases .

Phase 01: the safety factor of the inial phase.

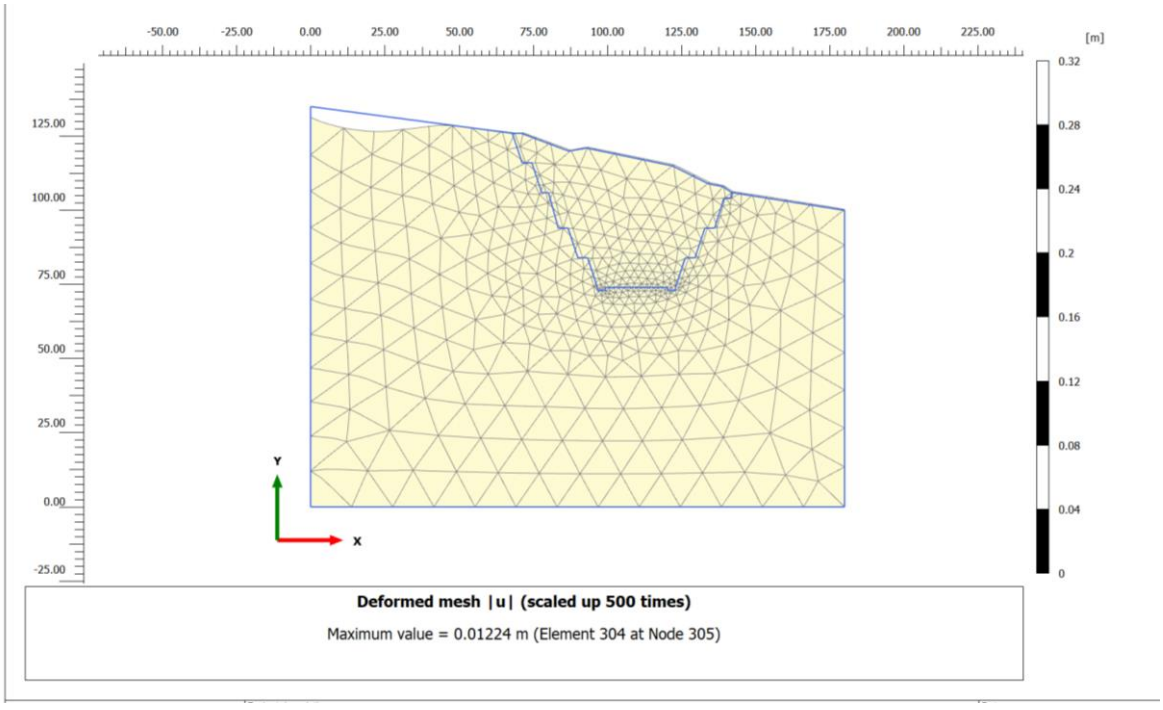


Fig IV.37 :Mesh Deformation during Phase 01.

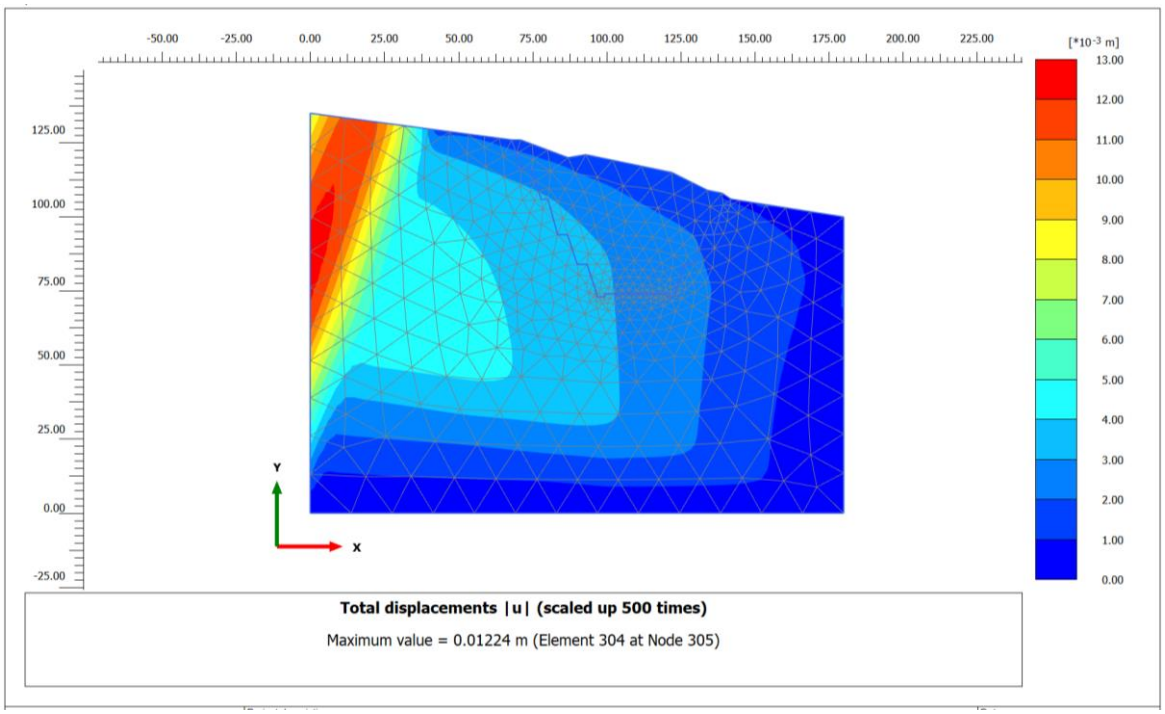


Fig IV.38:Total Deformation during Phase 01

Phase 02: Excavation phase:plastic phase calculation type.

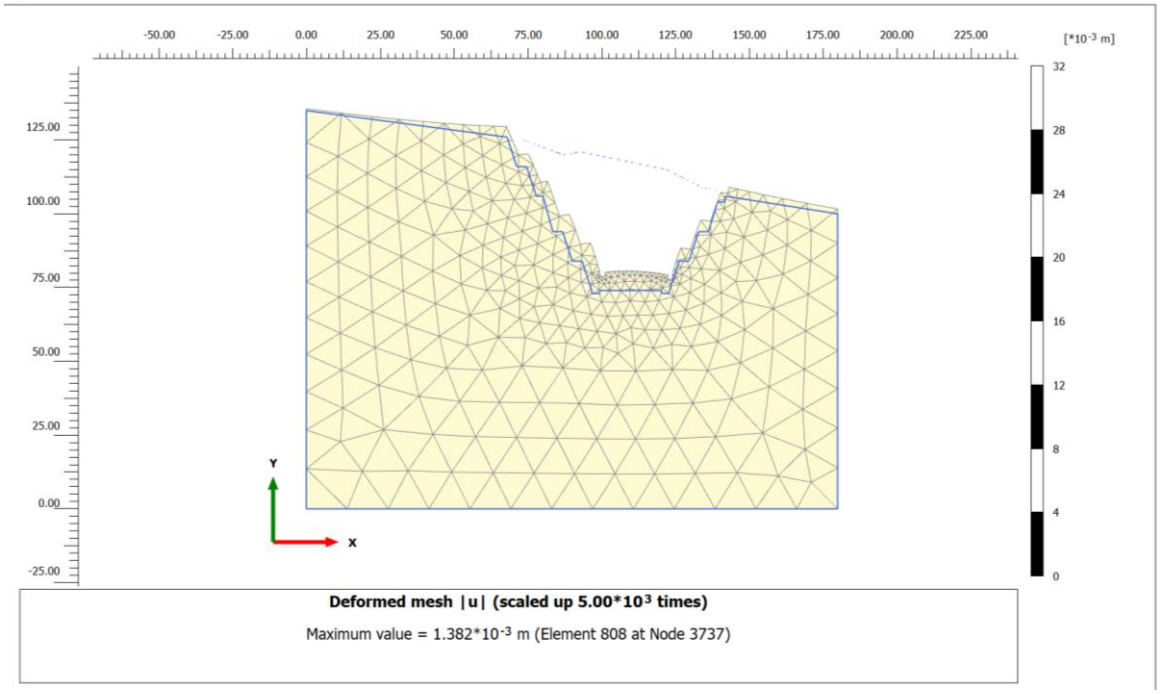


Fig IV.39:Mesh Deformation during Excavation Phase.

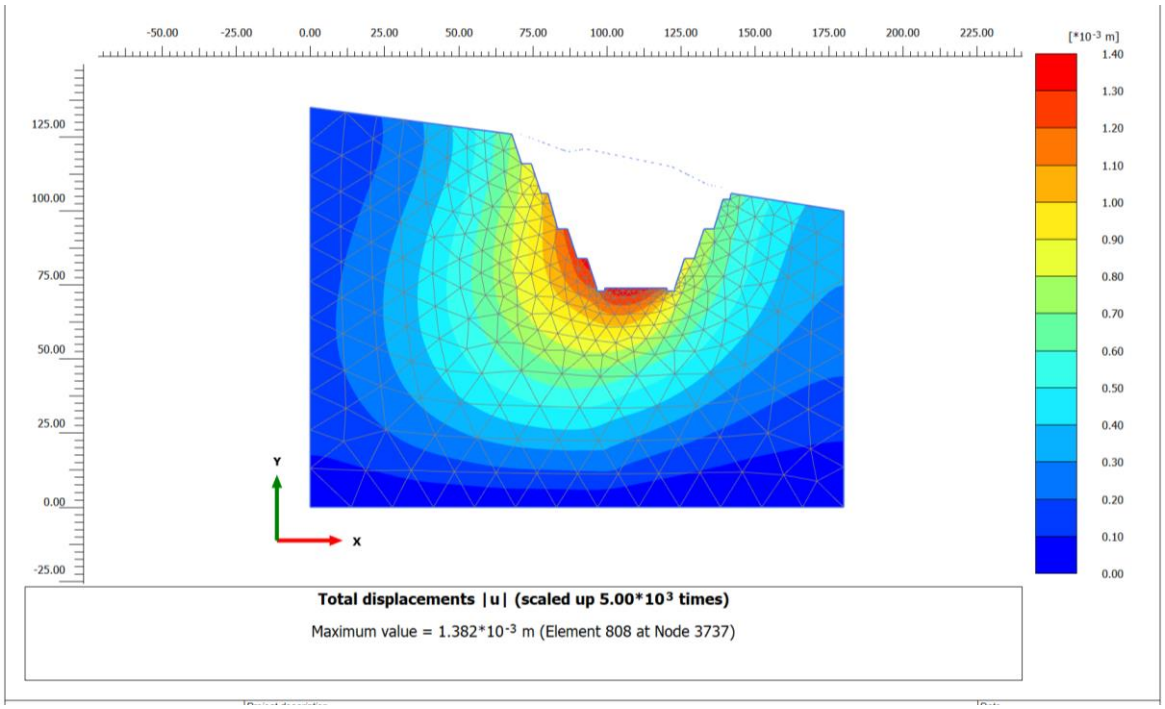


Fig IV.40:Total Deformation during Excavation Phase.

Phase 03: The safety factor of the Excavation phase.

FS Excavation [Phase_3]			
Initial			
Classical mode			
Safety			
False			
Picos			
64 bit			
2.000			
0.01187E-3			
		ΣM_{Weight}	1.000
M_{sf}	2.115E-3	ΣM_{sf}	2.037

Fig IV.41 :The safety factor of the Excavation phase.

Phase 04: Railway phase: plastic phase calculation type.

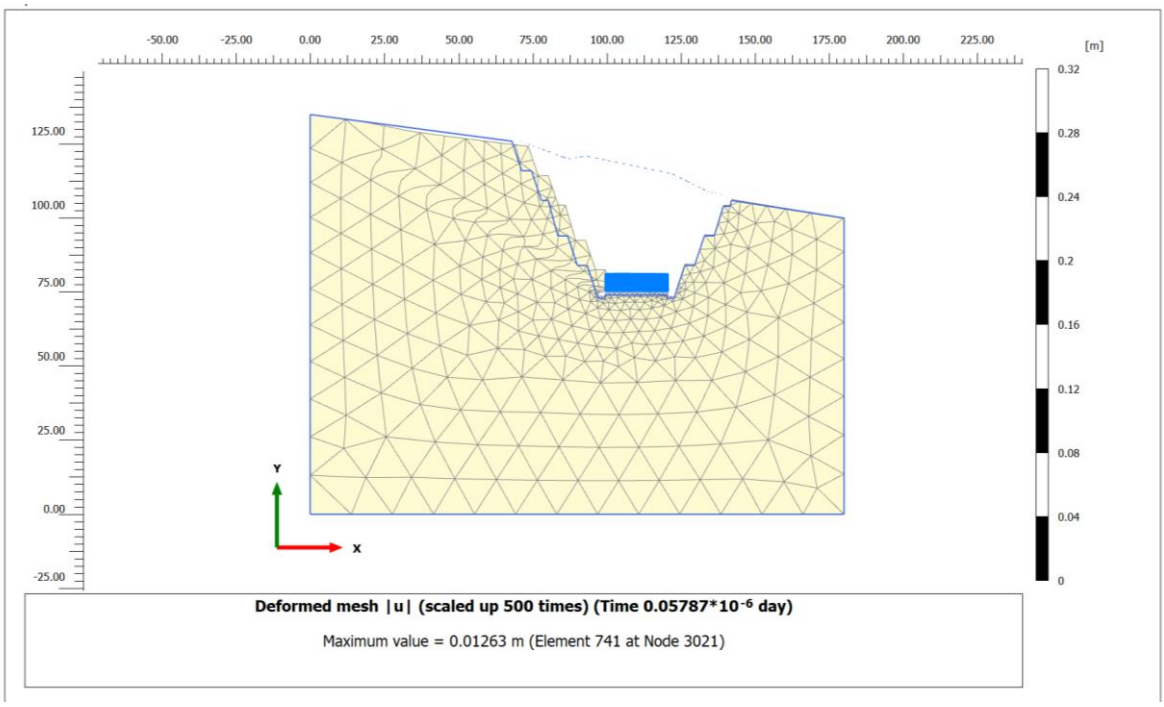


Fig IV.42:Mesh Deformation during Phase 04

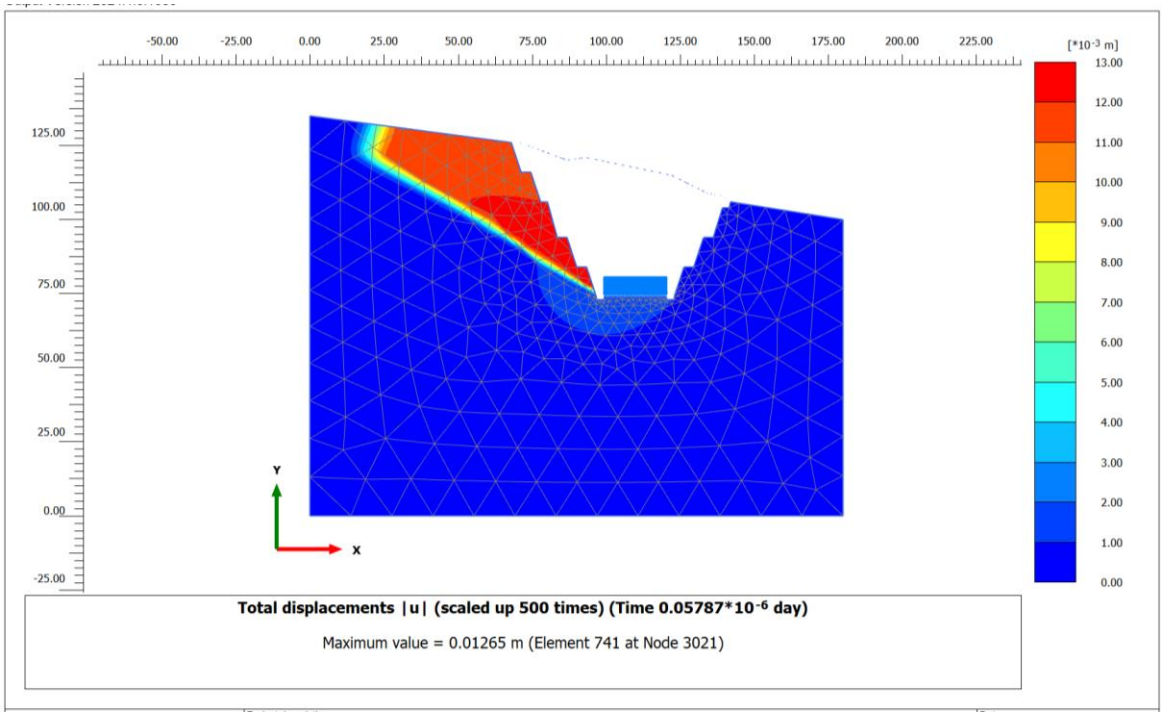


Fig IV.43:Total Deformation during Phase 04

Phase 05: The safety factor of the phase 04.

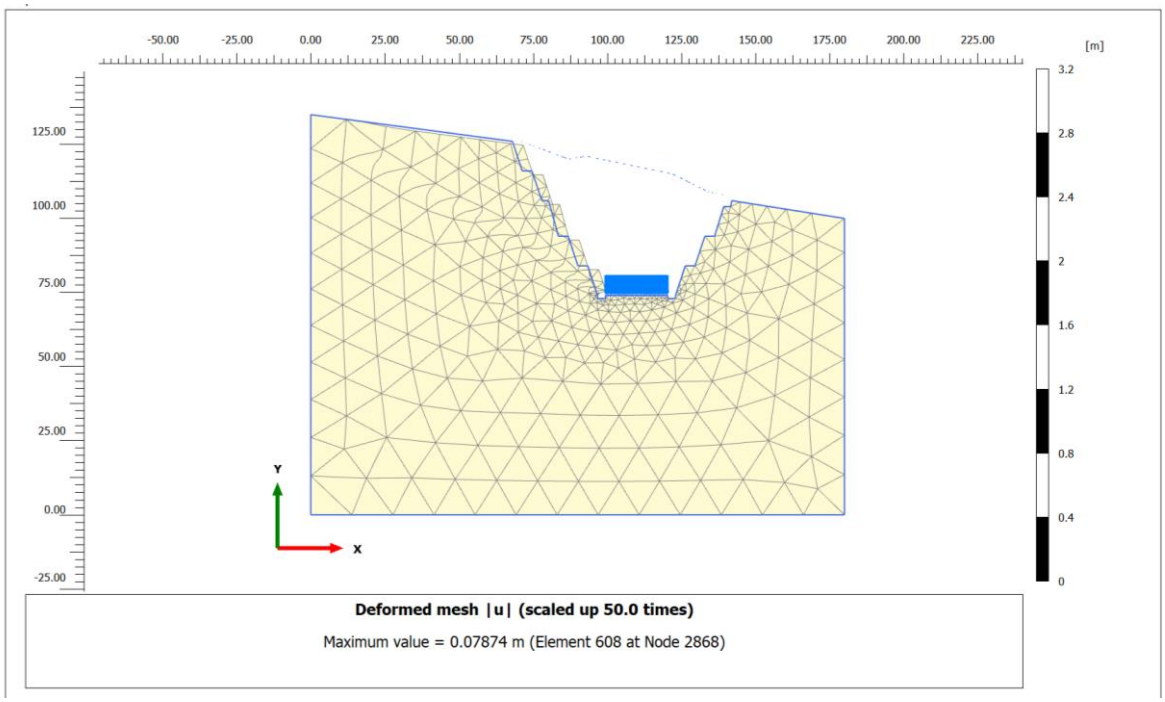


Fig IV.44:Mesh Deformation during Phase 05

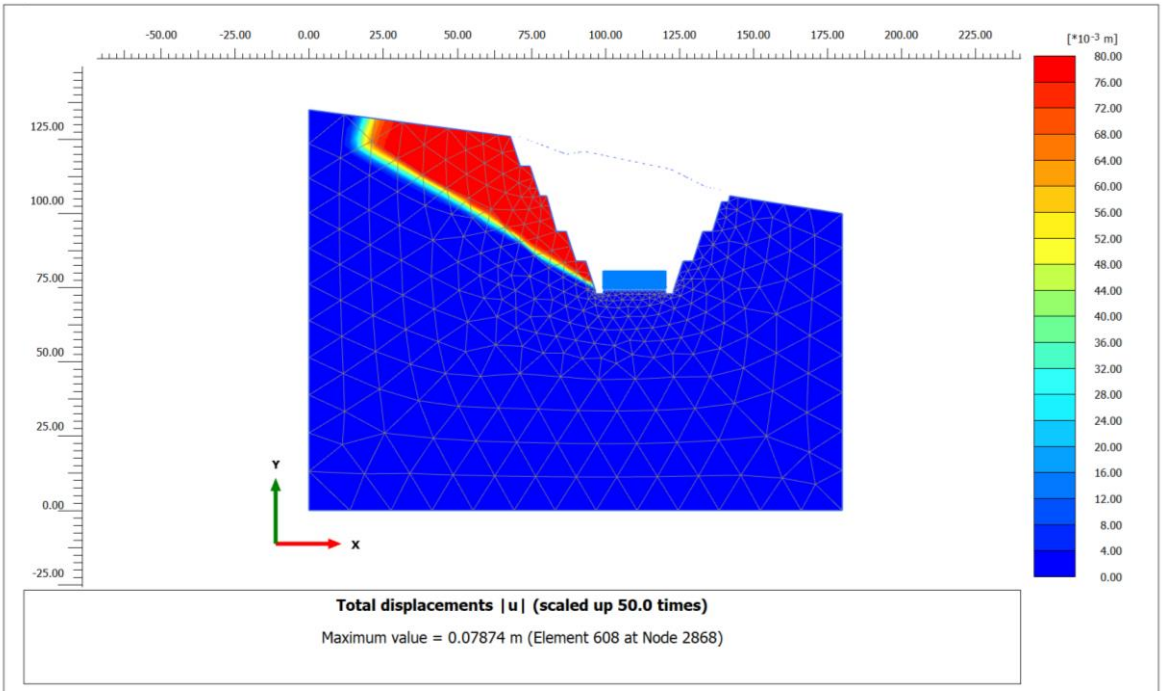


Fig IV.45**:** TotalDeformation during Phase 05.

Fs railway [Phase_5]			
Initial			
Classical mode			
Safety			
False			
Picos			
64 bit			
2.000			
-0.07353E-3			
		ΣM_{Weight}	1.000
M_{sf}	-4.917E-3	ΣM_{sf}	2.074

Fig IV.46:The safety factor of phase 05.

Phase 06: Dynamic phase:dynamics phase calculation type.

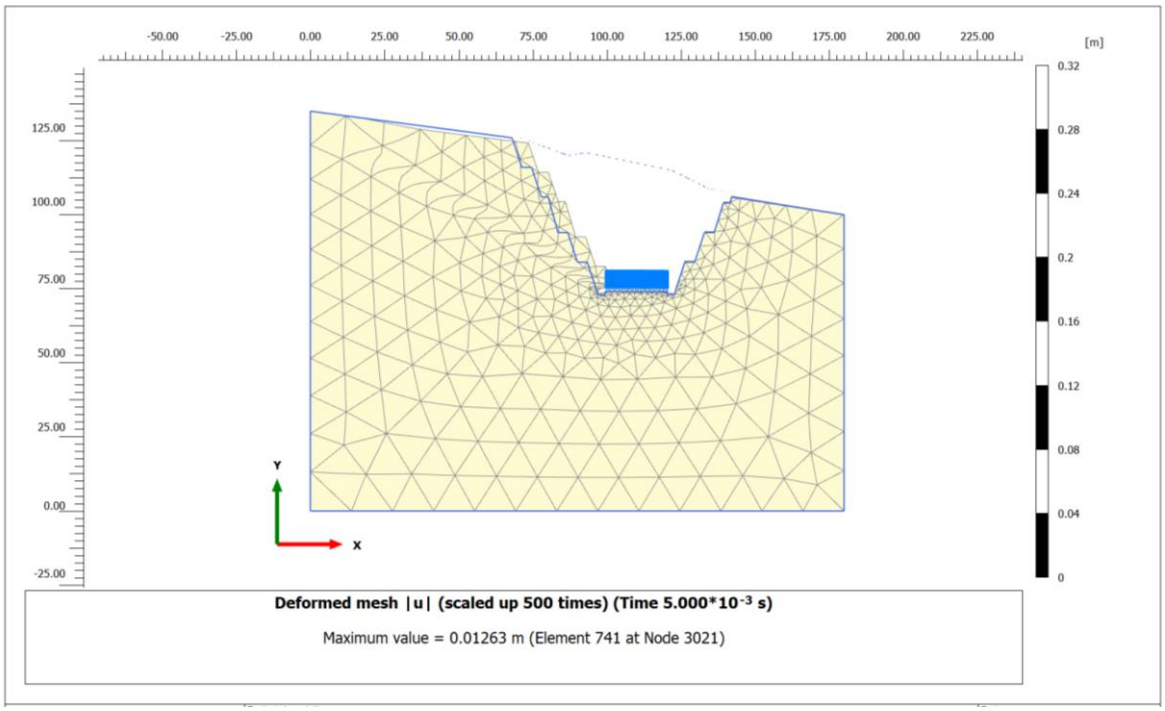


Fig IV.47:Mesh Deformation during Phase 06(dynamic)

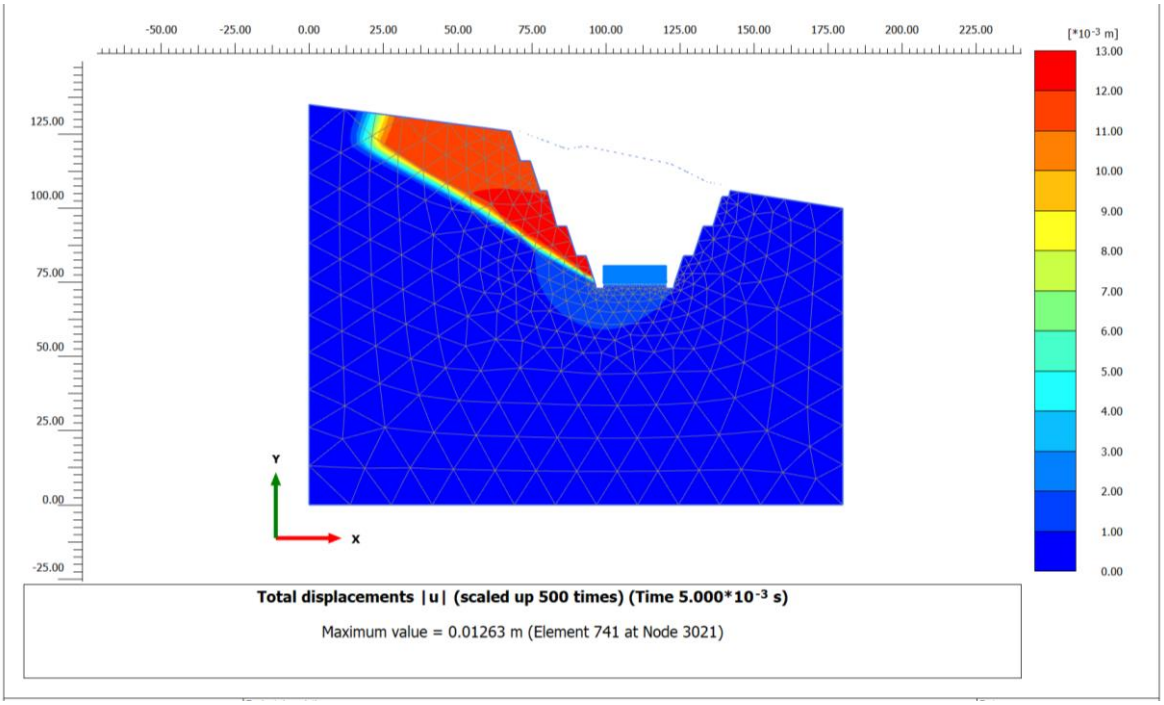


Fig IV.48:Total displacement during phase 06 (dynamic)

Phase 07: Rainfall phase (0.01m/day): fully coupled flow-deformation calculation type.

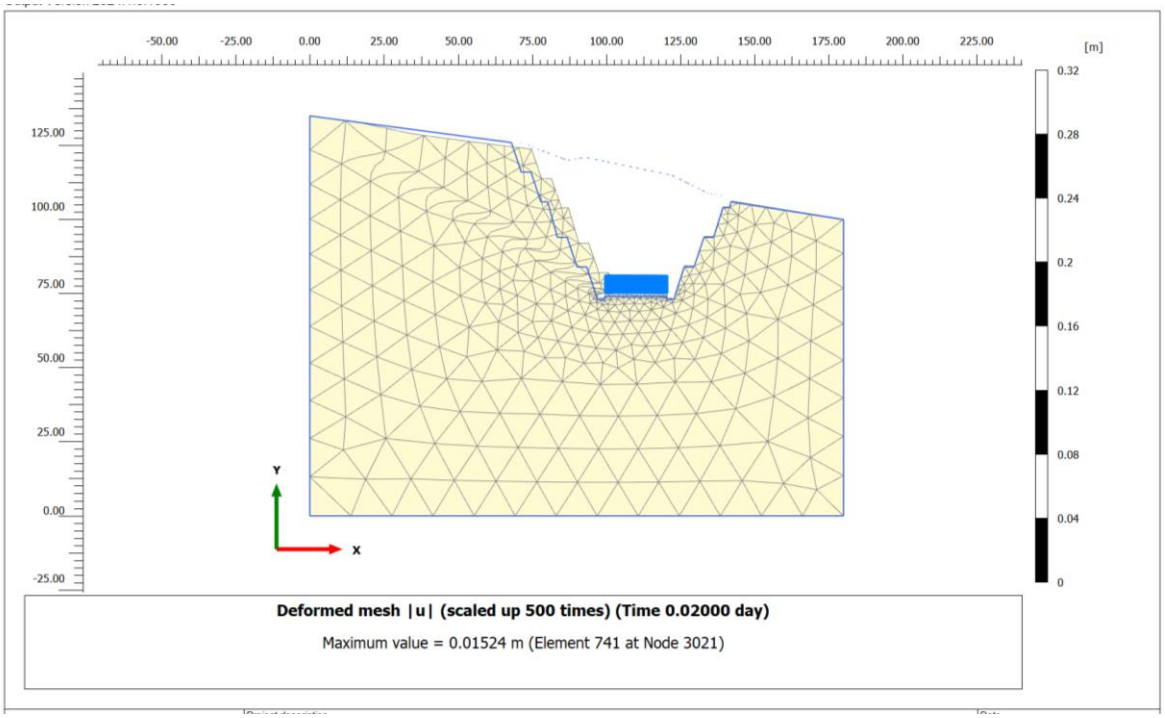
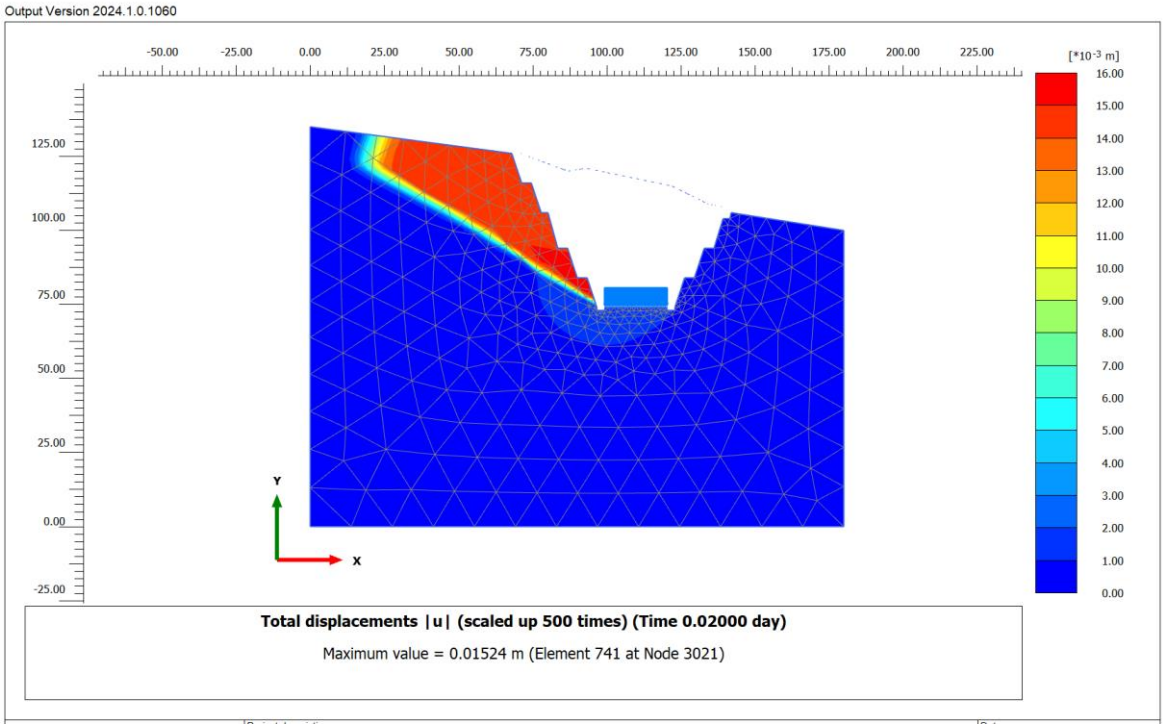


Fig IV.49:Mesh Deformation during Phase 07(rainfall).



FigIV.50:Total displacement during phase 07(rainfall).

Phase 08: The safety factor of the phase07.

Fs Rainfal [Phase_7]			
Initial			
Classical mode			
Safety			
False			
Picos			
64 bit			
2.000			
-2.452E-6			
		ΣM_{Weight}	1.000
M_{sf}	4.600E-3	ΣM_{sf}	2.117

C

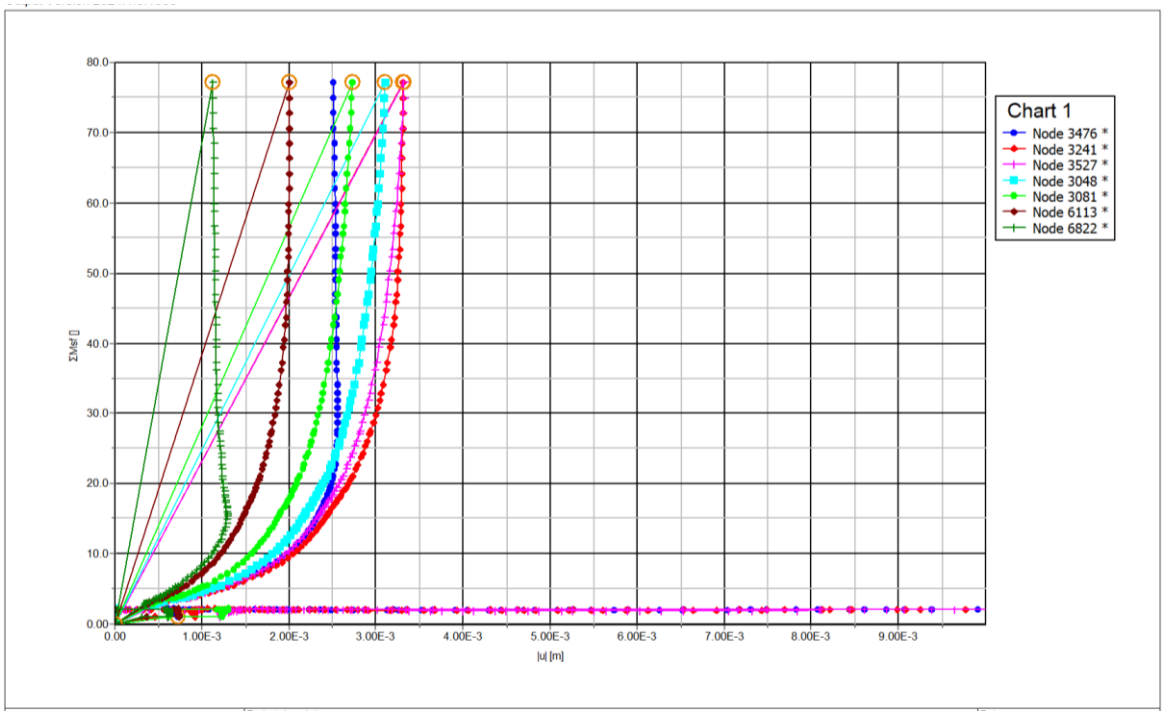


Fig IV.51 :Displacement versus Strngth Reduction Factor (Msf)

IV.2.6Interpritation (Limestone):

The Limestone facies demonstrates exceptional stability across all calculation phases, maintaining high safety factors regardless of external conditions, including rainfall infiltration. Its inherent strength and low permeability prevent significant pore pressure buildup, ensuring consistent performance even under hydraulic loading. Unlike the Clayey facies, this material shows no susceptibility to water-induced weakening or deformation. The robust nature of the Limestone facies eliminates the need for additional stabilization measures, making it the most reliable and low-risk material in the slope design.

IV.2.7 Diapiric clayey soil formation (Triasic facies) :

A) Define the Geometry: from the cross section imported as DXF AutoCAD file sheet and Material properties has been introduced

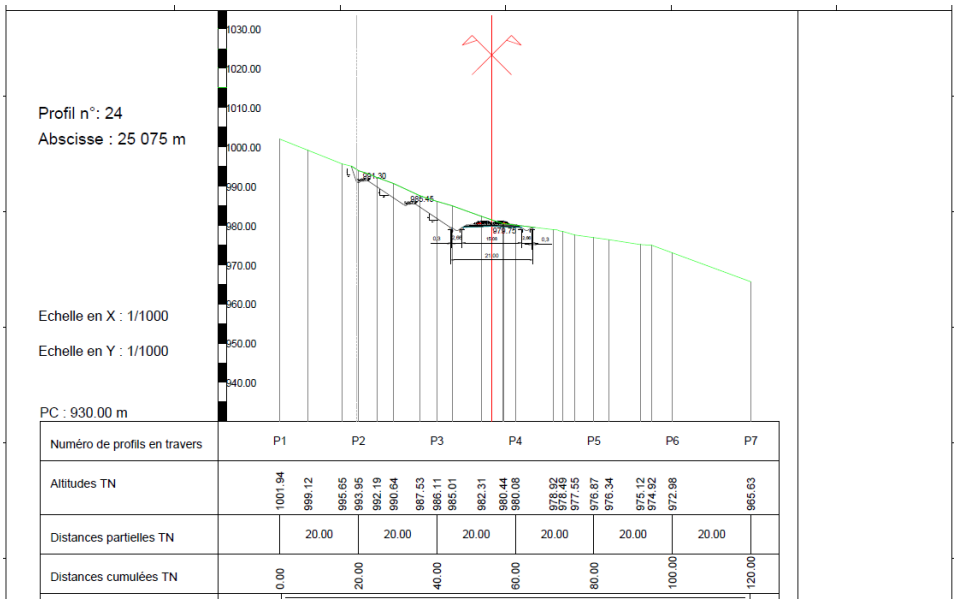


Fig IV.52: The Cross section of clayey soil.

B) Geometrical modeling of the Triassic layer:



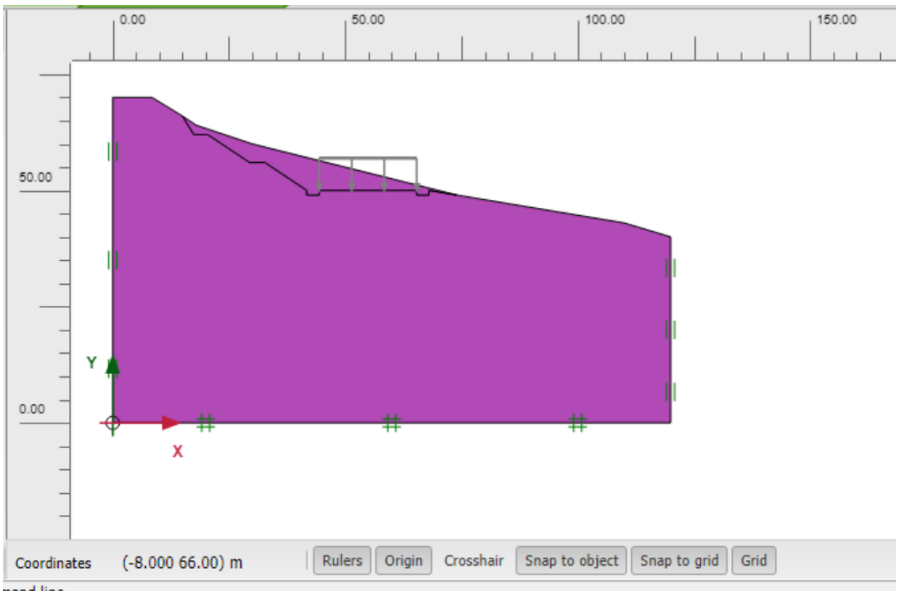
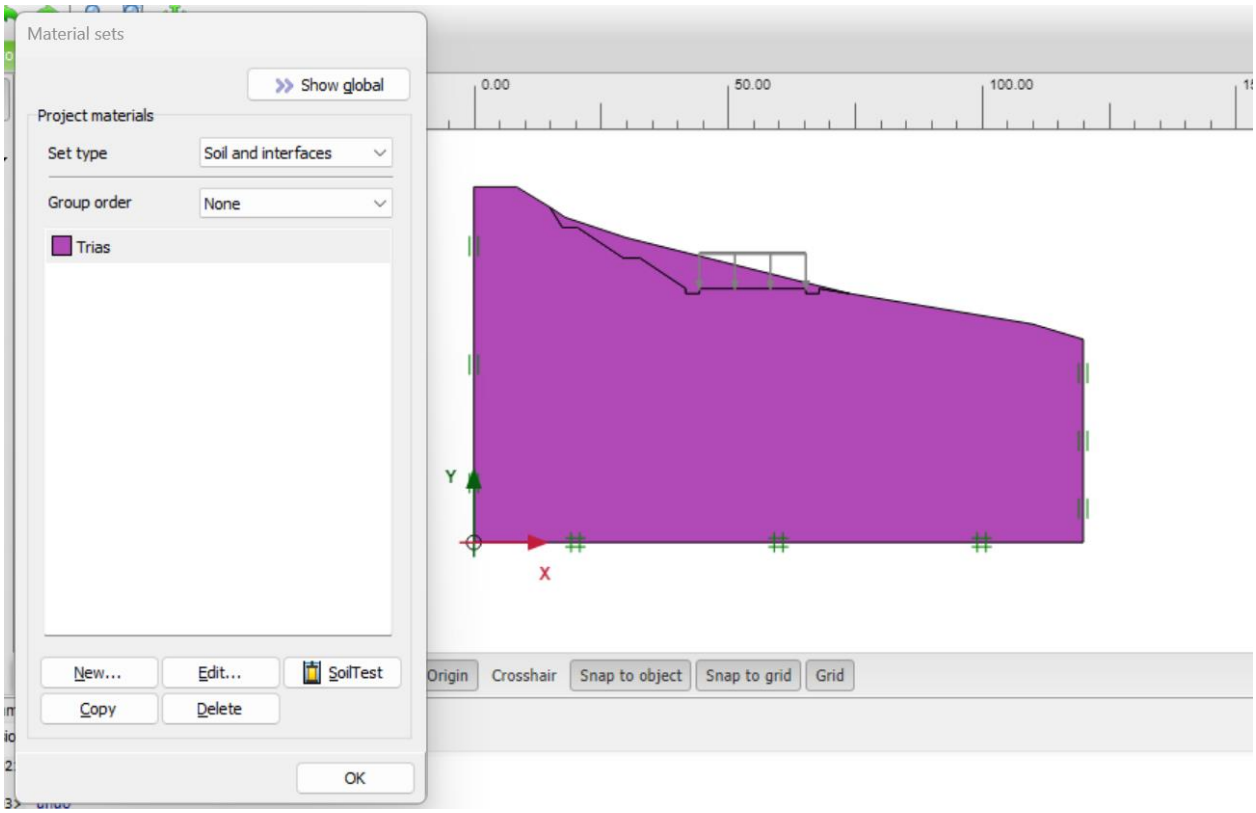


Fig IV.53: The Geometry Clayey Layer.

C) Material Properties:

Parameter	Name	Value	Unit
Material model	Model	Mohr-Coulomb	-
Type of material behavior	Type	Drained	-
Saturated Unit Weight	γ_{sat}	21.5	KN/m^3
Unsaturated Unit Weight	γ_{unsat}	19	KN/m^3
Young's modulus	E'	500000	KN/m^2
Poisson's ratio	**N**	0.23	-

Table IV.03:Clay (Turonian)layer properties.



FigIV.54:Input material .

D).Boundaries Conditions:

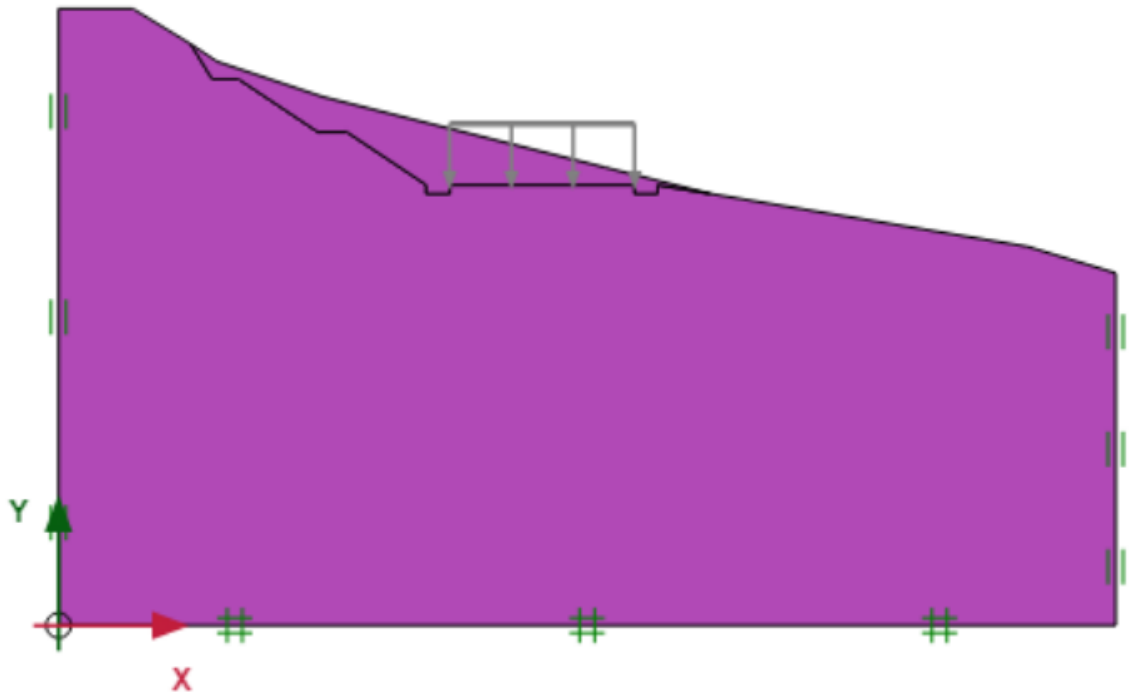
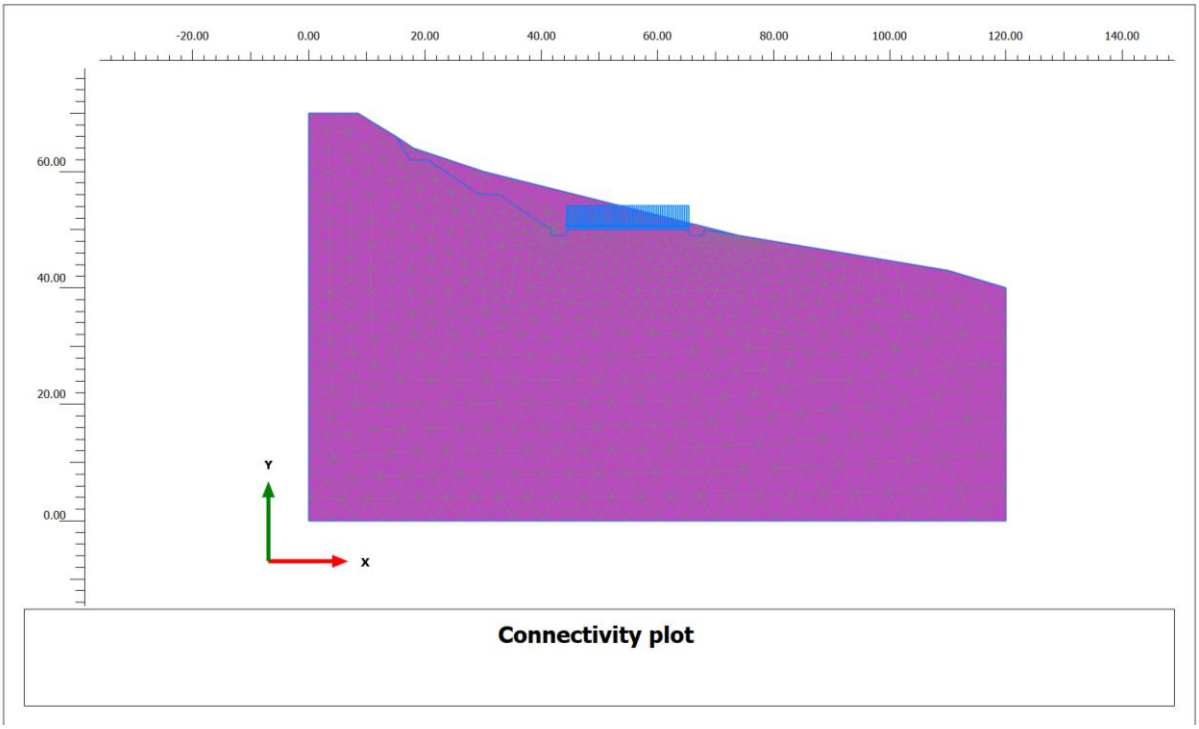


Fig IV.55: Boundaries Conditions.

E). Mesh generation:



F). Flow conditions:

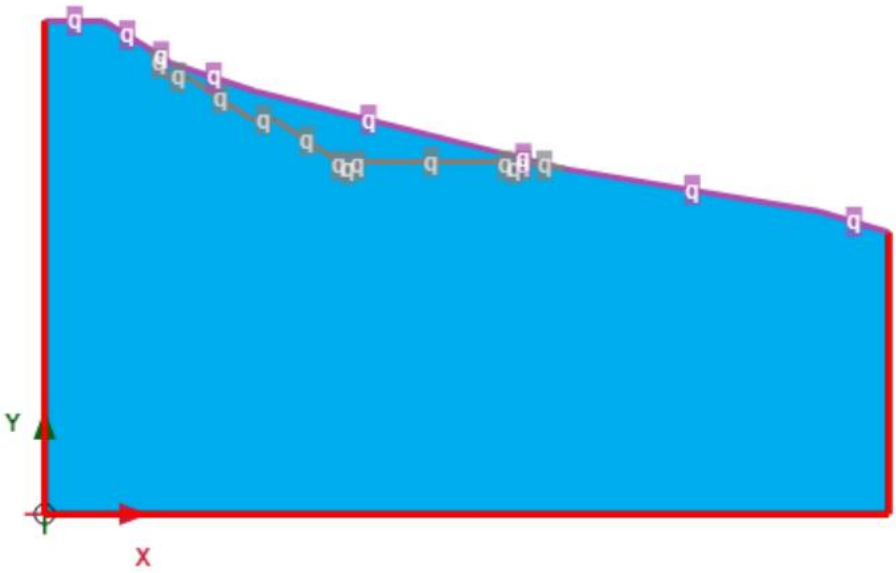


Fig IV.57: Flow condition.

G). Construction stages and calculation Types:

Sequence of Calculation Phases:

- Initial phase: using K_0 Procedure calculation type.

- Phase 01: the safety factor of the initial phase.

- Phase 02: Excavation phase: plastic phase calculation type.

- Phase 03: the safety factor of excavation phase.

-Phase04 :Railway phase: plastic phase calculation type.

- Phase 05: The safety factor of the railway phase.

- Phase 06: Dynamic phase: dynamics phase calculation type.

-Phase 07: Rainfall phase (0.01m/day): fully coupled flow-deformation calculation type.

-Phase 08: The safety factor of the rainfall phase.

This step-by-step procedure allows for a comprehensive understanding of slope behavior under both static and dynamic loads, capturing the key deformation and failure mechanisms that may occur.

IV.2.8Results and discussion:

This section presents and interprets the simulation results of all phases:

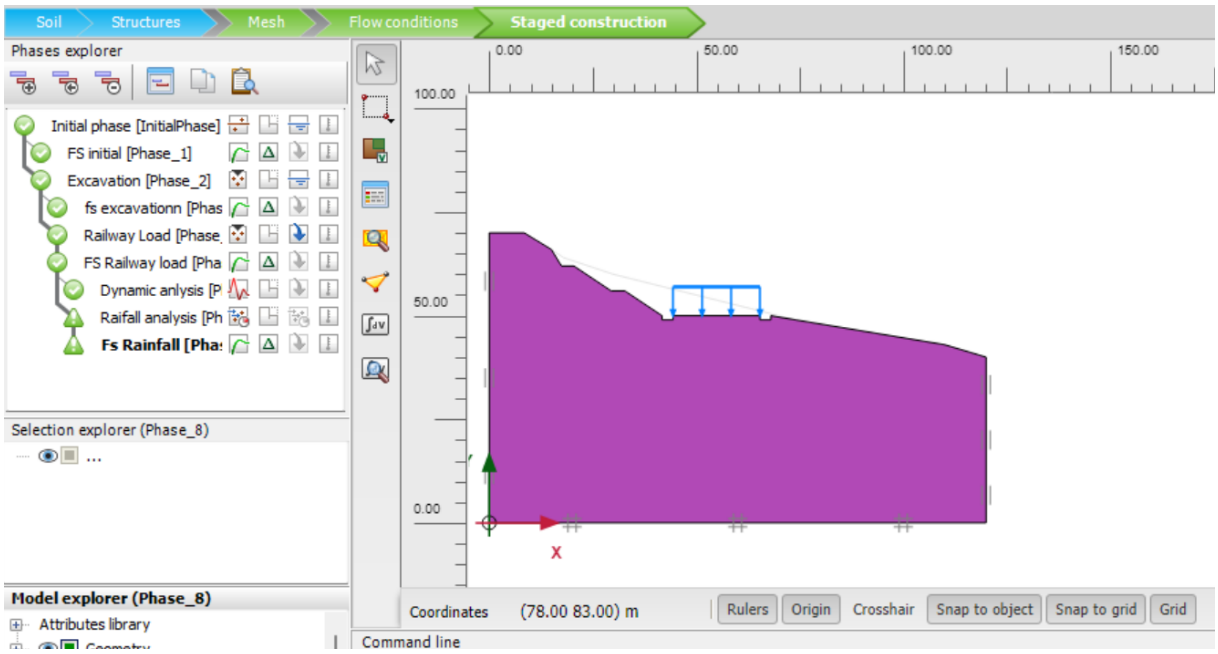


Fig IV.58: Configuration and calculation phases in PLAXIS 2D.

Initial phase:using K_0Procedure calculation type:

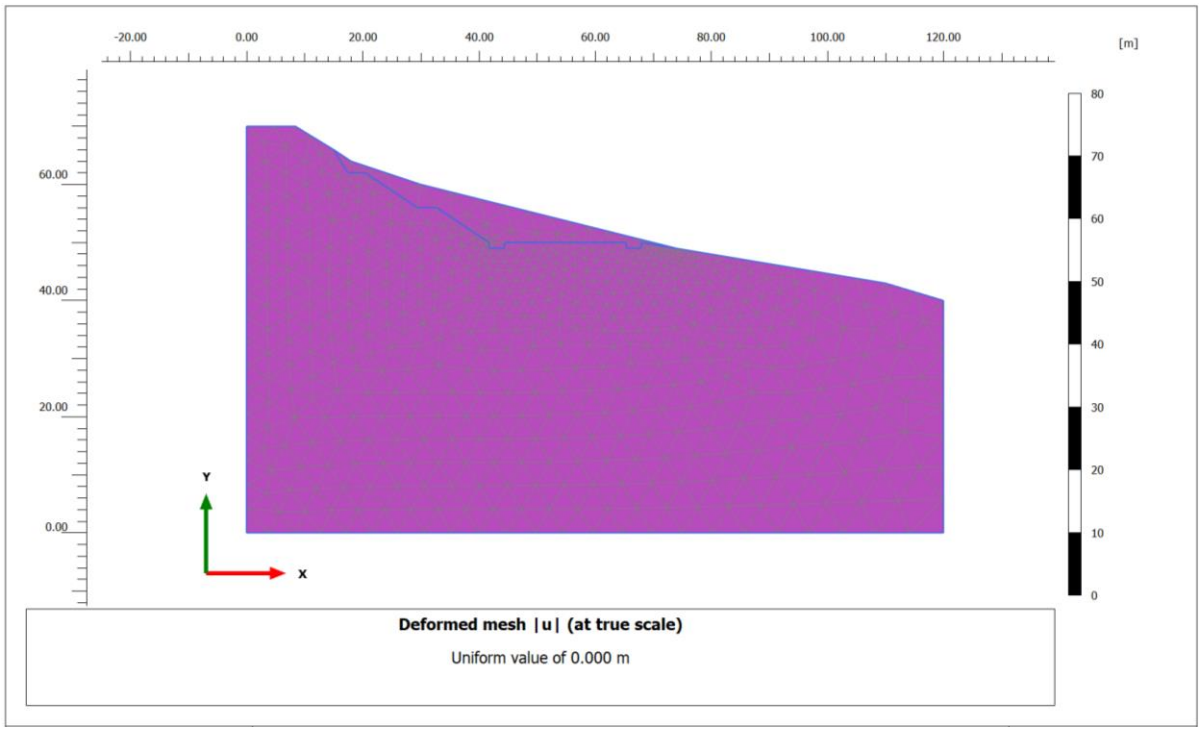
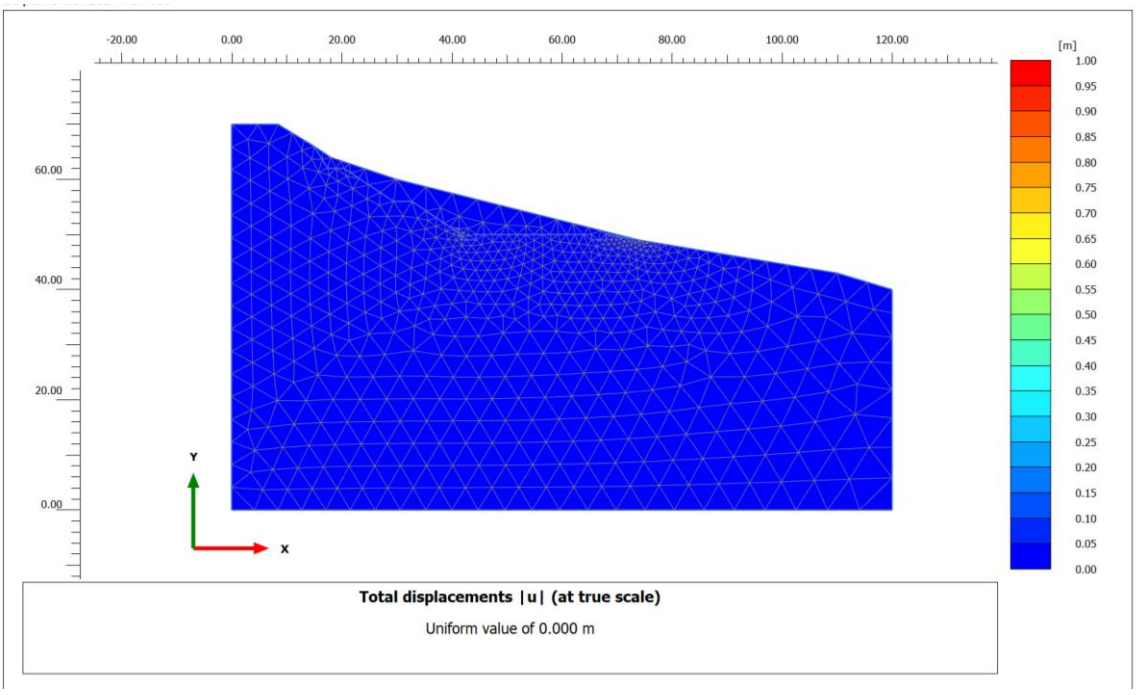


Fig IV.60:MeshDeformation during Initial Phases



FigIV.61 :Total Deformation during Initial Phases

Phase 01: the safety factor of the first phase.

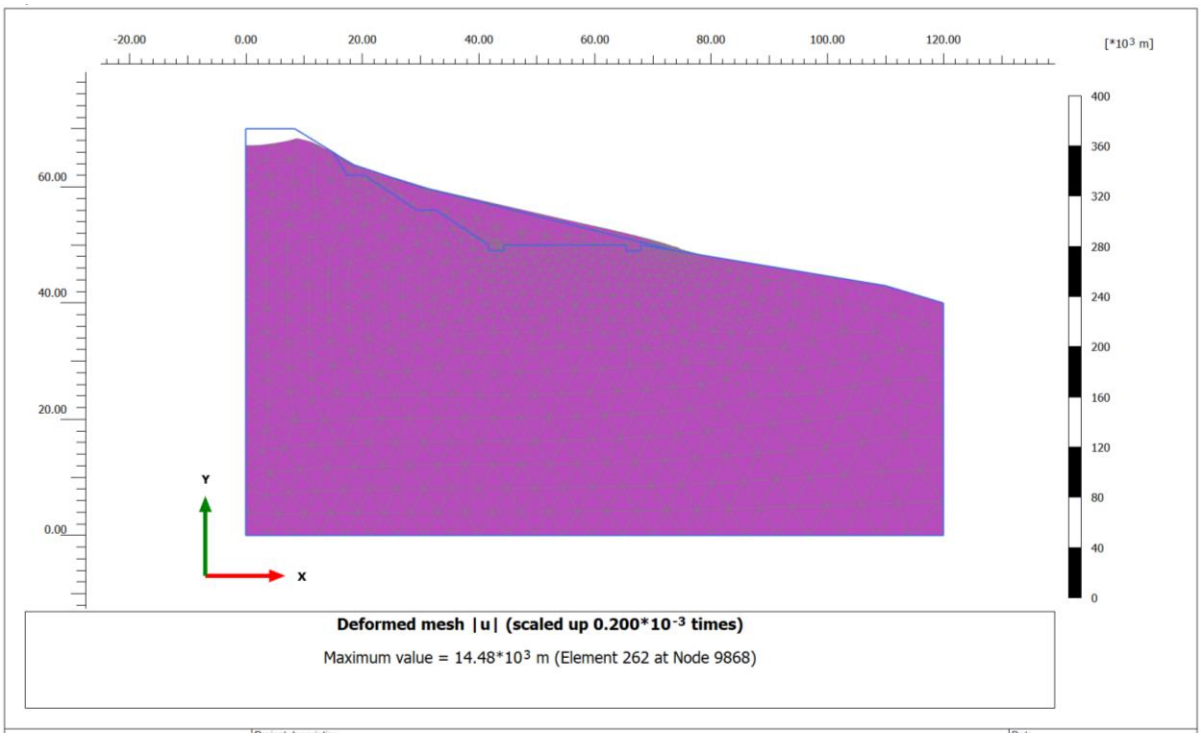


Fig IV.62:MeshDeformation during Phase 01

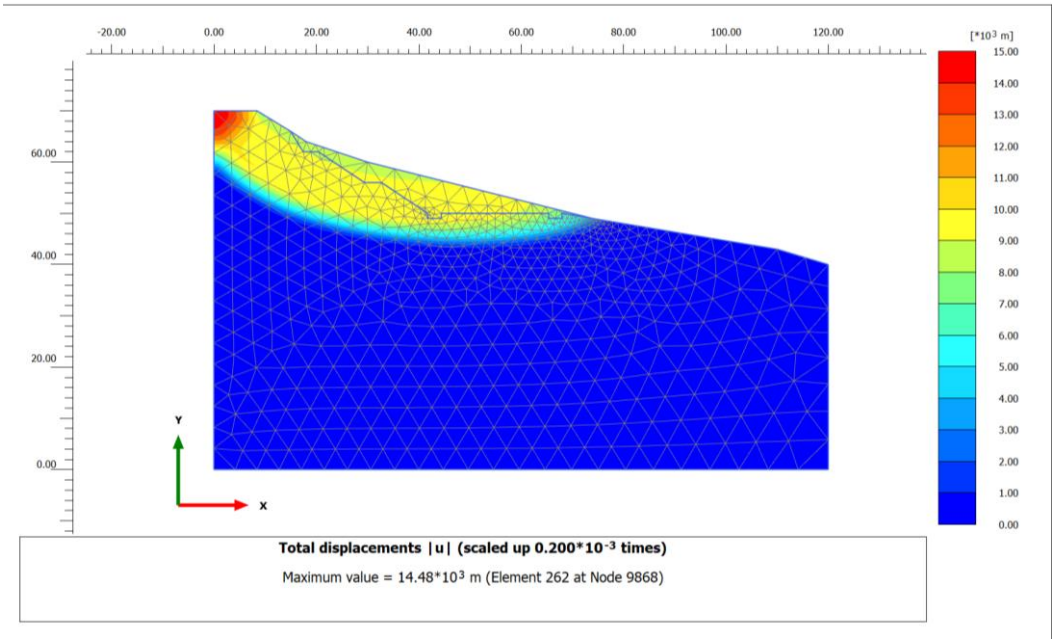


Fig IV.63:Total Deformation during Phase 01

Phase 02: Excavation phase:plastic phase calculation type.

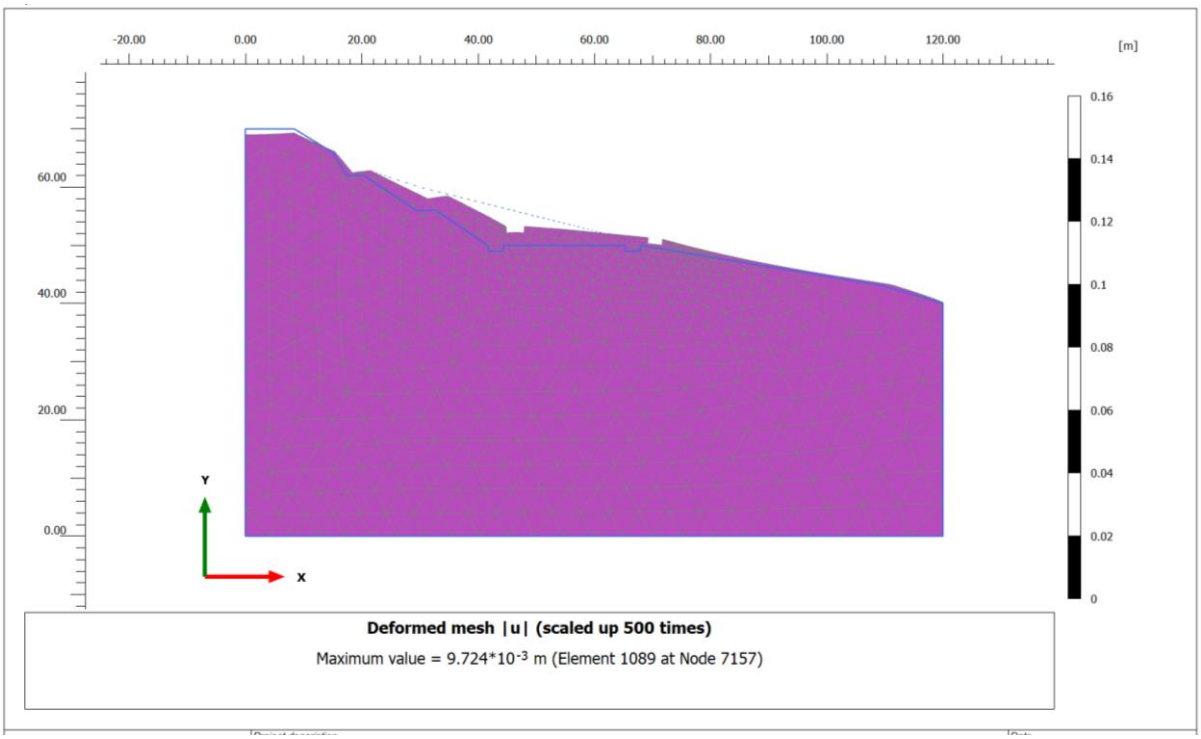


Fig IV.64:MeshDeformation during Excavation Phase

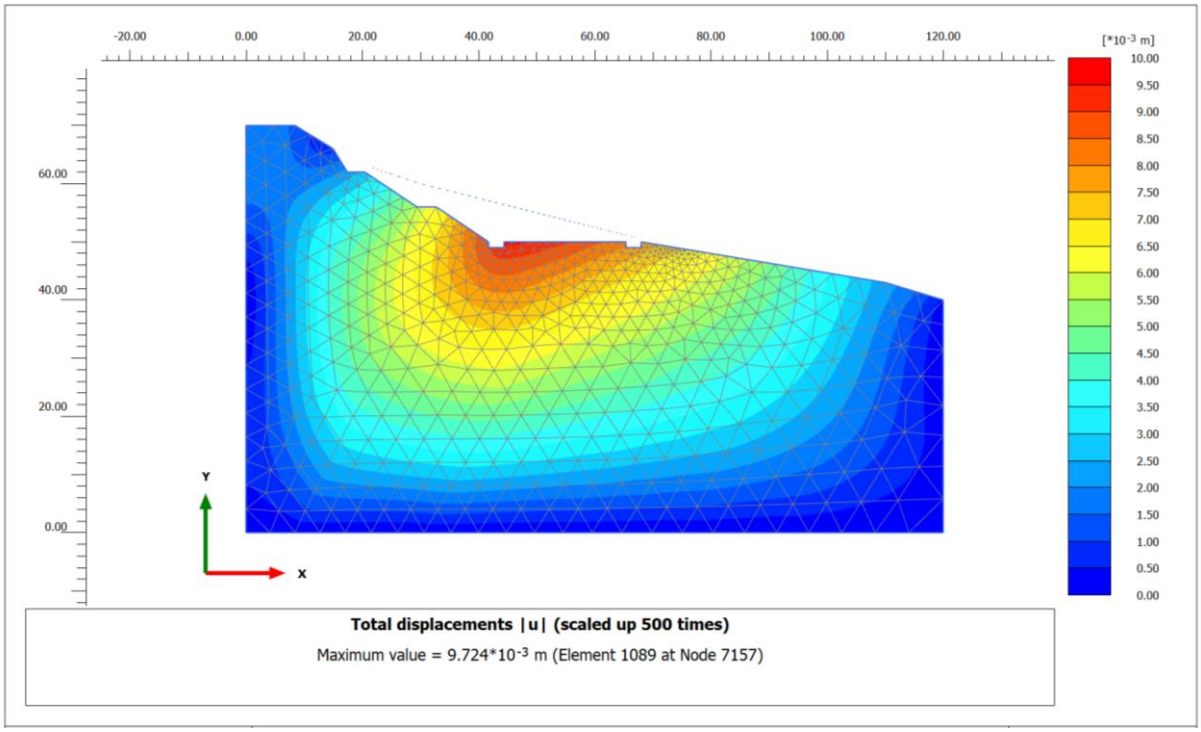


Fig IV.65:TotalDeformationduring Excavation Phase.

Phase 03: The safety factor of the Excavation phase.

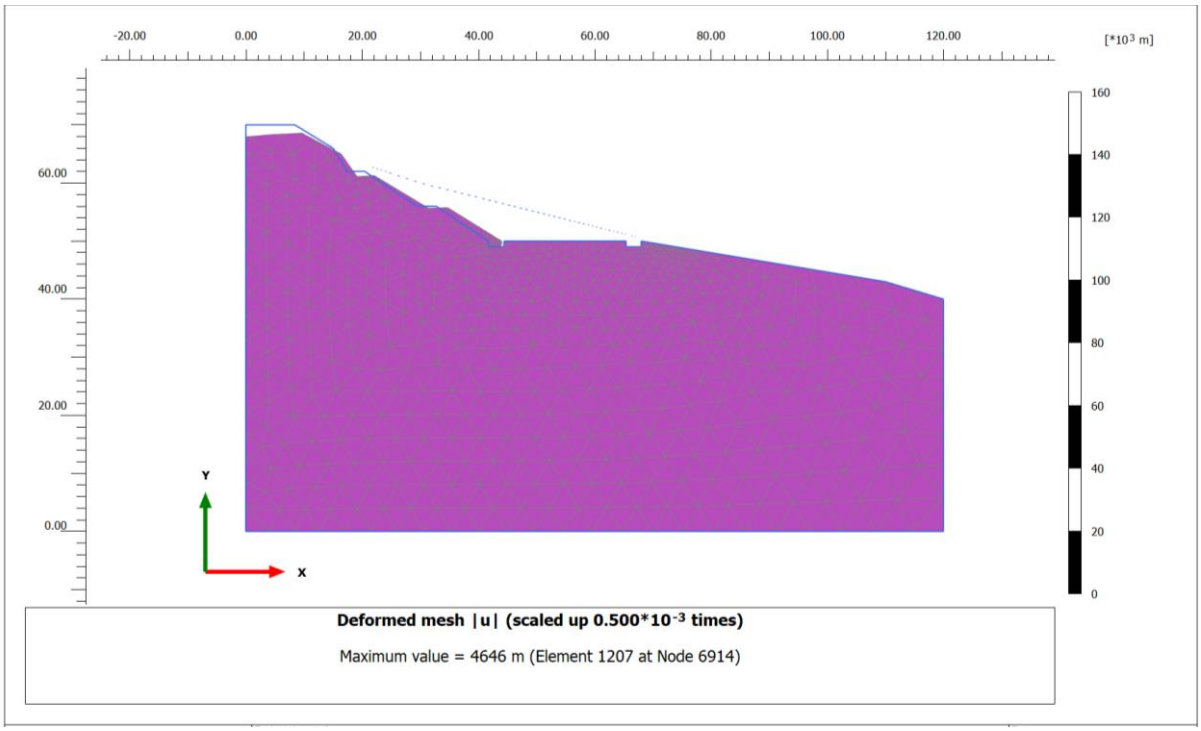


Fig IV.66Mesh Deformation during phase 03

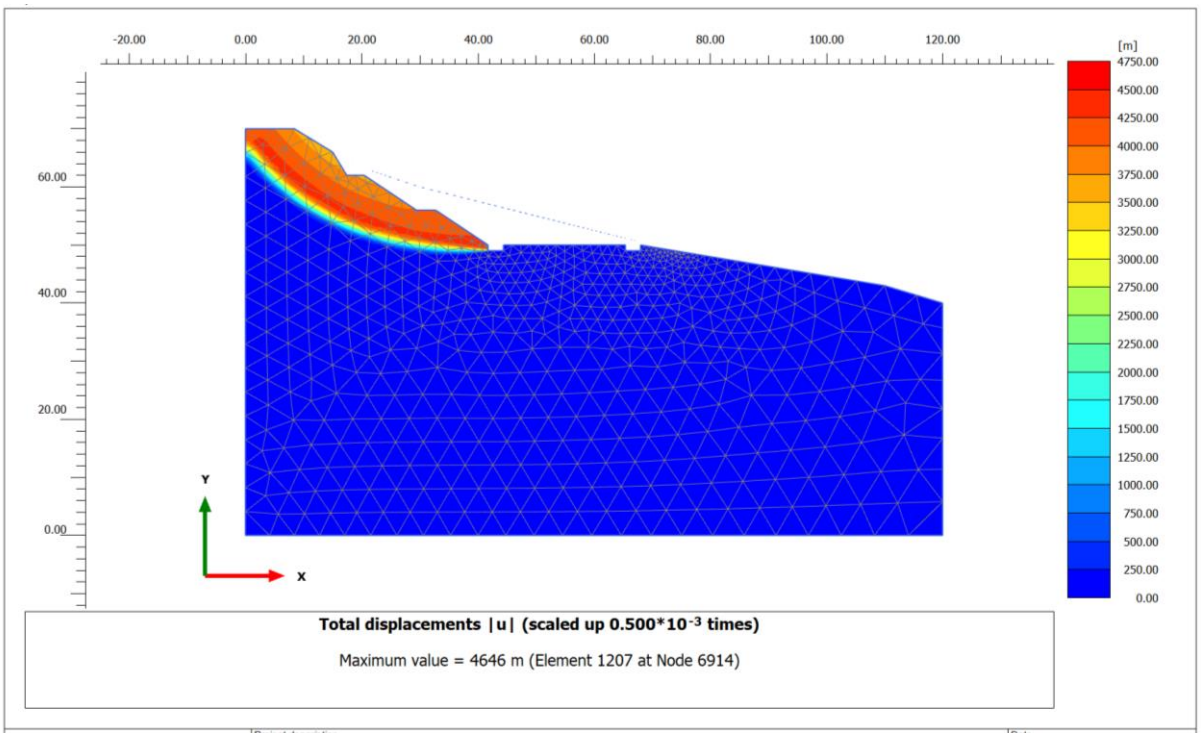
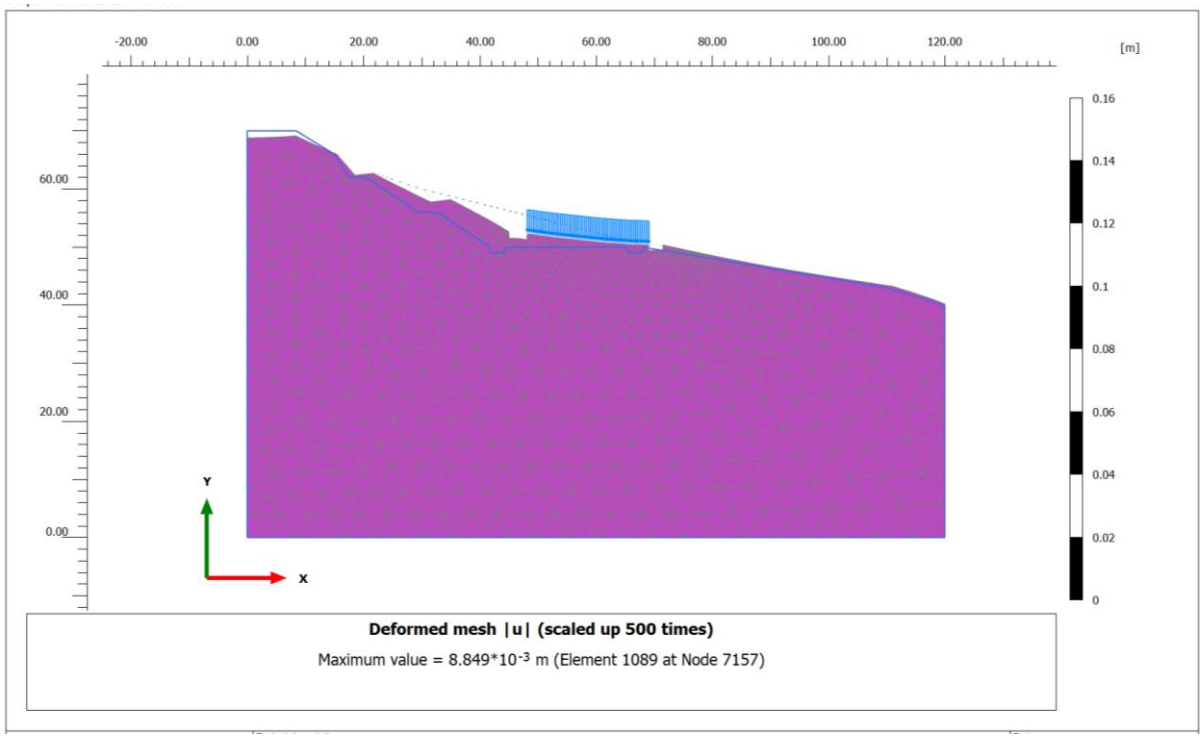


Fig IV.67 :Total displacement during phase 03



FigIV.68 :Mesh Deformation during Phase 04

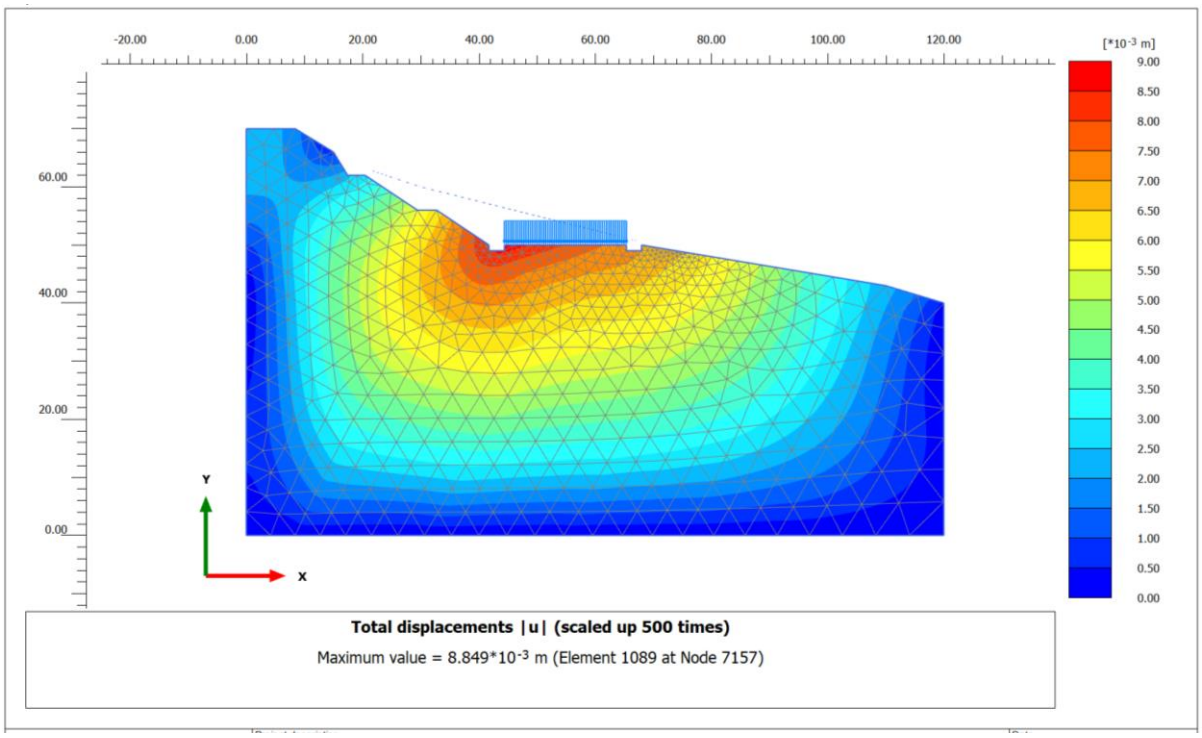


Fig IV.69:Total Deformation during Phase 04

Phase 05: The safety factor of the fourth phase.

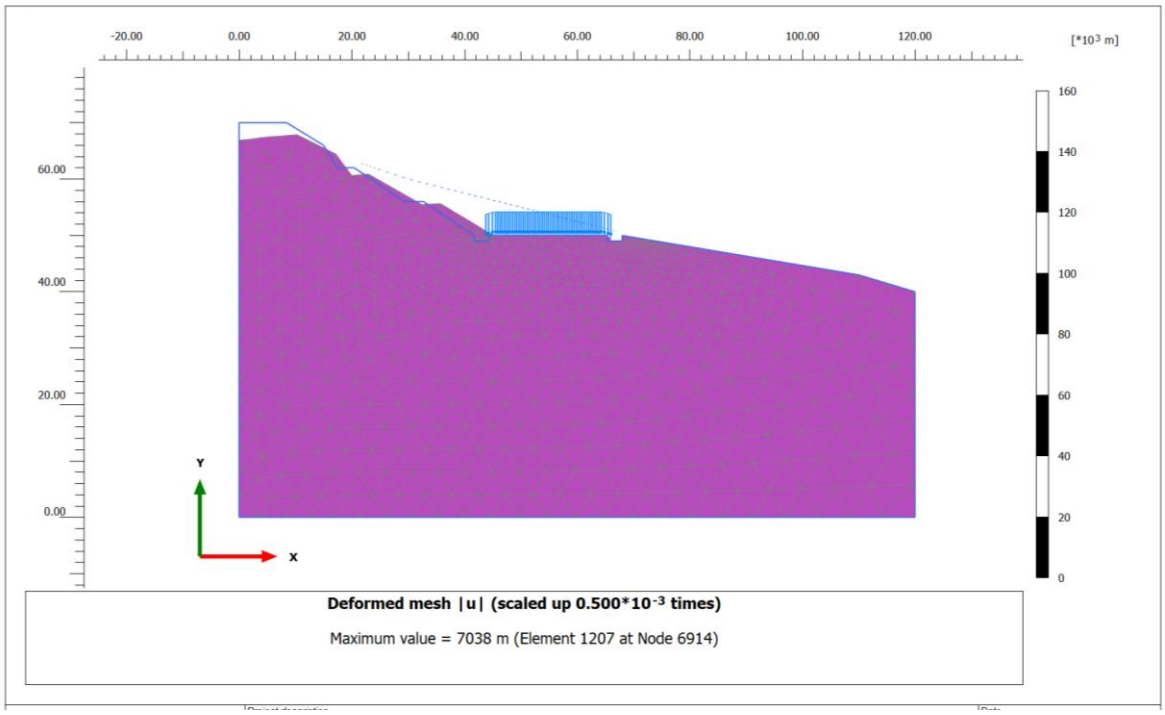


Fig IV.70:Mesh Deformation during Phase 05

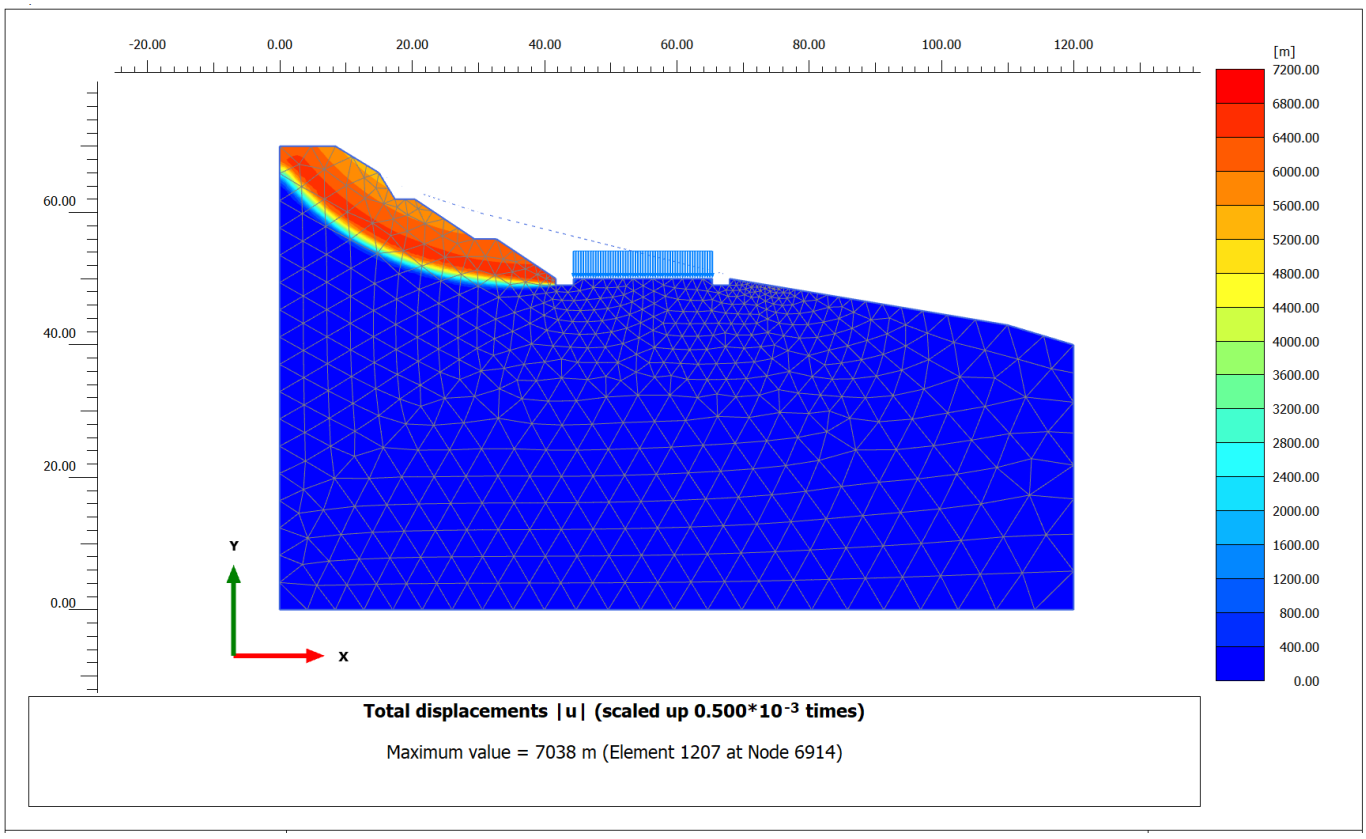
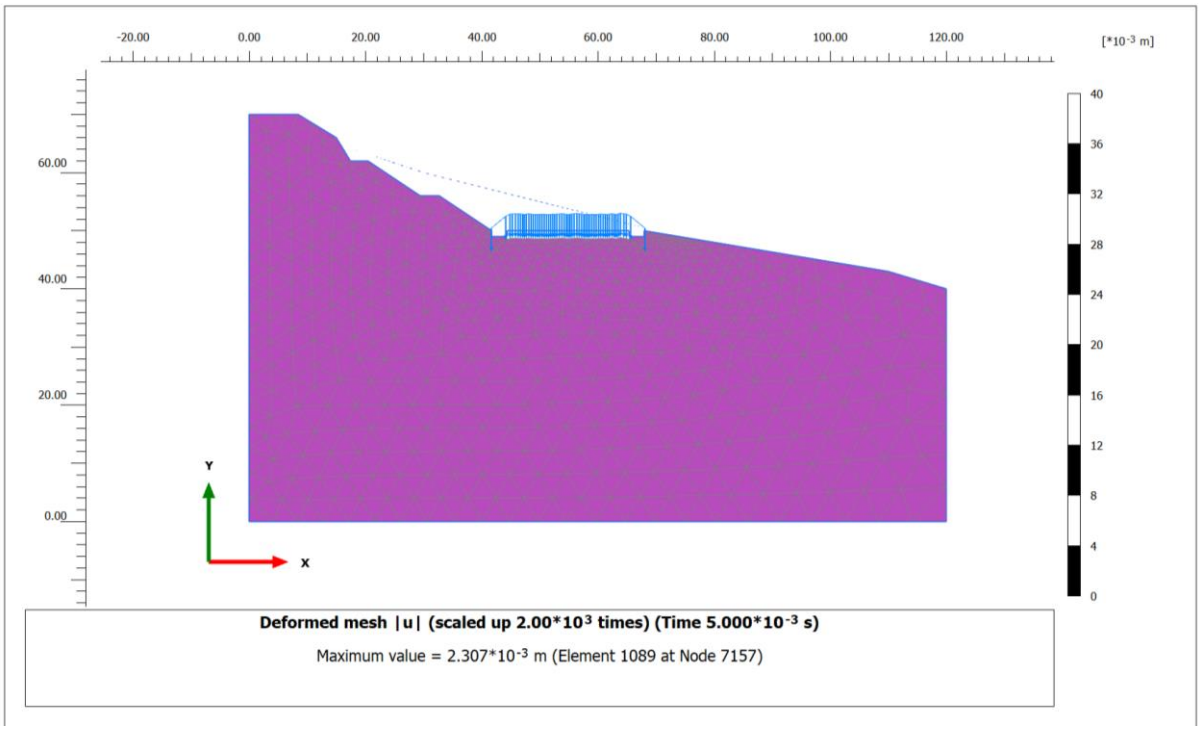


Fig IV.71:TotalDeformation during Phase 05.

Phase 06: Dynamic phase:dynamics phase calculation type.



FigIV.72:MeshDeformation during Phase 06(dynamic)

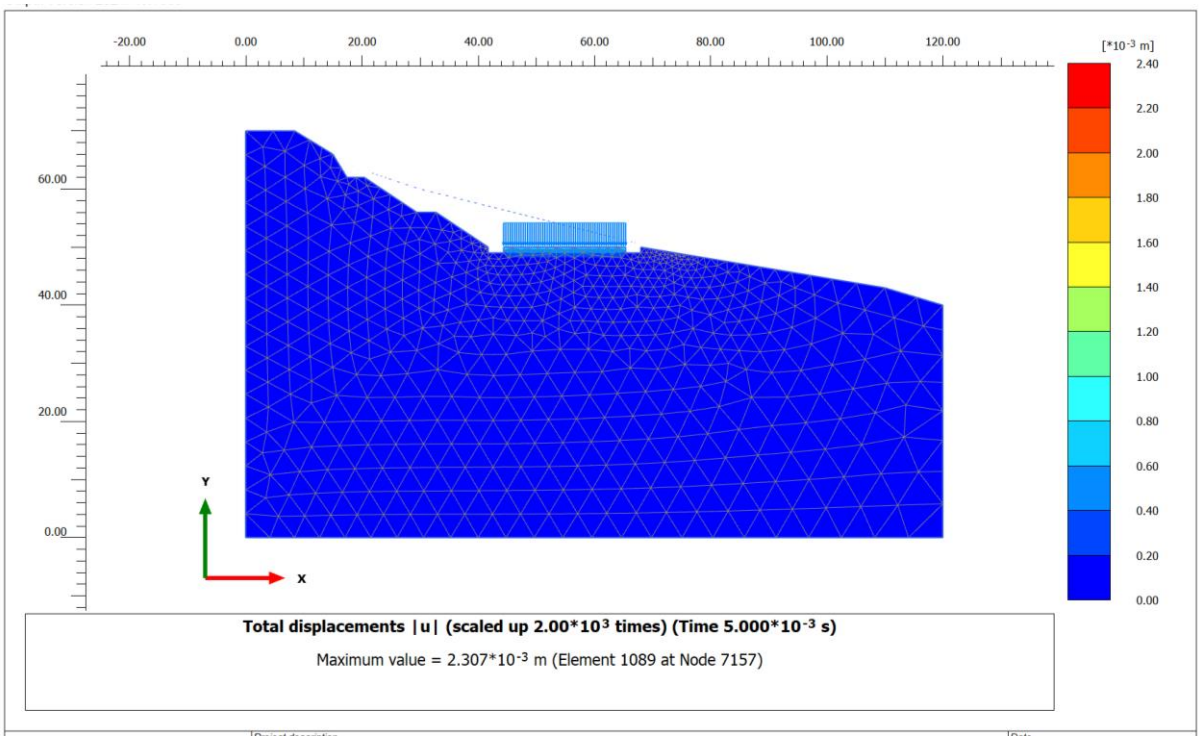


Fig IV.73: Total displacement during phase 06 (dynamic)

Step info				
Phase	Dynamic anlysis [Phase_6]			
Step	Initial			
Calulation mode	Classical mode			
Step type	Dynamics analysis			
Updated mesh	False			
Solver type	Picos			
Kernel type	64 bit			
Extrapolation factor	0.000			
Relative stiffness	0.4225			
Multipliers				
Soil weight			ΣM_{Weight}	1.000
Strength reduction factor	M_{sf}	0.000	ΣM_{sf}	2.229
Time	Increment	0.000	End time	0.05787E-6
Dynamic time	Increment	0.05000E-3	End time	5.000E-3
Staged construction				
Active proportion total area	M_{Area}	0.000	ΣM_{Area}	0.9694
Active proportion of stage	M_{Stage}	0.000	ΣM_{Stage}	0.000
Forces				
F_X	0.000 kN/m			
F_Y	0.000 kN/m			
Consolidation				
Realised $P_{Excess,Max}$	0.000 kN/m²			

Fig IV. 74:The safety factor of the phase dynamic.

Phase 07: Rainfall phase (0.01m/day): fully coupled flow-deformation calculation type.

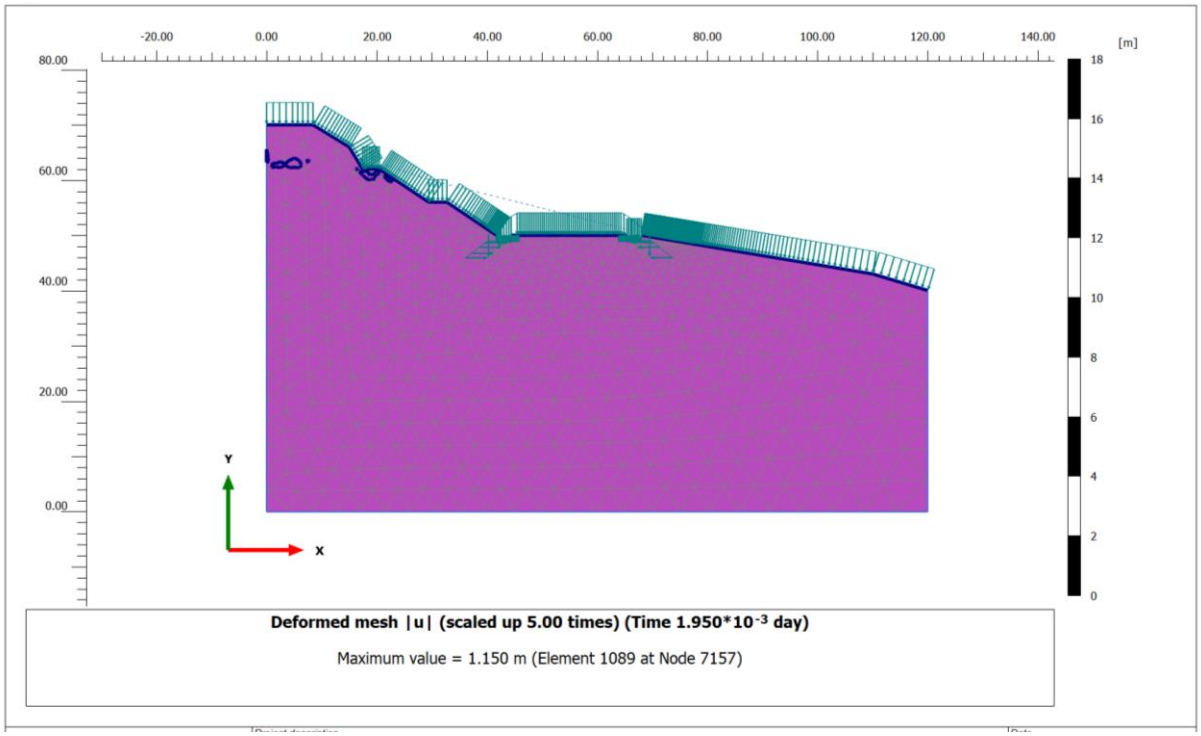


Fig IV. 75:Mesh deformation .

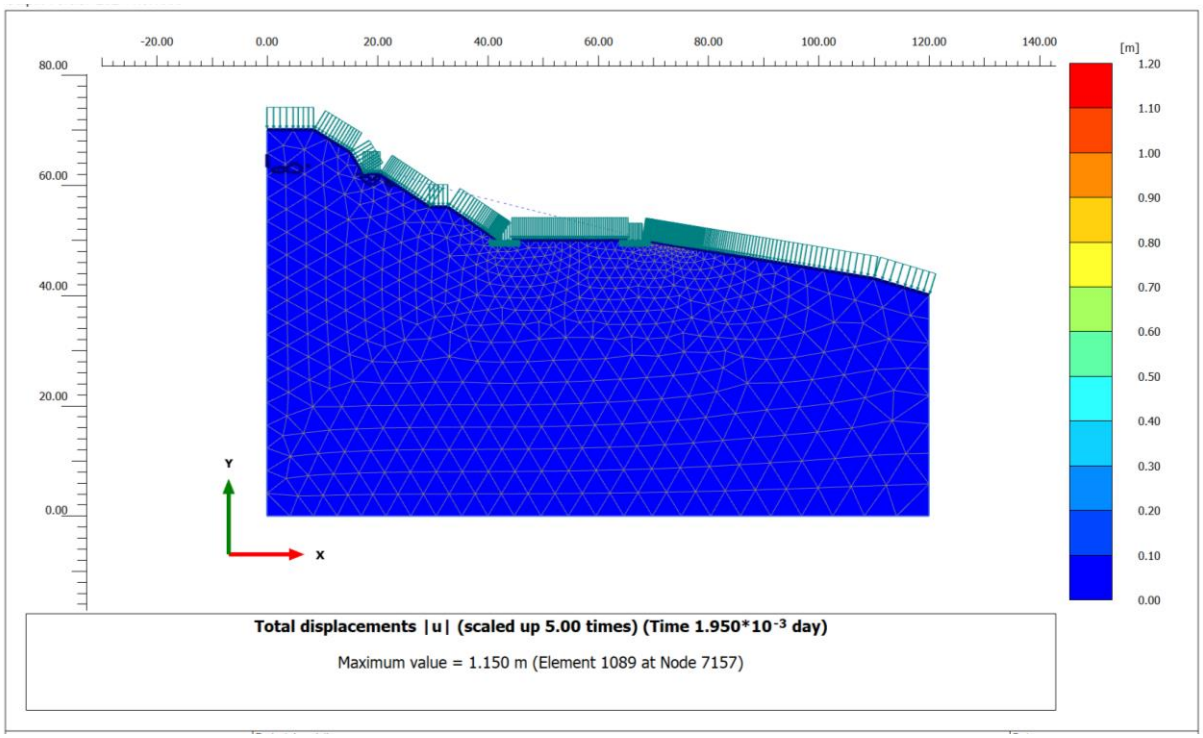
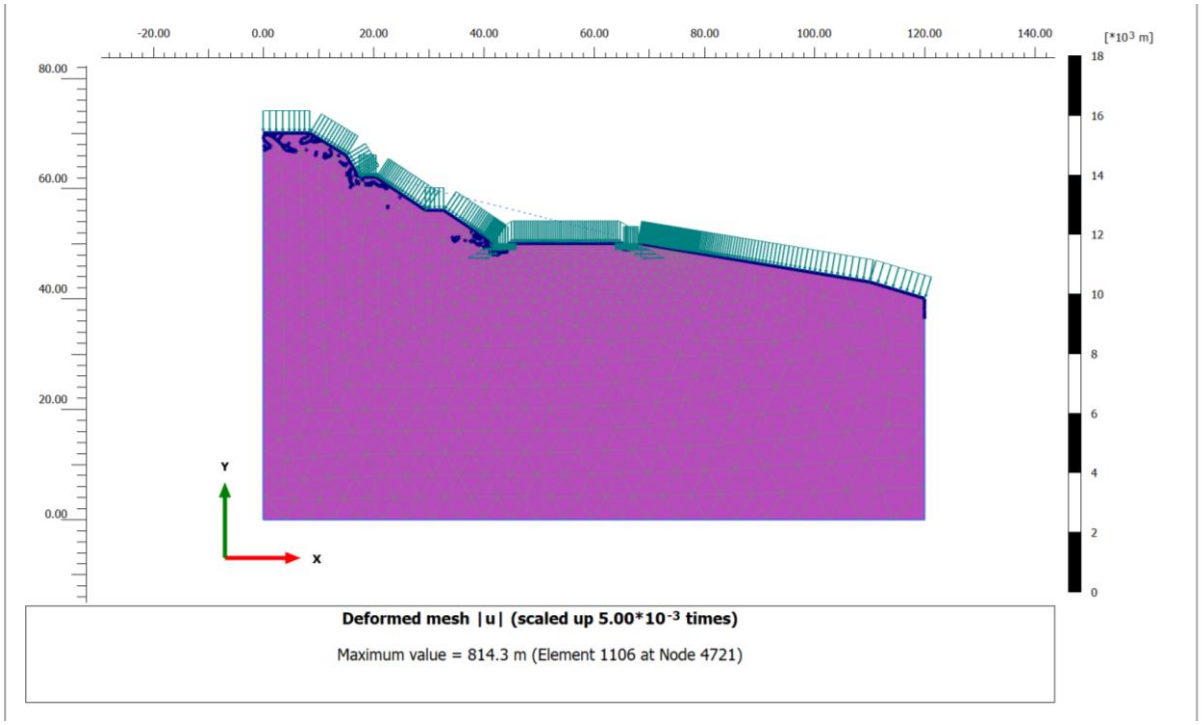


Fig IV. 76:Total displacement during phase 07(rainfall).

Phase 08: The safety factor of the phase 07.



FigIV.77:MeshDeformation during phase 08



FigIV.78:The safety factor of the phase07.

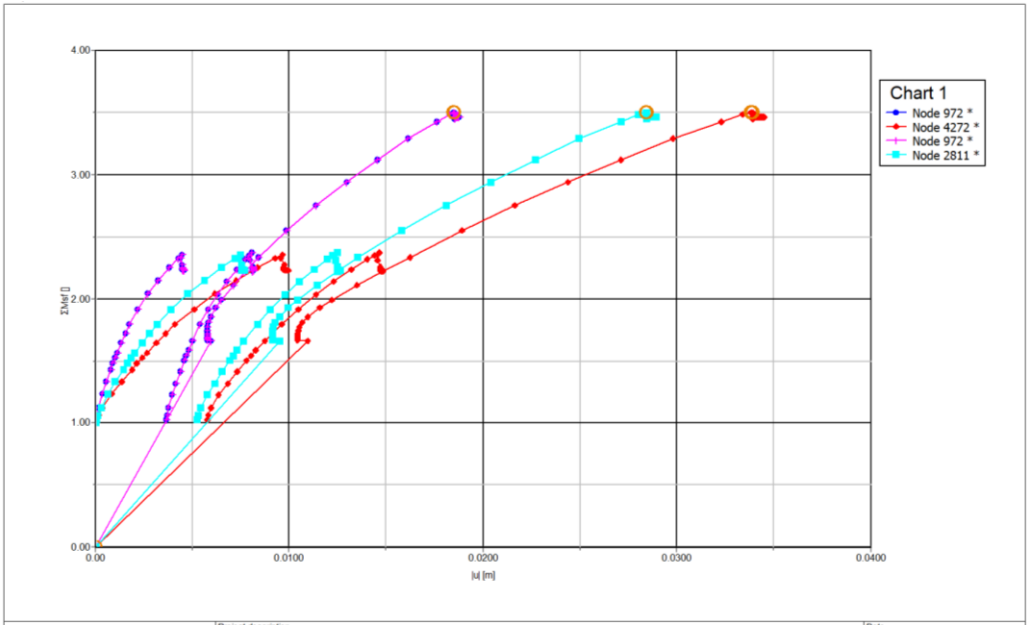


Fig IV.79 :Displacement versus Strngth Reduction Factor (Msf)

IV.2.8 Interpretation (gypsum clayey facies Triassic)

All phases of earthworks show, after equilibrium finite element analysis in PLAXIS, a high safety factor in this facies—except in the final calculation phase when rainfall conditions are applied. Under these conditions, the safety factor drops below 1, indicating instability. The gypsum clayey diapiric facies remains stable under normal circumstances, but water infiltration acts as a critical destabilizing factor, triggering material dissolution, movement, and sliding deformations. Given the high risk in this scenario, remediation measures must be implemented to ensure long-term slope stability.

IV.2.9 Risk Assessment Recommendations & Remediation Measures for Unstable Facies

IV.2.9.1 Gypsum Clayey Diapiric Facies (Triassic)

Risk Assessment:

- High risk of **rapid strength loss** upon water infiltration due to gypsum dissolution and clay softening.
- Potential for **sudden slope failure** under prolonged rainfall.
- **Progressive deformations** may occur even before full collapse.

Remediation Measures:

- **Surface & Subsurface Drainage:**
  - Install **horizontal drains** or **vertical wells** to lower groundwater levels.
  - Use **geocomposite drainage layers** to divert surface water away from the slope.
- **Slope Protection & Erosion Control:**
  - Apply **shotcrete** or **geotextile-reinforced vegetation** to prevent surface erosion.
  - Construct **gabion walls** or **riprap** at the slope toe to reduce undercutting.
- **Chemical Stabilization (if applicable):**
  - Use **lime or cement stabilization** to reduce solubility of gypsum.
  - Inject **grouting materials** to fill dissolution voids.
- **Slope Geometry Modification:**
  - **Flatten slopes** to reduce driving forces.
  - Implement **benching (terracing)** to improve stability.

IV.2.9.2 Clayey Facies

Risk Assessment:

- **Chronic instability** due to low shear strength and high plasticity.
- **Extreme sensitivity to rainfall**—rapid pore pressure buildup leads to failure.
- **Long-term creep deformations** possible even without immediate collapse.

Remediation Measures:

- **Deep & Shallow Drainage Systems:**
  - **Vertical sand drains** or **wick drains** to accelerate consolidation.
  - **French drains** or **interceptor trenches** to prevent surface water infiltration.
- **Slope Reinforcement:**
  - **Soil nailing** or **anchored retaining walls** for deep stabilization.
  - **Geogrid reinforcement** in embankments to enhance tensile strength.
- **Material Replacement/Improvement:**

  - **Remove and replace** highly plastic clay with engineered fill (e.g., granular backfill).
  - **Lime/cement modification** to reduce plasticity and increase strength.
- **Real-Time Monitoring:**
  - Install **piezometers** and **inclinometers** to track pore pressure and movement.
  - Use **slope stability radar (SSR)** for early warning of deformations.

IV.3 Conclusion

The stability analysis reveals significant contrasts in the behavior of the three facies under investigation. The **Clayey facies** presents the most critical scenario, with persistently low safety factors that deteriorate further under rainfall infiltration. Water saturation leads to reduced shear strength, increased pore pressure, and a high risk of slope failure. Immediate remediation measures—such as enhanced drainage, slope reinforcement, or selective material replacement—are essential to mitigate these risks and ensure long-term stability.

In stark contrast, the **Limestone facies** exhibits exceptional stability across all phases, maintaining high safety factors even under adverse conditions. Its inherent strength and low permeability prevent water-induced weakening, eliminating the need for additional stabilization. This facies represents the most reliable geological unit in the slope design, requiring no intervention.

The **Gypsum Clayey Diapiric facies (Triassic)** displays intermediate behavior, remaining stable under normal conditions but becoming highly unstable when subjected to rainfall. The drastic drop in safety factor (below 1) upon water infiltration highlights the material's susceptibility to dissolution and sliding deformations. Targeted remediation—such as waterproofing measures, slope regrading, or chemical stabilization—must be prioritized in zones with this facies to prevent sudden failures. Collectively, these findings underscore the necessity of facies-specific slope design and risk management strategies to address varying geological vulnerabilities.

General Conclusion

This research has systematically bridged theoretical geomechanical principles with practical engineering challenges in a complex mountainous terrain, yielding significant insights into slope stability mechanisms under varied geological and environmental conditions. Through comprehensive numerical modeling and field validation, the study demonstrates that lithological heterogeneity exerts primary control on slope performance, with distinct behavioral patterns emerging across the three principal geological facies.

The diapiric facies, comprising gypsum-clay formations, consistently demonstrated unstable behavior in all simulation scenarios. Excavation-induced stress redistribution triggered progressive failure mechanisms, while rainfall infiltration further reduced factors of safety by 25-40% through pore pressure elevation and strength degradation. These findings necessitate systematic reinforcement measures, including soil improvement techniques and structural stabilization, for any engineering works in these formations.

In marked contrast, limestone units exhibited exceptional stability across all modeled conditions. The jointed rock model simulations confirmed robust performance even under dynamic loading, with factors of safety consistently exceeding 2.0. This competence suggests that minimal stabilization measures are required in these zones, though careful attention to karst features remains essential.

The plastic clay formations presented particularly challenging conditions, with all numerical models indicating marginal stability (FoS < 1.3) under both static and dynamic conditions. The material's high compressibility and strain-softening behavior led to progressive failure development, exacerbated by seasonal groundwater fluctuations. These results underscore the critical need for comprehensive protection systems, including drainage networks and retaining structures, to ensure long-term stability.

This study contributes to geotechnical field include the following keys:

1. Development of a validated modeling framework for anisotropic, multi-lithological terrains
2. Quantification of hydro-mechanical coupling effects in diapiric formations

3. Demonstration of strain-accumulation patterns in plastic clays under cyclic loading
4. Establishment of design thresholds for benched excavations in mixed geological settings

Practical recommendations emerging from this research emphasize:

• Implementation of real-time monitoring systems combining piezometers

• Adoption of 3D modeling approaches to capture cross-sectional variability

• Application of soil improvement techniques in plastic clay zones

• Development of adaptive excavation protocols responsive to real-time instrumentation data

This study advances slope stability assessment methodologies by providing a replicable, data-driven framework for infrastructure projects in geologically complex environments. The findings offer both immediate solutions for the current project and fundamental insights applicable to similar challenges worldwide, particularly in mining transportation corridors through mountainous terrain. Future research directions should focus on long-term performance monitoring and the development of machine learning tools for predictive stability assessment in such variable geological settings.

REFERENCES

References

- Acharya, B., Kundu, J., Sarkar, K., & Chawla, S. (2017). Stability assessment of a critical slope near Nathpa region, Himachal Pradesh, India. In Proceedings of the Indian Geotechnical Conference 2017 (GeoNEst), 14–16 December 2017.
- ANESRIF. (2022). National Agency for the Study and Monitoring of Railway Investment Projects.
- ANRH. (2018). National Agency for Water Resources, Hydrogeological study of the Eastern High Plains.
- Bishop, A. W. (1955). The use of the slip circle in the stability analysis of slopes. Géotechnique, 5(1), 7-17.
- Budhu, M. (2010). Soil Mechanics and Foundations (3rd ed.). John Wiley & Sons.
- Budhu, M. (2011). Soil Mechanics and Foundations (3rd ed.). John Wiley & Sons.
- CGI International Geotechnical Center. (2024). *Wedge failure on slopes: Analysis and stabilization*. CGI International Geotechnical Center. https://www.cgiearth.com/reports/wedge_failure_2024.pdf
- CRAAG. (2020). Seismological Survey of Algeria.
- Cruden, D. M., &Varnes, D. J. (1996). Landslide types and processes. In Landslides: Investigation and mitigation (pp. 36–75). Transportation Research Board.
- Crosta, G. B., Imposimato, S., &Roddeman, D. G. (2008). Numerical modelling of large landslide evolution. International Journal of Geomechanics, 8(5), 310–321.
- Das, B. M., & Sobhan, K. (2017). Principles of Geotechnical Engineering (9th ed.). Cengage Learning.
- Dikau, R., Brunsden, D., Schrott, L., & Ibsen, M.-L. (1996). Landslide Recognition: Identification, Movement and Causes. Wiley.
- Duncan, J. M., & Wright, S. G. (2005). Soil Strength and Slope Stability. John Wiley & Sons.
- Fell, R., & Fry, J. J. (2007). The stability of slopes. In: Geotechnical Engineering Handbook.
- Ghrieb, S. (2010; 2011). Hydrogeological dynamics and structural geology of Tébessa.
- Griffiths, D. V., & Lane, P. A. (1999). Slope stability analysis by finite elements. Géotechnique, 49(3), 387–403.

- Hadji, R., Boumezbeur, A., Bensalem, S., & Bouchelaghem, F. (2017). Karst development and geohazards in northeastern Algeria: The case of the Bekkaria area. Journal of African Earth Sciences, 134, 478–489.
- Idriss, I. M., & Boulanger, R. W. (2008). Soil Liquefaction During Earthquakes. Earthquake Engineering Research Institute.
- Itasca. (2012). FLAC: Fast Lagrangian Analysis of Continua. Minneapolis, USA.
- Janbu, N. (1954). Application of composite slip surfaces for stability analysis. European Conference on Stability of Earth Slopes.
- Janbu, N. (1956). Stability analysis of slopes with dimensionless parameters. Harvard Soil Mechanics Series, (46).
- Keefer, D. K. (2016, July 28). Illgraben debris-flow video. The Landslide Blog. https://blogs.agu.org/landslideblog/2016/07/28/illgraben-debris-flow-video/
- Kolapo, P., Oniyide, G. O., Said, K. O., Lawal, A. I., Onifade, M., & Munemo, P. (2022). An overview of slope failure in mining operations. Mining, 2(2), 350–384.
- Kramer, S. L. (1996). Geotechnical Earthquake Engineering. Prentice Hall.
- Kumari, S. (2022, October 10). Narrow escape for 30 passengers as bus gets stuck in flooded river in Uttarakhand's Haldwani. India Today.
- Legrioui, M., Hadji, R., &Hamimed, A. (2017). Karstification and geohazards in carbonate terrains of northeastern Algeria: Case study of Bekkaria region. Journal of African Earth Sciences.
- Maáfat, M., & Slimani, S. (2005). Tectonic evolution of the Tellian Atlas in northeastern Algeria: Implications for groundwater structure.
- Mebrouk, A. (2014). Tectonic Activity and Fault Systems in North-Eastern Algeria. Geomechanical Studies, 19(3), 77-90.
- Mrad, A., et al. (2018). Transient perched water tables and slope stability.
- ONM. (2020). Climatic analysis of semi-arid zones in northeastern Algeria (2010–2020).
- ONS. (2020). National Office of Statistics, Population distribution by commune, Algeria.
- Perrodon, J. (1957). Mesozoic Geology and Stratigraphy of the Tébessa Region. Bulletin of the Geological Society, 14(1), 22-35.
- Peters, S., & Liu, J. (2024). Detecting coseismic landslides in GEE using machine learning algorithms on combined optical and radar imagery. Remote Sensing, 16(10), 1722. https://doi.org/10.3390/rs16101722

- Petley, D. N. (2012). Global patterns of loss of life from landslides. Geology, 40(10), 927–930.
- Potts, D. M., &Zdravkovic, L. (2001). Finite Element Analysis in Geotechnical Engineering. Thomas Telford.
- Schematics Inkage. (2024, July). Formation of an earthquake diagram.
- Smith, J., & Doe, A. (2018). Modern Mining Techniques. 3rd ed. Mining Publications.
- Smith, I. M., & Griffiths, D. V. (2004). Programming the Finite Element Method (4th ed.). John Wiley & Sons.
- Smith, R., Martin, L., & Dupont, P. (2018). Tectono-sedimentary evolution of the eastern Saharan Atlas: New insights. Journal of African Earth Sciences, 144, 45-59.
- Taylor, D. W. (1937). Stability of earth slopes. Journal of the Boston Society of Civil Engineers, 24(1), 197–246.
- U.S. Geological Survey. (2004). Landslide types and processes (Fact Sheet 2004–3072). U.S. Department of the Interior. https://pubs.usgs.gov/fs/2004/3072/fs-2004-3072.html
- U.S. Geological Survey. (2023, April 19).
- UNDRR. (2020). Global Assessment Report on Disaster Risk Reduction. United Nations Office for Disaster Risk Reduction.
- Vila, E. (1980). Tectonic Evolution of the Eastern Saharan Atlas. Geological Journal, 15(4), 133-148.
- Waltham, T. (2009). Foundations of Engineering Geology (3rd ed.). Taylor & Francis.
- Wyllie, D. C., & Mah, C. W. (2004). Rock slope engineering: Civil and mining (4th ed.). London: CRC Press. Figure 85 adapted from Goodman & Bray.
- Zerrouki, A., et al. (2013). Post-Miocene Tectonics and Basin Evolution in the Tébessa Region. Tectonic Research Journal, 29(1), 120-135.

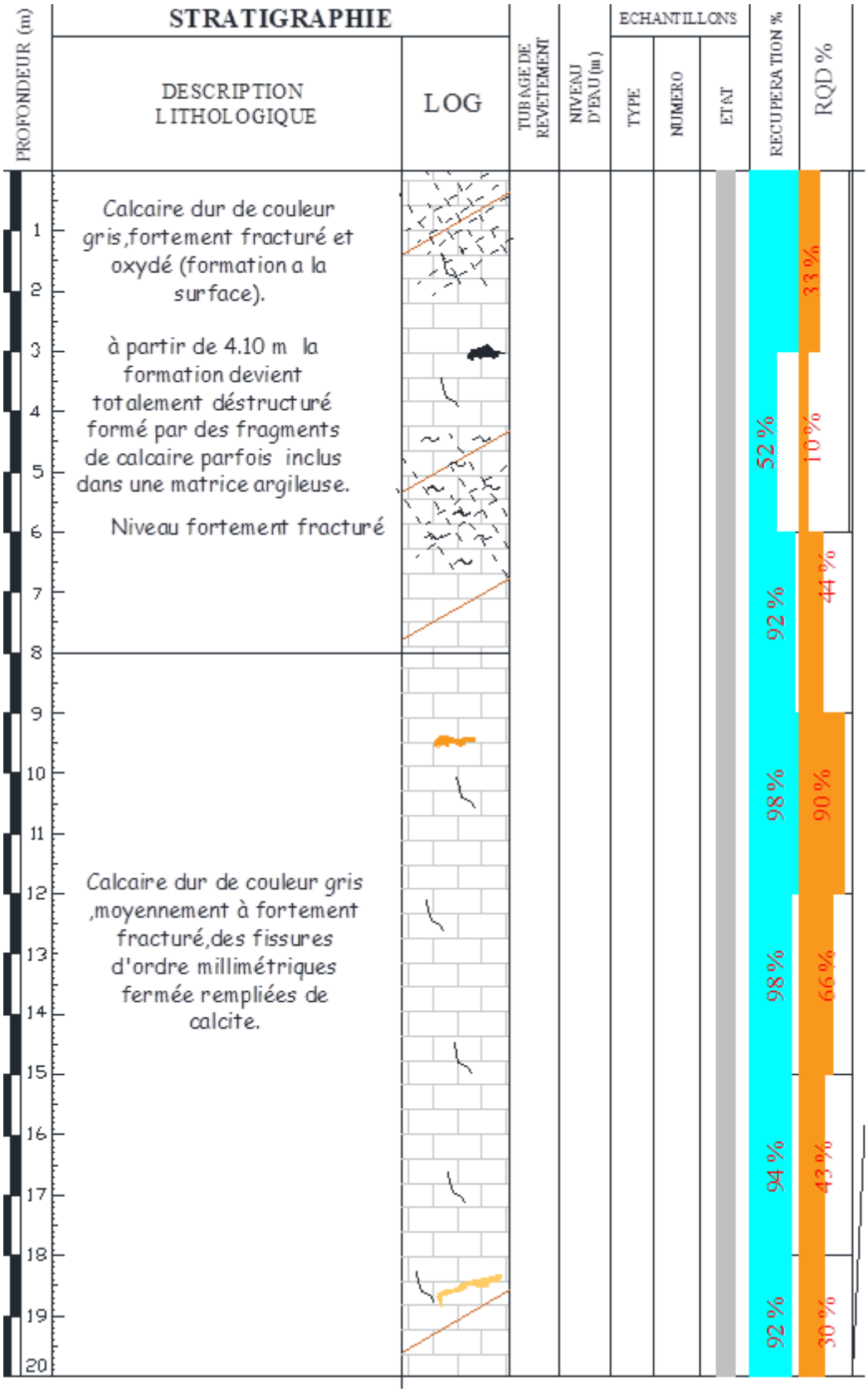
Blogs and website:

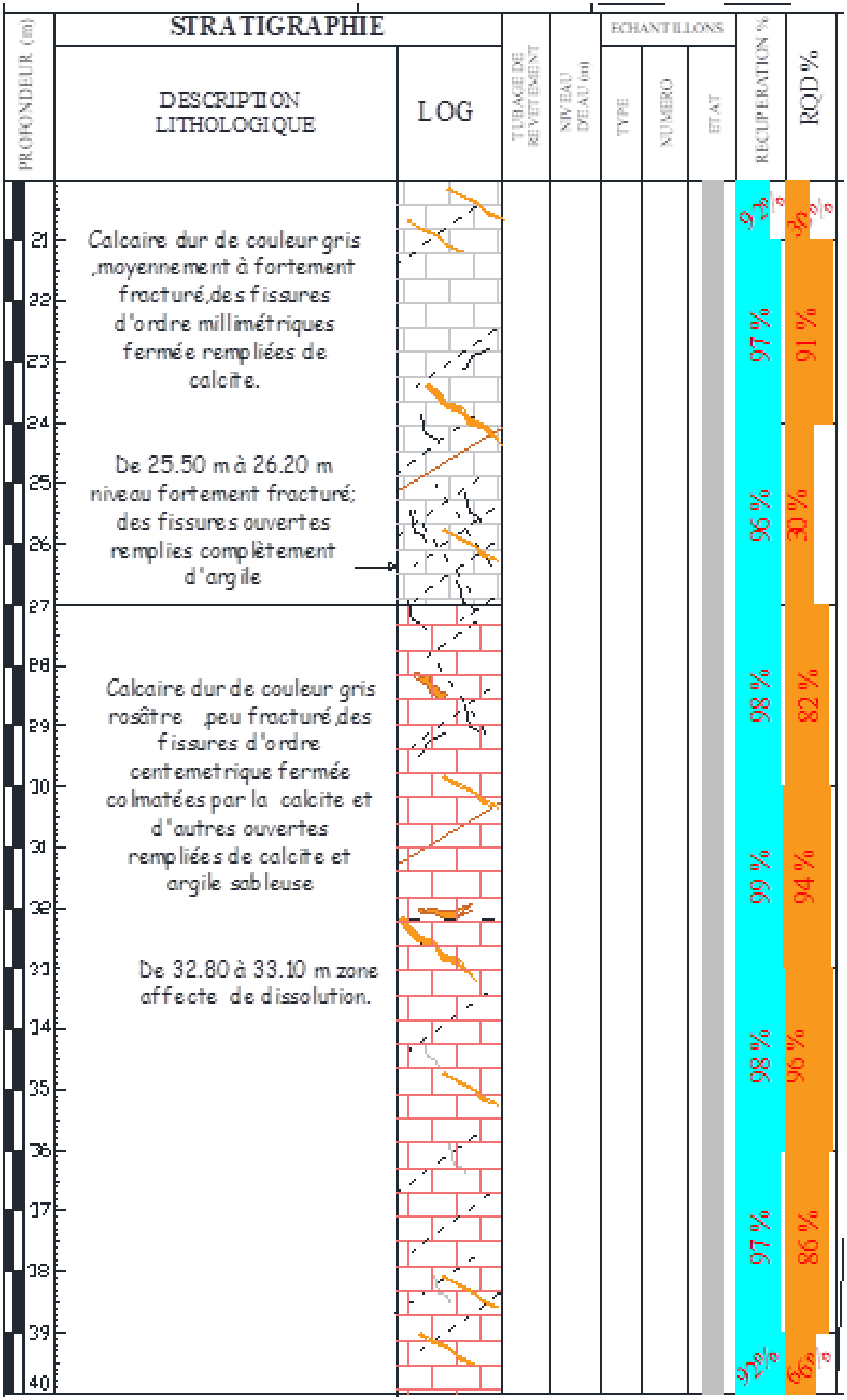
- notasingenierocivil.blogspot.com. (2011). Ábacos de Taylor. Retrieved from https://notasingenierocivil.blogspot.com/2011/05/abacos-de-taylor.html
- InspiredPencil. (2023). Rockfall Diagram. https://ar.inspiredpencil.com
- Climate Charts.com. (n.d.). Monthly data table for Tébessa, Algeria – Precipitation and temperature. from https://www.climatecharts.com/Locations/a/AL60475.html

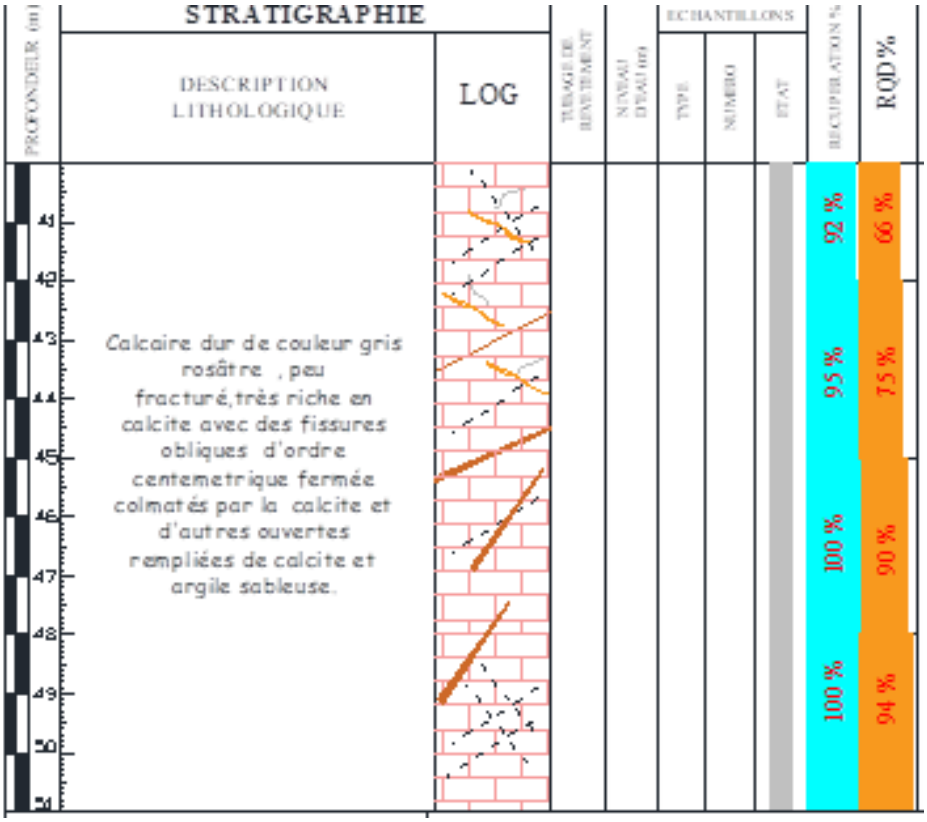
- Drias, T., Belloula, M., Badraddine, S., &Saibi, H. (2022). Groundwater modelling of the TebessaMorsott alluvial aquifer (northeastern Algeria): A geostatistical approach. Groundwater for SustainableDevelopment, 16, 100687.

ANNEX

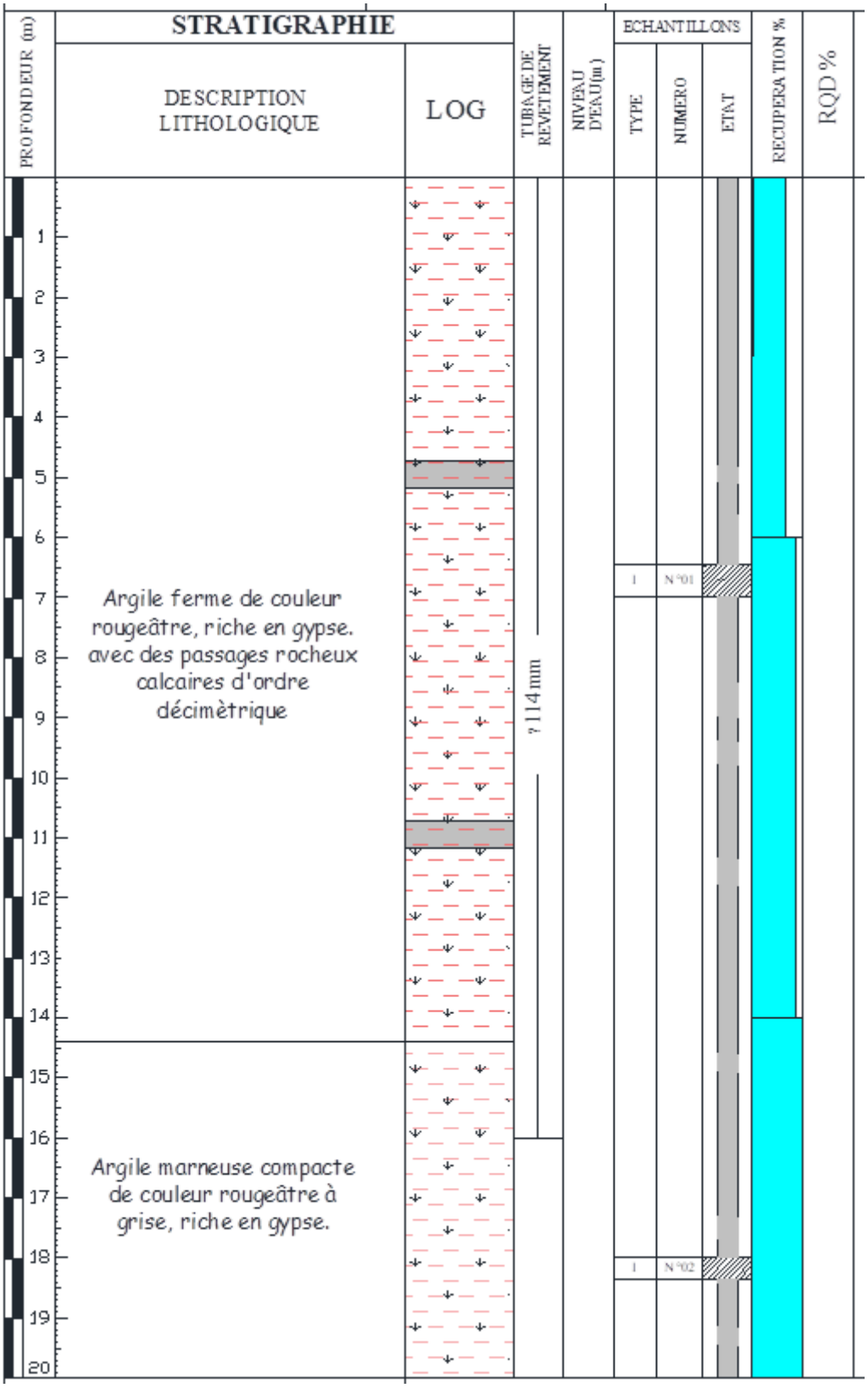
Annex 1.Bore Hole 01 (Limestone) :

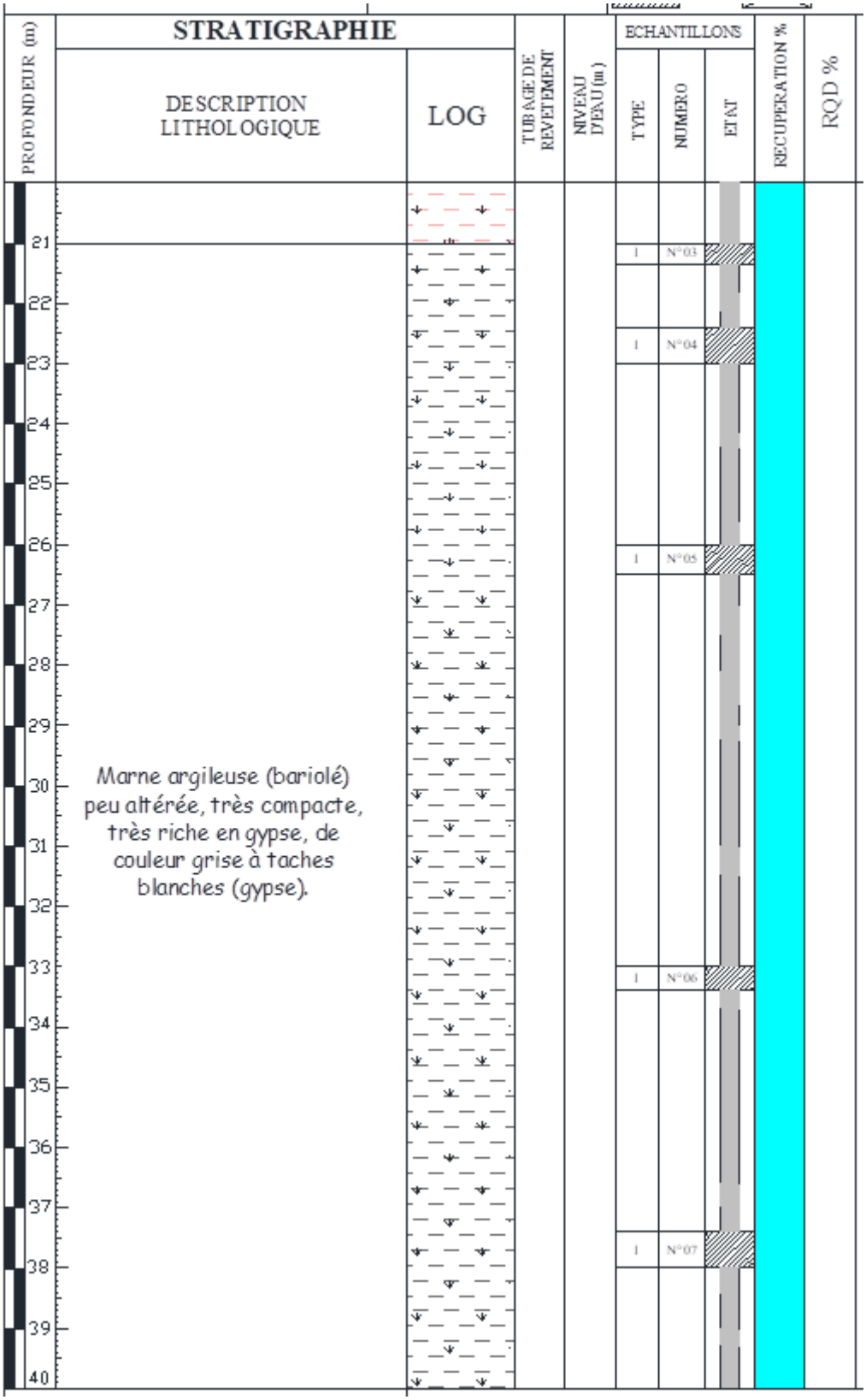


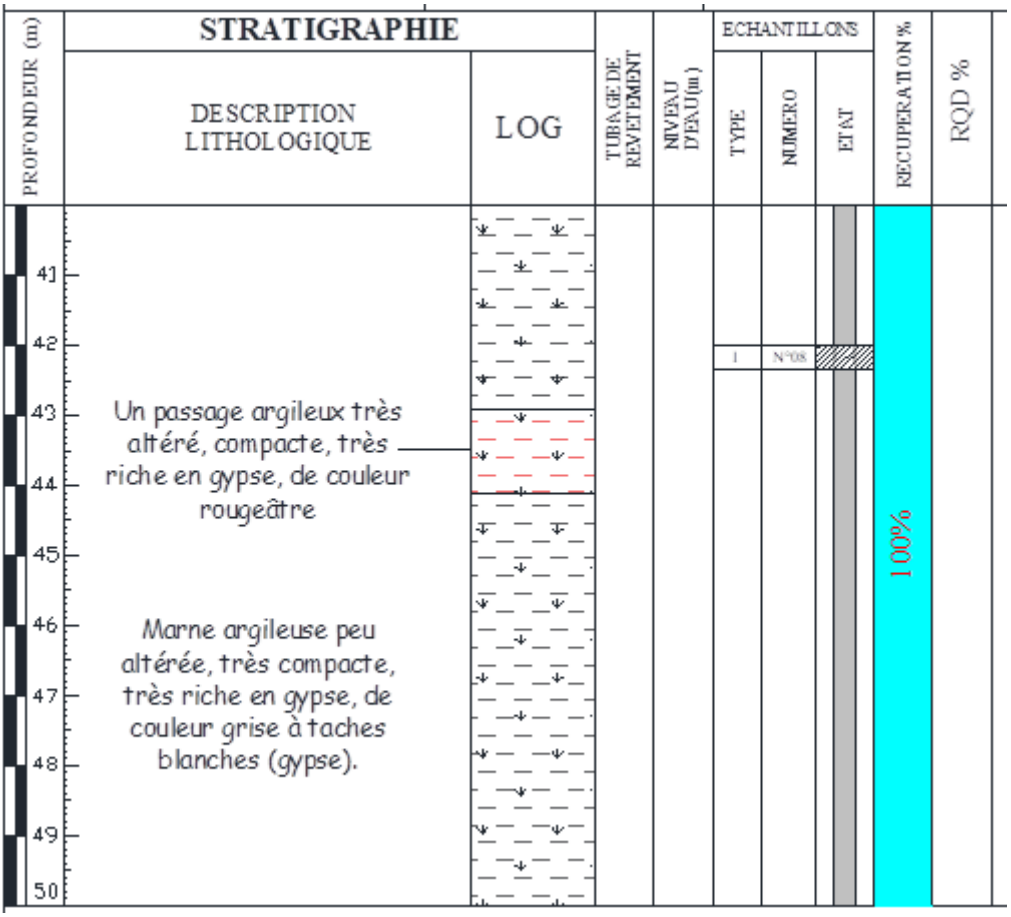

STRATIGRAPHIE
PROFONDEUR (m)
DESCRIPTION LITHOLOGIQUE
LOG
TUBAGE DE REVETEMENT
NIVEAU D'EAU (m)
ECHANTILLONS
TYPE
NUMERO
ETAT
RECUPERATION %
RQD %
Calcaire dur de couleur gris ,moyennement à fortement fracturé,des fissures d'ordre millimétriques fermée rempliées de calcite.
De 25.50 m à 26.20 m niveau fortement fracturé; des fissures ouvertes remplies complètement d'argile
Calcaire dur de couleur gris rosâtre peu fracturé,des fissures d'ordre centemetrique fermée colmatées par la calcite et d'autres ouvertes rempliées de calcite et argile sableuse
De 32.80 à 33.10 m zone affecte de dissolution.
21
22
23
24
25
26
27
28
29
30
31
32
33
34
35
36
37
38
39
40
97 %
91 %
96 %
30 %
98 %
82 %
99 %
94 %
98 %
96 %
97 %
86 %


STRATIGRAPHIE
PROFONDEUR (m)
DESCRIPTION LITHOLOGIQUE
LOG
TUBAGE DE REVETEMENT
NIVEAU D'EAU (m)
ECHANTILLONS
TYPE
NUMERO
ETAT
RECUPERATION %
RQD %
41
42
43
44
45
46
47
48
49
50
51
Calcaire dur de couleur gris rosâtre , peu fracturé,très riche en calcite avec des fissures obliques d'ordre centemetrique fermée colmatés par la calcite et d'autres ouvertes rempliées de calcite et argile sableuse.
92 %
95 %
100 %
100 %
66 %
75 %
90 %
94 %

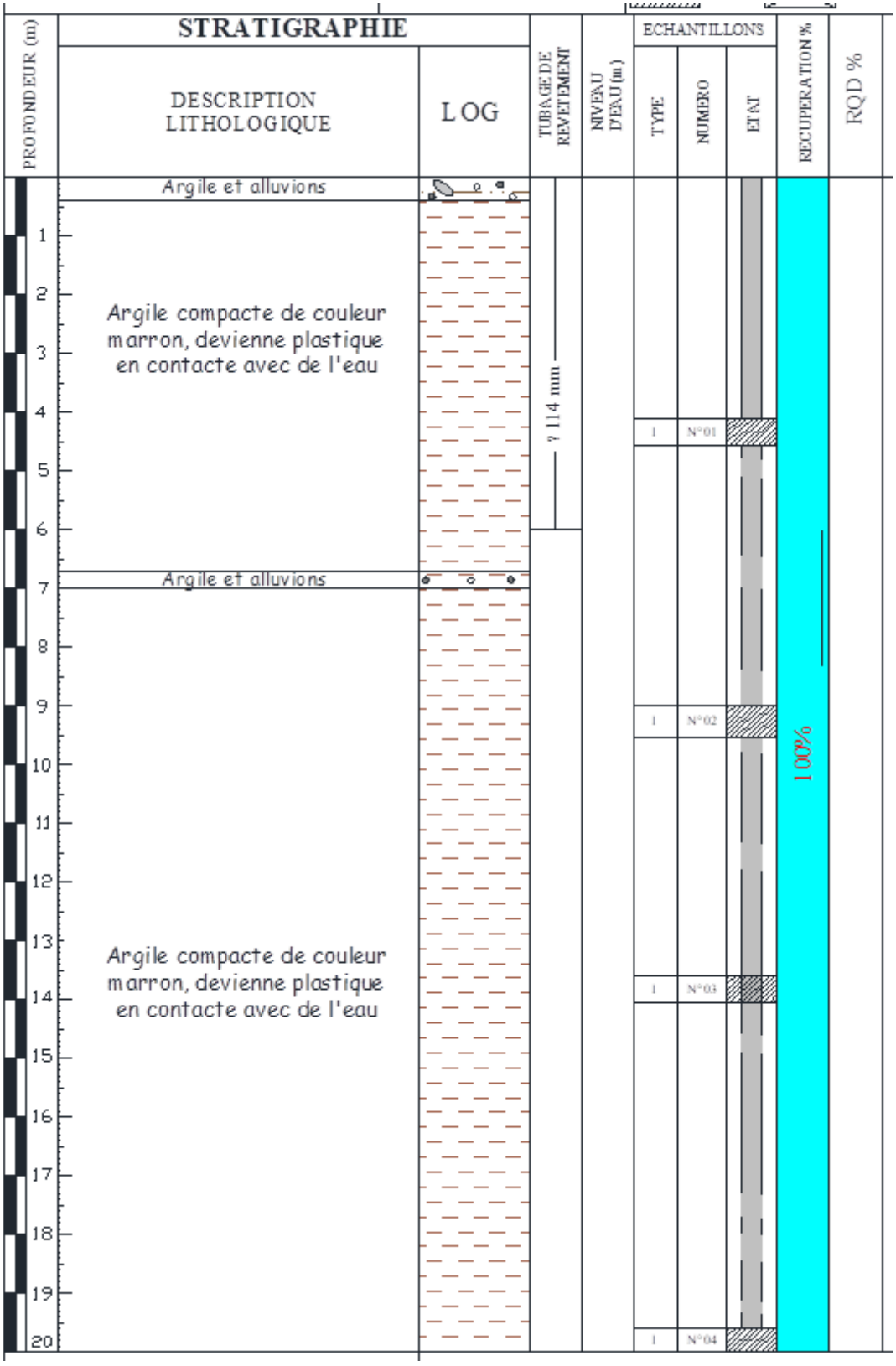
Annex 2 :Bore Hole 02 (Trias) :

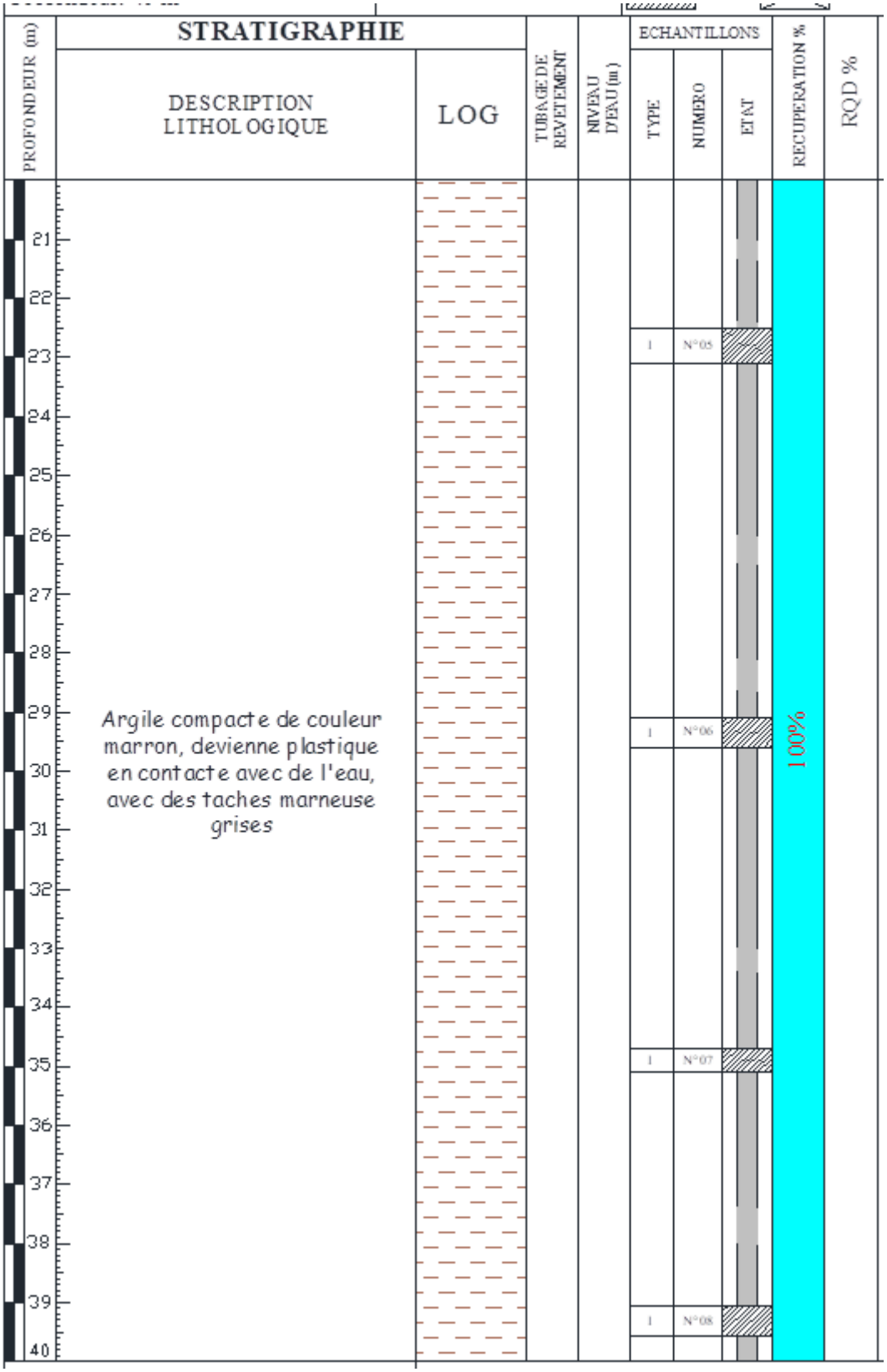



STRATIGRAPHIE
PROFONDEUR (m)
DESCRIPTION LITHOLOGIQUE
LOG
TUBAGE DE REVETEMENT
NIVEAU D'EAU (m)
ECHANTILLONS
TYPE
NUMERO
ETAT
RECUPERATION %
RQD %
21
22
23
24
25
26
27
28
29
30
31
32
33
34
35
36
37
38
39
40
Marne argileuse (bariolé) peu altérée, très compacte, très riche en gypse, de couleur grise à taches blanches (gypse).
1 N°03
1 N°04
1 N°05
1 N°06
1 N°07


PROFONDEUR (m)
STRATIGRAPHIE
DESCRIPTION LITHOLOGIQUE
LOG
TUBAGE DE REVETEMENT
NIVEAU D'EAU(m)
ECHANTILLONS
TYPE
NUMERO
ETAT
RECUPERATION %
RQD %
41
42
43
44
45
46
47
48
49
50
Un passage argileux très altéré, compacte, très riche en gypse, de couleur rougeâtre
Marne argileuse peu altérée, très compacte, très riche en gypse, de couleur grise à taches blanches (gypse).
1
N°08
100%

Annex 3 : Bore Hole 06(Clay) :




PROFONDEUR (m)
STRATIGRAPHIE
DESCRIPTION LITHOLOGIQUE
LOG
TUBAGE DE REVETEMENT
NIVEAU D'EAU (m)
ECHANTILLONS
TYPE
NUMERO
ETAT
RECUPERATION %
RQD %
Argile compacte de couleur marron, devienne plastique en contacte avec de l'eau, avec des taches marneuse grises
1 N°05
1 N°06
1 N°07
1 N°08
100%
21
22
23
24
25
26
27
28
29
30
31
32
33
34
35
36
37
38
39
40